DM

Preparation of complexes based on Laponite®, polydopamine, and polyethyleneimine for doxorubicin delivery

MASTER DISSERTATION

Emanuel Pedro Rodrigues Costa
MASTER IN APPLIED BIOCHEMISTRY

UNIVERSIDADE da MADEIRA
A Nossa Universidade
www.uma.pt

September | 2024

Preparation of complexes based on Laponite®, polydopamine, and polyethyleneimine for doxorubicin delivery

MASTER DISSERTATION

Emanuel Pedro Rodrigues Costa
MASTER IN APPLIED BIOCHEMISTRY

SUPERVISOR
Mara Isabel Jesus Gonçalves

Preparation of complexes based on Laponite®, polydopamine, and polyethyleneimine for doxorubicin delivery

Dissertation submitted to the University of Madeira in fulfilment of the requirements for the degree of Master in Applied Biochemistry

By Emanuel Pedro Rodrigues Costa

Work developed under the supervision of

Dr. Mara Isabel Jesus Gonçalves

Faculdade de Ciências Exatas e da Engenharia

Centro de Química da Madeira

Universidade da Madeira

Funchal – Portugal

2024

ORIGINALITY STATEMENT

“Plagiarism consists of the presentation, as your own and even if there has been translation, of ideas, opinions, phrases/texts, results, or conclusions of others. The practice of plagiarism is a serious violation of academic ethics and may lead to failure or withdrawal of the withdrawal of the degree, as well as civil, criminal, and disciplinary liability.”

I hereby declare on my honour that this dissertation is of my own exclusive authorship, it is original, and that I have referenced and quoted all sources used in it.

September | 2024

Emanuel Pedro Rodrigues Costa

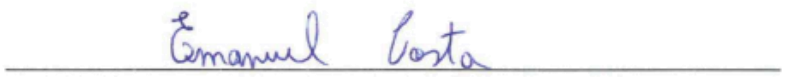

Acknowledgments

This thesis represents the culmination of a journey that would not have been possible without the invaluable support and assistance of many people. I wish to extend my heartfelt thanks and express my sincere gratitude to everyone who, in various ways, contributed to the completion of this work.

First and foremost, I would like to thank the Centro de Química da Madeira (CQM) and Professor João Rodrigues for welcoming me into the research group and providing all the necessary conditions to complete my work. I also extend my gratitude to all the funding institutions involved: Fundação para a Ciência e a Tecnologia (FCT), through the CQM Base Fund - UIDB/00674/2020, and Programmatic Fund - UIDP/00674/2020, and Agência Regional para o Desenvolvimento da Investigação Tecnologia e Inovação (ARDITI) for funding the CQM.

My deepest thanks go to my supervisor, Dr. Mara Gonçalves, for accepting my proposal and believing in my abilities. Thank you for your guidance, unwavering support, and insightful suggestions that helped me navigate through challenges and dead ends. Above all, thank you for always taking the time to listen, even amidst numerous other responsibilities, and for your comforting words.

I am also profoundly grateful to Rita Castro and Dina Maciel for their invaluable assistance in the lab, their constant willingness to help, and their kindness throughout this time. Special thanks to lab technicians Paula Andrade and Paula Vieira for always being available to assist with material and reagent requests.

A huge thank you to all my CQM friends Henrique Sousa, Duarte Fernandes (better known as Baljeet), Lydia dos Órfãos, Fátima Mendes, Jaison Jeevanandam, and especially João Carreira, Bárbara Pedra, and Jéni Monroy for all the encouragement, laughter, and good times. You all made this journey lighter and more enjoyable. Without you, I might have gone crazy, just kidding (or maybe not). Thank you for making my work breaks fun and interesting, it was a pleasure working with you all. In particular, I would also like to express my appreciation to Phineas, Perry, and Buford for always making lunch breaks enjoyable and for being my confidants in the lab and beyond. We've been on this journey together, and it's because of that camaraderie that we're here today, submitting our theses (except for Buford, but he knows what I mean).

I would also like to express my gratitude for the friendship I made this year with John Carreiras, for being a wonderful companion during the countless hours spent in the lab, singing songs to brighten our days. Thank you, John, for all the laughs and good times. It was a great pleasure working with you, and don't forget, when this is all over, we'll have that Spanish song to sing.

I also want to acknowledge my dear unemployed friend Ana Salvação for her unwavering support and for reminding me that life is about more than just work. Thank you for listening to my

endless thesis talk, even when it made no sense to you. I promise to respond to your messages more promptly from now on!

To my long-time friends Francisco “Maionese” Olim, André “Scooter” Dias, Yonathan “Hallaca” Reis, and Fábio “Wally” Leal, thank you for all the unforgettable moments we've spent over the years, whether on trips, festivals, or simple get-togethers. Even without knowing it, you've helped me reach where I am today by taking me to the best moments and refreshing my ideas. Without you, university life wouldn't have been as exciting.

I couldn't fail to thank to Afonso Teles, Sara Gil, Nance Hontman, Jéssica Gonçalves, João Pedro Ribeiro, “Canhota”, “Sola da Bota”, “Joker” and Joel Remesso for their companionship throughout this challenging dissertation journey. Thank you for always motivating me, for our coffee breaks, and for all the shared gossip; without you, the days would have been much darker.

To my family, I owe everything. Without your unwavering support and love, I could not have come this far. You have taught me to never give up on my dreams and to always strive for my best, and it is because of your guidance that I have reached this point. Thank you for your constant encouragement throughout my life.

I'd also like to thank my second family, which doesn't unite us by blood, but by camaraderie, TUMa - Tuna Universitária da Madeira, for all the good times I've had at this university and for making this academic journey more than just a phase, but the best years of my life. It was thanks to them that I was able to discover the true meaning of academic life. So here's a new rhyme:

Aqui vai uma rima!

Hoje vou agradecer à diocese!

Quem bebe?

Eu porque finalmente acabei a Tese!

Finally, a deep and sincere thank you to all those who have contributed, directly or indirectly, to my academic career. Without you, this work would have been impossible.

Abstract

Cancer continues to be one of the leading causes of death worldwide, with the number of cases expected to rise. Despite advances in medical science, many types of cancer still lack treatments capable of fully eradicating tumors due to their unique characteristics. Chemotherapy remains a common treatment, but it often comes with severe side effects and can sometimes be ineffective. Nanoparticles have gained attention for their ability to enhance cancer treatment by improving drug solubility, targeting tumors more effectively, increasing bioavailability, reducing side effects, and prolonging circulation time.

This study focuses on the synthesis and characterization of Laponite®-based nanocomplexes for targeted doxorubicin delivery, aiming to improve therapeutic efficacy while minimizing side effects. The complexes were developed by incorporating polydopamine and polyethyleneimine coatings onto Laponite nanodisks, with additional functionalization using FI-PEG-FA for enhanced targeting.

The study successfully synthesized and characterized LAP/DOX/PDA(FI-PEG-FA) and LAP/DOX/PEI(FI-PEG-FA) complexes through various physicochemical techniques, including Nuclear Magnetic Resonance, Dynamic Light Scattering, Electrophoretic Light Scattering, and Ultraviolet/Visible spectroscopy. The encapsulation efficiency and loading capacity of DOX were calculated, achieving 99.68% and 28.53%, respectively. The LAP/DOX/PDA(FI-PEG-FA) complex exhibited a diameter of 214.10 nm, a PdI value of 0.45 and a negative surface charge of -16.60 mV. The LAP/DOX/PEI(FI-PEG-FA) complex displayed a diameter of 880.40 nm, a PdI value of 0.41 and a positive surface charge of 20.85 mV.

The LAP/DOX/PEI(FI-PEG-FA) complex demonstrated superior effectiveness in sustaining DOX release under physiological conditions compared to the LAP/DOX/PDA(FI-PEG-FA) complex. Furthermore, *In vitro* cytotoxicity assays were performed to assess the impact of these complexes on cancer cell viability, with LAP/DOX/PEI(FI-PEG-FA) demonstrating the most significant reduction in cell viability. At 0.1 μM, the activity is around 60% and drops drastically to about 20% at 2 μM. Cells with the LAP/DOX/PDA(FI-PEG-FA) complex maintained relatively high metabolic activity, ranging from 85% to 100% across all concentrations.

The results suggest that these Laponite-based nanocomplexes, particularly those functionalized with FI-PEI-PEG-FA, hold promise as effective vehicles for the controlled release of DOX, with potential applications in targeted cancer therapy. Further studies are recommended to optimize these complexes and assess their performance in vivo.

Keywords: Cancer, Drug Delivery Systems, DOX, Laponite®, PEI, PDA.

Resumo

O cancro continua a ser uma das principais causas de morte em todo o mundo, prevendo-se que o número de casos aumente. Apesar dos avanços da ciência médica, muitos tipos de cancro ainda não dispõem de tratamentos capazes de erradicar totalmente os tumores devido às suas caraterísticas únicas. A quimioterapia continua a ser um tratamento comum, mas tem frequentemente efeitos secundários graves e pode, por vezes, ser ineficaz. Nanopartículas ganharam atenção pela sua capacidade de melhorar o tratamento do cancro, melhorando a solubilidade dos fármacos, visando os tumores de forma mais eficaz, aumentando a biodisponibilidade, reduzindo os efeitos secundários e prolongando o tempo de circulação.

Este estudo centra-se na síntese e caraterização de nanocomplexos à base de Laponite® para a administração de doxorrubicina, com o objetivo de melhorar a eficácia terapêutica e minimizar os efeitos secundários. Os complexos foram desenvolvidos através da incorporação de revestimentos de polidopamina e polietilenoimina em nanodiscos de Laponite, com funcionalização adicional utilizando FI-PEG-FA para melhorar o direcionamento.

Neste estudo sintetizou-se e caracterizou-se com sucesso os complexos LAP/DOX/PDA(FI-PEG-FA) e LAP/DOX/PEI(FI-PEG-FA) através de várias técnicas físico-químicas, incluindo Ressonância Magnética Nuclear, Espalhamento Dinâmico de Luz, Espalhamento Electroforético de Luz e Espectroscopia Ultravioleta/Visível. A eficiência de encapsulação e a capacidade de carga da DOX foram calculadas, atingindo 99,68% e 28,53%, respetivamente. O complexo LAP/DOX/PDA(FI-PEG-FA) apresentou um diâmetro de 214,10 nm, um valor de PdI de 0,45 e uma carga superficial negativa de -16,60 mV. O complexo LAP/DOX/PEI(FI-PEG-FA) apresentou um diâmetro de 880,40 nm, um valor de PdI de 0,41 e uma carga superficial positiva de 20,85 mV.

O complexo LAP/DOX/PEI(FI-PEG-FA) demonstrou uma eficácia superior na libertação de DOX em condições fisiológicas, em comparação com o complexo LAP/DOX/PDA(FI-PEG-FA). Além disso, foram efectuados ensaios de citotoxicidade in vitro para avaliar o impacto destes complexos na viabilidade celular, tendo o complexo LAP/DOX/PEI(FI-PEG-FA) demonstrado a redução mais significativa da viabilidade celular. A 0,1 μM, a atividade é por volta de 60%, e cai drasticamente para cerca de 20% a 2 μM. Células na presença do complexo LAP/DOX/PDA(FI-PEG-FA) mantiveram uma atividade metabólica relativamente elevada, variando entre 85% e 100% em todas as concentrações.

Os resultados sugerem que estes nanocomplexos à base de Laponite, particularmente os funcionalizados com FI-PEI-PEG-FA, são promissores como veículos eficazes para a libertação controlada de DOX, com potenciais aplicações na terapia do cancro. Recomenda-se a realização de mais estudos para otimizar estes complexos e avaliar o seu desempenho in vivo.

Palavras-Chave: Cancro, Sistemas de administração de medicamentos, DOX, Laponite®, PEI, PDA.

Index

Figures Index

Tables Index

Abbreviations

AA	Antibiotic-antimycotic
CR	Cumulative release
D_2O	Deuterium oxide
DAPI	40 ,6-diamidino-2- phenylindole
DDS	Drug delivery systems
DLS	Dynamic Light Scattering
DMSO	Dimethyl sulfoxide
DNR	Daunorubicin
DOX	Doxorubicin
DSPE-PEG	1,2-distearoyl-sn-glycero-3-phosphoethanolamine-N-(methoxy-PEG)
EDC	1-ethyl-3-(3-dimethylaminopropy) carbodiimide hydrochloride
EE	Encapsulation efficiency
Egg PC	Egg phosphatidylcholine
ELS	Electrophoretic Light Scattering
EPR	Enhanced permeability and retention
FA	Folic acid
FBS	Fetal bovine serum
FI	Fluorescein Isothiocyanate
HSPC	Hydrogenated soy phosphatidylcholine
LAP	Laponite®
LC	Loading capacity
MOE	Molecular Operating Environment
MWCO	Molecular weight cut-off
NHS	N-hydroxysuccinimide
NMR	Nuclear Magnetic Resonance
NPs	Nanoparticles
PBS	Phosphate-buffered saline
PDA	Polydopamine
PdI	Polydispersity index
PEG	Polyethylene glycol
PEI	Polyethyleneimine
ROS	Reactive oxygen species
RPMI	Roswell Park Memorial Institute
UV/Vis	Ultraviolet/Visible spectroscopy
VEGF	Vascular endothelial growth factor

Chapter 1 – Introduction

1. Cancer

Cancer represents a significant challenge to human health, largely due to the uncontrolled proliferation and dissemination of anomalous cells. As reported by Bray *et al*., 2024, [1], nearly 20 million new cancer cases were reported, along with 9.7 million cancer-related deaths in 2022, and it is estimated that there will be 35 million new cases of cancer by 2050 [1]. The early identification and treatment of cancer are now achievable thanks to recent advancements in nanotechnology and the synthesis of nanomaterials [2–4]. These nanomaterials, defined as materials that have at least one dimension at the nanoscale, can be designed to carry drugs and nucleic acids, releasing them inside the target cells in a controlled and efficacious way [5–7]. Nevertheless, despite these advances, cancer remains one of the most challenging diseases to treat and one of the major global causes of morbidity and mortality.

The vision of cancer treatment has been dramatically transformed by the advancement of our understanding of molecular and tumor biology in recent years. The traditional approach of categorizing and treating cancer based solely on the origin of organs or basic histomorphological features has been superseded. It has become evident that the pursuit of molecularly targeted therapies and treatment decisions guided by specific molecular alterations is imperative [8].

This paradigm shift has been driven by two fundamental developments: the acquisition of new technologies for the profiling of tumor molecular characteristics and the identification of predictive molecular targets. The convergence of these efforts has resulted in the emergence of two transformative revolutions in cancer treatment. The first of these innovations focuses on genotype-directed precision oncology, a strategy that tailors personalized therapies to subgroups marked by distinct genomic abnormalities across various tumor types. The second innovation turns around the manipulation of elements within the tumor microenvironment, particularly the immune system and its antitumor immune responses. These combined efforts usher in a new era of cancer treatment marked by precision and a comprehensive understanding of the intricate tumor biology [8].

Conventional chemotherapy is a commonly used approach to prevent cancer cells from spreading and dividing throughout the body [3]. For many years, chemotherapy has been the first choice in the treatment of malignant tumors [9]. However, the severe systemic toxicity associated with a low biodistribution, the unsatisfactory therapeutic effect, and nonspecific distribution, may result in the damage of healthy tissue during the delivery [10,11]. Given the limits of conventional chemotherapy, the development of nanoscale delivery systems (e.g., nanoparticles (NPs) or nanotubes) is essential for the targeted delivery of chemotherapeutic drugs to cancer cells [10]. An example of using NPs is the study conducted by Amiryaghoubi N, *et al.* [12], which utilized various nanometric drug delivery systems for bone cancer therapy. Another example is the study

by Liu X, *et al*. [13], which demonstrates the use of nanotubes for the photothermal ablation of tumors. The role of chemotherapy will continue to expand and become even more significant in improving both the survival and quality of life for patients with cancer.

2. Doxorubicin

Anthracyclines belong to an important class of chemotherapeutic agents employed in the treatment of cancer, obtained from the *Streptomyces bacterium* [14]. Their therapeutic efficacy has been demonstrated in a wide range of cancers, including not only leukemias and lymphomas but also breast, uterine, ovarian, bladder, and lung cancers. Anthracyclines represent some of the most potent and successful cancer therapies ever developed, demonstrating efficacy against a broader group of cancer types when compared to other chemotherapeutic category [15–17]. This is due to their ability to function regardless of the cell cycle stage and the fact that anthracyclines have numerous molecular targets, which makes them the most widely used and potent antitumor medications [18]. In clinical practice, the most noteworthy anthracyclines are daunorubicin (DNR), doxorubicin (DOX), epirubicin, and idarubicin [15].

The initial two anthracyclines, DOX and DNR, were extracted from the pigment-producing *Streptomyces peucetius*. Both drugs exhibit aglyconic and sugar moieties (Figure 1). The aglycone exhibits a tetracyclic ring featuring an adjacent quinone-hydroquinone group, a methoxy substitute, and a brief side chain containing a carbonyl group. The sugar, known as daunosamine, is connected to one of the rings by a glycosidic bond. This sugar consists of a 3-amino-2,3,6-trideoxyL-fucosyl moiety. The only distinction between these two molecules lies in the termination of the side chain. In the case of DOX, it is terminated with a primary alcohol, whereas in DNR, it ends with a methyl group, as shown in Figure 1. Although anthracyclines are widely employed, their cytotoxic effects vary considerably. Cardiotoxicity is the most recognized adverse outcome [19].

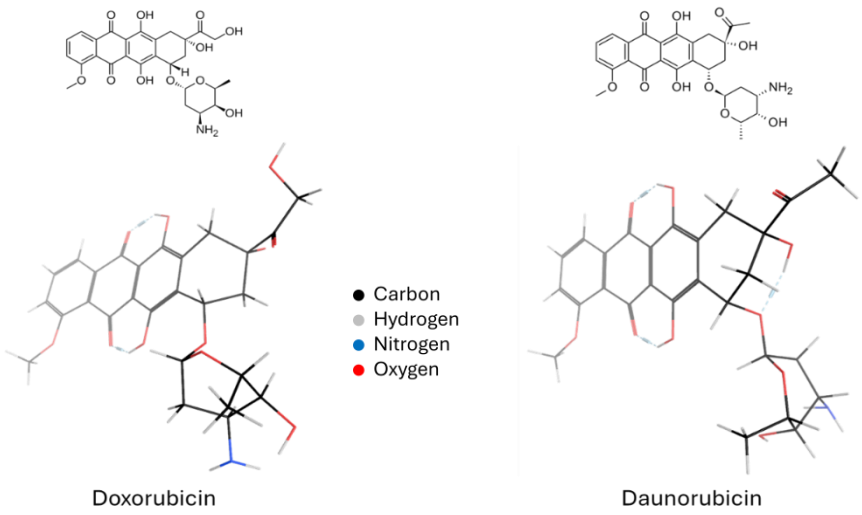

Figure 1. Chemical structures of DOX and DNR. Structures created in Molecular Operating Environment (MOE) 2015.10 software [20].

The identification of DNR was first reported in the 1950s, derived from a strain of the soil-based microorganism *Streptomyces peucetius* [21]. Later on, DNR entered clinical trials and demonstrated efficacy in the treatment of lymphoma and acute leukemia. However, it was also associated with the development of fatal cardiac complications [22]. A few years later, in the 1960s, a team of researchers at *Farmitalia Research Laboratories,* in Italy discovered DOX. Arcamone and colleagues [23] induced a genetic mutation in the *Streptomyces peucetius* strain. The colonies that were still alive began to produce a reddish substance called adriamycin, which was later renamed DOX. The anticancer activity of this substance was found to be superior to that of DNR. Subsequently, it was developed as a chemotherapeutic drug, and significant research has been conducted over the past few decades to determine its precise mechanism of action [23–26]. DOX can be synthesized directly from DNR or by fermentation using *Streptomyces peucetius var. caesius*, followed by solvent extraction and chromatographic purification [23]. In 1974, the United States approved its use as a medical treatment, and the World Health Organization subsequently included it on its List of Essential Medicines [25–27]**.**

DOX represents one of the most potent antineoplastic medications, either administered alone or in combination with other anticancer agents. It maintains its distinction as the most versatile compound within its category, exhibiting activity across a broad range of indications. Unquestionably, DOX is advantageous in treating both solid tumors and hematological malignancies. Its applications cover a broad spectrum of conditions, including breast cancer [28,29], liver cancer [30], bone cancer [31], ovarian cancer, lymphomas, leukemias, and soft tissue sarcomas [24,32]. In addition, DOX has been used to treat childhood solid tumors, osteosarcomas, soft tissue sarcomas, Kaposi's sarcoma, acute myeloblastic and lymphoblastic leukemia, as well as Wilms Tumor [19].

2.1. Mechanisms of action

DOX is used in both adjuvant and neoadjuvant therapy, depending on the type and stage of cancer. It is typically administered intravenously, although it can also be given orally. In adjuvant therapy, DOX is administered following surgical resection to eradicate any residual cancer cells and prevent a recurrence. In neoadjuvant therapy, DOX is given before surgery to reduce the size of the tumor and facilitate its removal. The dosage and schedule of administration are dependent upon the type and stage of the cancer, as well as the patient's overall health and other factors. Furthermore, DOX is also used in palliative care to relieve symptoms and enhance the life quality in patients with advanced cancer [33,34]. DOX has multiple molecular targets, and its primary cytotoxic effects are attributed to two phenomena, DNA intercalation and reactive oxygen species (ROS) production.

2.1.1. DNA intercalation

Firstly, like other anthracyclines, DOX intercalates within the DNA by forming hydrogen bonds with guanines in adjacent GC base pairs [35]. This implies that DOX molecules are inserted between the base pairs of the DNA double helix [24,32]. As a result, it inhibits the activity of topoisomerase II, an enzyme that relaxes the DNA supercoils for transcription [24,36]. Consequently, the replication of cancer cells is inhibited, preventing them from dividing and proliferating [24,32]. This results in the prevention of DNA replication and transcription, which leads to the cancer cells death.

Nevertheless, according to Kciuk *et al.*[35], the specific mechanisms underlying this interaction remain relatively unknown. One hypothesis regarding the impact of DOX on cancer cells is that the intercalation into the DNA molecule causes an untwisting of the DNA helix, leading to a positive supercoiling. Additionally, there is supporting evidence indicating that DOX enhances the turnover of nucleosomes surrounding promoters of active genes due to its intercalation, thereby inducing alterations in DNA topology. It is established that the untwisting of DNA caused by DOX's intercalation exerts a significant degree of positive torsional stress that destabilizes the nucleosome’s structure. Furthermore, research has shown that the formation of DOX–DNA adducts has the potential to trigger the DNA damage response pathway independently of the drug's effect on topoisomerase II. It is evident that DOX–DNA adducts are detectable even at clinically relevant drug doses. This indicates that the formation of these adducts occurs during chemotherapy administration. Despite that, the formation of these adducts may not represent the principal mechanism of DOX action [35].

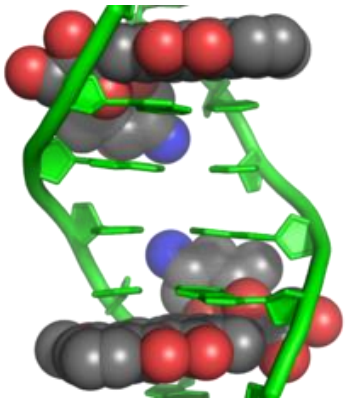

Figure 2. Diagram of two DOX molecules intercalating DNA, from PDB: 1D12 [37].

2.1.2. ROS production

Another phenomenon worthy of consideration is the ROS production. As described by Kciuk *et al.* [35], ROS can be generated within aerobic organisms through various mechanisms, including the activity of catabolic oxidases, peroxisome metabolism, and the electron transport chain. In the absence of elevated ROS concentrations, these molecules serve as cellular messengers in redox signaling processes [38]. However, excessive production of ROS can contribute to DNA damage, where radicals affect DNA bases and the sugar-phosphate backbone. In the absence of repair, this damage can lead to apoptosis and cell cycle arrest, ultimately resulting in the cancer cells' death [35].

2.2. Properties

The non-selective anthracycline DOX has a structural composition based on a water-insoluble aglycone (adriamycinone) that possesses lipophilic characteristics, and an amino-sugar moiety (daunosamine) that exhibits hydrophilic character. The quinine-hydroquinone group is located next to a tetracyclic ring in the adriamycinone compound. A glycosidic bond connects one of the rings to the amino-sugar moiety [39,40].

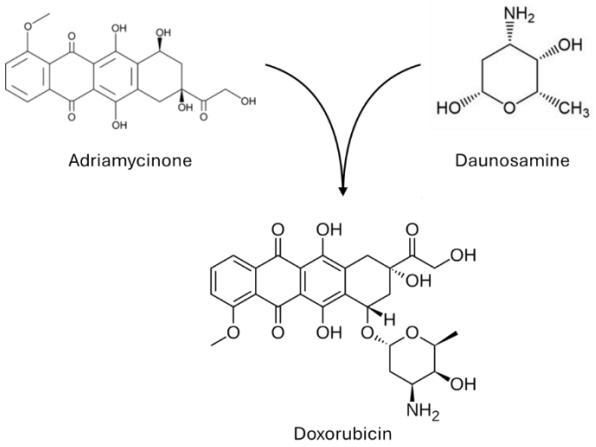

Figure 3. Chemical structure of DOX. Created in Biorender.

In addition, DOX exhibits both acidic and basic properties, classifying it as an amphoteric molecule. It contains three ionizable groups, corresponding to the amino group at daunosamine, the hydroxyl group at C11, and the hydroxyl group at C6, with pKa values of 8.2, 10.2, and 13.2, respectively [41]. Moreover, DOX can be used as a pH indicator, as evidenced by the shift in color from orange-red at neutral pH to blue-violet at a pH of 9 (Figure 4). This color shift is attributed to the chromophore present in the DOX molecule (dihydroxyanthraquinone) [40].

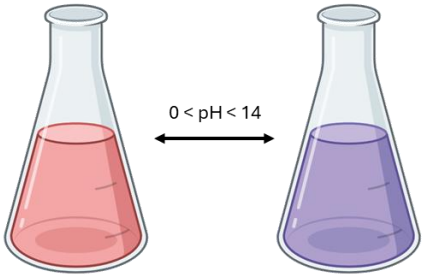

Figure 4. The color transition of DOX solution in an acidic and basic environment. Created in Biorender.

In addition, the DOX molecule exhibits intrinsic fluorescence properties. This fluorescence is frequently employed to track the uptake and localization of DOX within cells. The signal's intensity may change depending on the interaction between the molecule and the cell membrane, proteins, and/or DNA [42–44]. Given this, some studies have been performed to assess the relationship between solvent composition and fluorescence intensity [45,46]. Karukstis *et al*. [45] found that DOX fluorescence decreases with both an increase in concentration and a reduction in the pH of the surrounding environment. Moreover, two aqueous solution emission characteristic peaks for DOX were identified at 560 and 593 nm.

2.3. Side effects

As previously mentioned, DOX is one of the most frequently used chemotherapy agents for cancer treatment. Its applications encompass a range of malignancies, including breast cancer [28,29], liver cancer [30], and bone cancer [31]. Despite its broad spectrum, the use of conventional DOX in clinical practice has been constrained due to the presence of negative side effects, including cardiotoxicity [24]. This was particularly the case for individuals requiring dose escalation due to advanced disease [47]. DOX exhibits a significant interaction with cellular macromolecules, resulting in a reduction in its therapeutic index [48]. Consequently, the administration of high doses or repeated cycles is normally required to achieve the desired therapeutic effect, which can simultaneously lead to several major side effects [19]. Furthermore, DOX exhibits high toxicity and low water solubility, which present significant challenges in its administration and distribution within the body. These properties can result in a range of side effects, some of which may be severe [26,32]. The most common side effects include nausea, sickness, hair loss, fatigue, and decreased appetite. More serious side effects may include heart damage, which can result in heart failure, myelosuppression, and an increased risk of developing secondary cancers [19,24,32].

One of the major challenges associated with the use of DOX is the development of drug resistance. Cancer cells can become resistant to DOX through a variety of mechanisms, similar to what happens with other anticancer drugs. These mechanisms include increased efflux of the drug from the cell, decreased uptake, activation of detoxifying, DNA repair, or alterations in the target of the drug [40,49].

To mitigate the risk of side effects, patients receiving DOX are typically monitored closely, and the drug may be given in combination with other drugs to improve its effectiveness and reduce toxicity [50]. Despite its long-standing use in the treatment of cancer, researchers are currently focused on improving its efficacy while reducing its side effects. Some strategies are being explored, including the development of new formulations of the drug, such as liposomal formulations that can improve its delivery to tumor cells and reduce its toxicity to healthy tissues [51,52].

Prior clinical research has demonstrated that liposomal anticancer medications exhibit reduced toxicity and improved tolerance [53]. For the administration of DOX, several drug delivery methods have been studied, including polymers [54,55], such as liposomes [56] and dendrimers [57], which have been shown to enhance their anticancer activity [58]. The development of precisely controlled drug release systems capable of enhancing DOX cellular uptake and releasing the drug into the cytoplasm upon activation by environmental stimuli remains a significant challenge. Such systems would enable DOX to reach the nucleus and exert the intended therapeutic effects, as evidenced by several studies [59–61].

3. Nanomaterials

In the intricate domain of nanotechnology, the classification of nanomaterials represents a fundamental framework that categorizes these materials based on their distinctive properties and structures at the nanoscale. As illustrated in Figure 5, nanomaterials can be categorized into five primary groups. Nanomaterials encompass a diverse array of types, each exhibiting unique characteristics that make them suitable for specific applications [62].

Nanomaterials find diverse applications across a multitude of industries; one noteworthy application is in the development of diagnostic and control tools for epidemic diseases. A pertinent example was the role of nanomaterials in addressing the COVID-19 pandemic, as documented in 2019 [62].

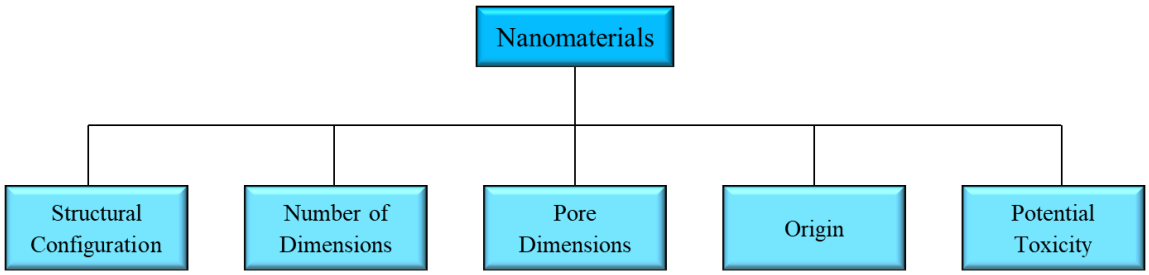

Figure 5. General classification of nanomaterials. Created in Biorender.

3.1. Nanomaterials for biomedical applications

NPs possess unique properties that make them attractive for biomedical applications. They can be designed to possess specific shapes, sizes, and surface properties, which can be used to control their interactions with biological systems [63]. For instance, NPs can be functionalized with targeting moieties such as antibodies [64] or peptides [65], which can enable them to selectively bind to specific cells or tissues, and can also be used to encapsulate drugs or other therapeutic agents, facilitating a controlled release and targeted delivery [63,66].

Nanomedicine is the application of nanotechnology to the field of medicine. The history of nanomedicine can be traced back to the 1950s when the concept of using tiny particles for drug delivery was first proposed. However, it was not until the 1980s that the field began to gain a boost, with the development of novel techniques for synthesizing and characterizing NPs [67]. Since then, considerable progress has been made in the development of nanomedicine, which has become a fast-growing field with applications in many areas of medicine [67,68].

Nanomedicine has the potential to improve the diagnosis, treatment, and prevention of a wide range of diseases, such as atherosclerosis, the novel coronavirus disease (COVID-19), cancer, infectious diseases, cardiovascular disease, and neurological disorders [44,69–73].

Among its most promising applications is regenerative medicine, where NPs can be used to create scaffolds for tissue engineering, providing a framework for the growth and regeneration of tissues and organs [74,75]. In drug delivery, NPs can be used to deliver drugs to specific cells or tissues, improving drug efficacy and reducing side effects, such as the systemic toxicity associated with conventional chemotherapy [71]. Liposomes, dendrimers, and polymer-based nanoparticles are some of the most commonly used drug delivery systems (DDS) [76]. Furthermore, in imaging, NPs can also be used as contrast agents in medical imaging, allowing for earlier detection and more accurate diagnosis [77,78], improving the sensitivity and specificity of diagnostic tests. Quantum dots, gold NPs, and iron oxide NPs are some examples of nanoparticle-based imaging agents [67,79]. Additionally, in diagnostics, NPs can be used as diagnostic tools, such as biosensors, for the early detection and monitoring of diseases. Nanoparticle-based diagnostic tests can be more sensitive and specific than traditional diagnostic tests [80]. Lastly, in tissue engineering, NPs can also be used as the development of scaffolds. NPs can promote cell adhesion, and proliferation, and can be used to deliver growth factors or other bioactive molecules [81].

3.2. Biological challenges

Although nanomedicine holds great promise for revolutionizing the healthcare system, its biomedical applications are still limited by challenges such as toxicity, stability, and target delivery. A primary concern is the potential toxicity of NPs. Some have been shown to exhibit toxicity towards cells and tissues, yet their long-term effects on human health remain incompletely understood. NPs have the potential to accumulate in tissues and organs, potentially increasing the risk of adverse effects [82]. Efforts have been made to develop biocompatible and biodegradable NPs and to optimize their properties to reduce toxicity [82]. Another challenge is the regulatory approval process for nanomedicine products, which is still developing guidelines for the use of nanomedicines. Due to their unique properties, nanomedicine products may require additional safety and efficacy testing before they can be approved for clinical use. This can make the development and commercialization of nanomedicine products more challenging and time-consuming [83]. Additionally, technical challenges are associated with the design and production of NPs. The production on a large scale is challenging, as their properties can be affected by factors such as size, shape, and surface chemistry [83]. Finally, this innovative frontier presents its own set of obstacles, particularly in the biological field. The interaction between nanomaterials and living organisms presents complex and intricate biological challenges that necessitate meticulous analysis, such as the case of biological barriers and targeting.

3.2.1. Passive targeting

The passive targeting process involves the transport of NPs through the capillaries of a tumor. This process relies on the distinct pore sizes present in the tumor's microvasculature compared to normal capillaries. By engineering the optimal size, NPs can enter the tumor tissues while remaining confined within the capillaries of normal tissues, thereby achieving precise targeting [84–86]. This process occurs via passive diffusion or convection, where the transport of low molecular weight compounds primarily takes place through diffusion [87]. This process involves the movement of molecules across the cell membrane in the absence of cellular energy. The process of selective accumulation of drugs and nanocarriers is carried throughout the enhanced permeability and retention (EPR) effect [87]. This is regarded as the gold standard in the design of cancer-targeting drugs. Nanocarriers, given their specific particle size and the association with the EPR effect, tend to gather and concentrate in tumor tissues [88,89]. The EPR effects can also be applied to all quickly growing solid tumours [90]. Passive targeting strategies rely solely on the EPR effect, which lacks tumor detection capabilities, as evidenced by studies conducted by Low *et al.* (2008) [91], Y. Yang *et al.* (2020) [89], and Zhang *et al.* (2019) [92].

It is becoming clear that the EPR effect is a prevalent phenomenon in the majority of human cancers, except for hypovascular tumors such as prostate and pancreatic cancers [93,94]. For the EPR effect to be most effective, nanocarriers must avoid detection by the immune system and remain circulating within the bloodstream for an extended period. Consequently, drug-loaded nanocarriers can accumulate in the tumor site to levels that are 10 to 50 times higher than those observed in normal tissues, with this accumulation occurring within a time frame of 1 to 2 days [95].

To achieve successful drug delivery, nanocarriers must possess specific characteristics. Firstly, the optimal size range for nanocarriers is 10 to 100 nm. Nanocarriers with a diameter of less than 400 nm can effectively pass through the leaky vasculature surrounding tumors. However, they must also be larger than 10 nm to avoid filtration by the kidneys and smaller than 100 nm to prevent specific capture by the liver. Secondly, the charge of the nanocarriers' particles should be either neutral or anionic. This charge property facilitates evasion of elimination by the kidneys, thereby increasing circulation time in the body and enhancing the possibility of reaching the tumour site. Finally, nanocarriers should be designed to avoid detection by the reticuloendothelial system, which is responsible for the removal of foreign materials through opsonization and phagocytosis. By remaining undetected, the nanocarriers can avoid premature clearance and destruction, thereby maximizing their potential to deliver drugs effectively to the targeted tumor site [96,97].

Nevertheless, it is important to acknowledge that there are certain limitations associated with the passive targeting of tumors using nanocarriers. The success of this approach relies on the extent of tumor vascularization and angiogenesis [98]. The overexpression of angiogenesis

regulators, such as vascular endothelial growth factor (VEGF), plays a role in creating chaotic tumor vessel architecture and increasing vascular permeability, ultimately leading to enhanced drug accumulation [99]. Consequently, the extravasation of nanocarriers may vary depending on the specific type and location of the tumor within the body. Moreover, solid tumors exhibit a high interstitial fluid pressure, which presents a challenge for efficient drug uptake and even distribution within the tumour mass [100]. This elevated pressure, in conjunction with inadequate lymphatic drainage, contributes to the correlation between nanocarrier size and the effectiveness of the EPR effect. It can be observed that larger nanocarriers, which are capable of circulating in the bloodstream for an extended period (approximately 100 nm) are more likely to be retained within the tumor. On the contrary, smaller molecules may easily disperse away from the target site [101].

3.2.2. Active targeting

Active targeting involves the customization of nanocarriers with special targeting ligands on their surface (Figure 6), such as small molecules, carbohydrates, hormones, antibodies, and peptides, which possess a specific affinity for molecular receptors overexpressed on the surface of target cells [40]. These strategies have emerged as promising approaches.

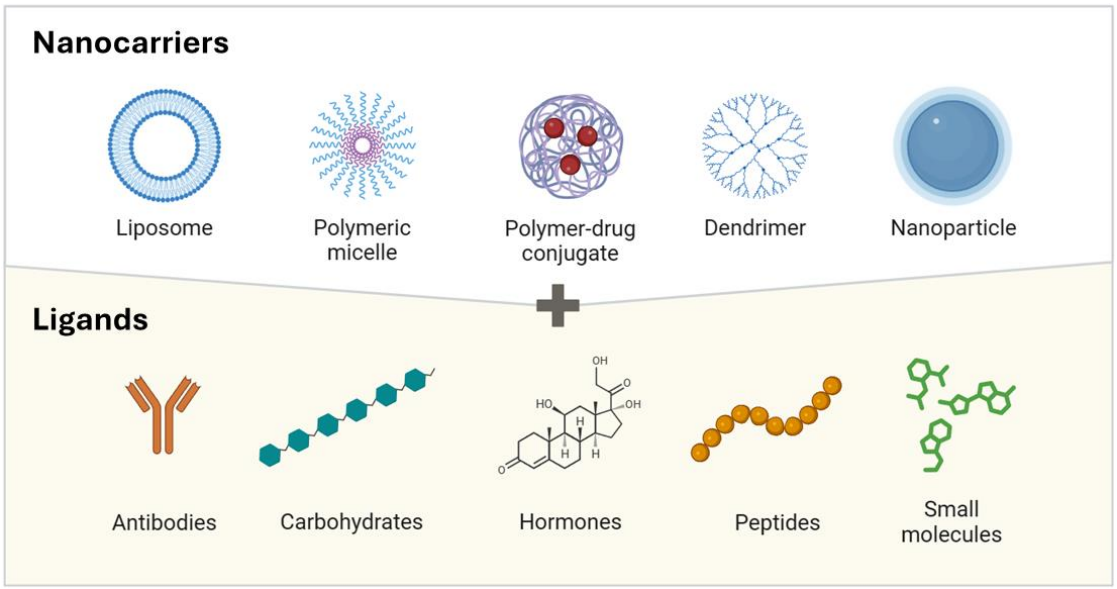

Figure 6. Schematic representation of distinct types of nanocarriers and ligands. Created in Biorender.

These ligands are designed to bind specifically to receptors found at the desired target site, as illustrated in Figure 7. The interaction between the ligand and the receptor triggers a receptor-mediated mechanism, facilitating the cellular internalization of the nanocarrier and

enhancing its effectiveness as a delivery system [102]. The selection of these ligands is crucial, as they must attach themselves to the receptors that are abundant in tumor cells or to the blood vessels surrounding the tumor [103].

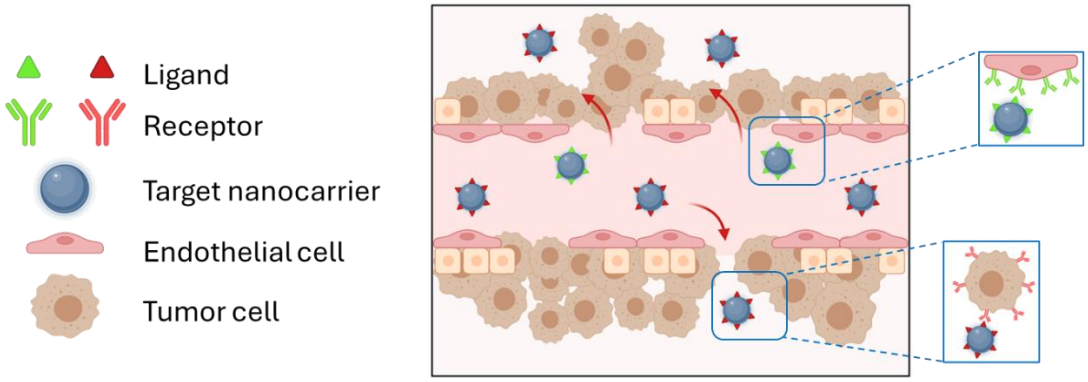

Figure 7. Active targeting strategies. Ligands grafted at the surface of nanocarriers bind to receptors overexpressed by cancer cells or endothelial cells. Created in Biorender.

The efficacy of active targeting relies on several factors, including the degree of receptor overexpression in the target cells and the strength of the bond between the targeting ligands and the receptors. This bond must overcome the "binding-site barrier" to effectively penetrate the tumor [40]. One great example is folic acid (FA), a commonly used targeting ligand that is frequently overexpressed in various cancer types, including those found in the ovary, brain, kidney, breast, colon, and lung [104]. As a result, it has been extensively employed in cancer treatment and detection [105].

When targeting accessible sites such as tumor vasculature, where the bloodstream flows dynamically, it is advantageous to have a high-affinity binding between the ligands and the receptors [106,107]. The term "ligand-targeted therapeutics" is a broad term that encompasses a variety of anti-cancer treatments that employ this targeting approach. These therapeutics can be classified into distinct categories based on their specific drug delivery methods [108].

One category of active targeting involves the use of antibodies, either monoclonal or fragments, to identify and engage with specific receptors. These antibodies can interfere with signal transduction pathways or regulate proto-oncogenes, which are crucial for the proliferation of cancer cells. Examples of such antibodies include trastuzumab (Herceptin®) which targets ERBB2, bevacizumab (Avastin®) which targets VEGF, and etaracizumab, a humanized anti-αvβ3 antibody (Abegrin™). In this approach, as illustrated in Figure 8, the active molecule plays a dual role, acting both as a targeting ligand and a drug. On the other hand, antibodies (or fragments) can function exclusively as targeting ligands when combined with therapeutic molecules [108]. For instance, ^{90}yttrium–ibritumomab tiuxetan (Zevalin®) targets *anti*-CD20 and represents the first radioimmunotherapeutic to gain clinical approval [109].

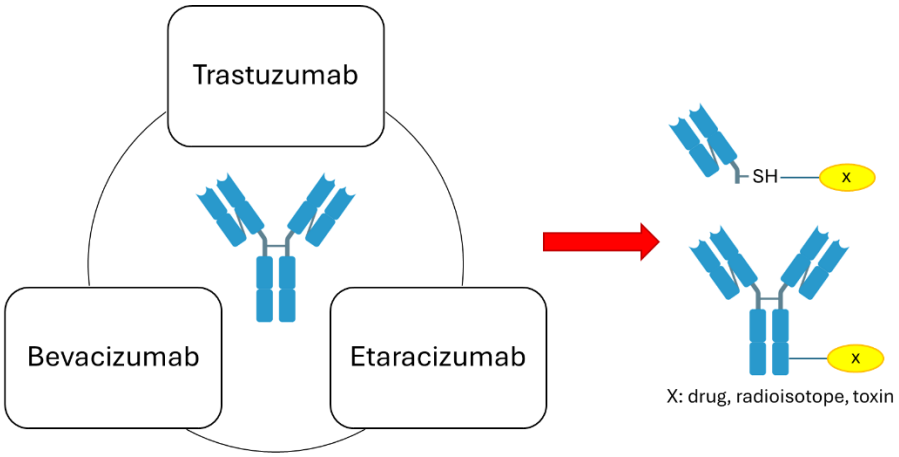

Figure 8. Active targeting using antibodies to detect specific receptors. Created in Biorender.

Another active targeting class involves the use of immuno-nanocarriers, in which cytotoxic drugs are encapsulated within nanocarriers, and antibodies (or fragments) serve as targeting ligands, attached to the nanocarrier's surface. Finally, targeted nanocarriers replace antibodies with specific molecules (peptidic or non-peptidic) that are designed to bind exclusively to certain receptors on the tumor cells as depicted in Figure 9 [108].

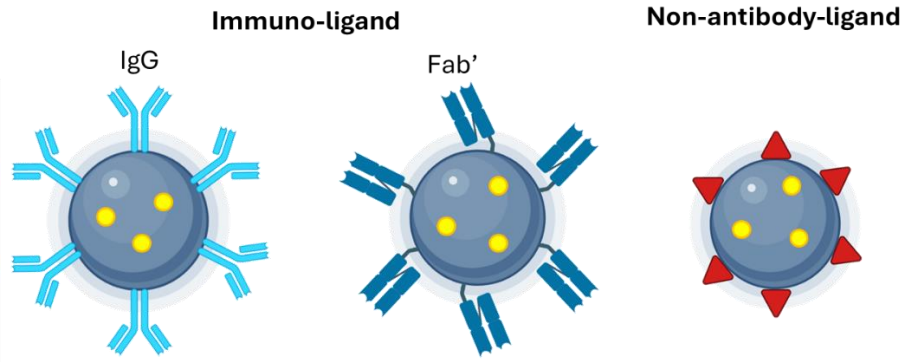

Figure 9. Nanocarriers presenting targeted ligands at the surface. The ligands are either monoclonal antibodies and antibody fragments (immuno-nanocarriers) or non-antibody ligands. Created in Biorender.

The combination of active targeting approaches with the EPR effect has the potential to significantly improve the efficacy of nanocarrier-based anticancer DDS [85,89]. The use of nanoscale DDS offers several advantages for targeted tumor therapy. Firstly, they take advantage of the EPR effect, which promotes the accumulation of nanocarriers within the tumor microenvironment [110]. Additionally, nanocarriers can be easily modified with biological ligands,

thus enabling active tumor targeting and improving specificity [111]. Moreover, these systems can incorporate stimuli-sensitive drug release mechanisms, allowing controlled and targeted drug delivery [112]. In the field of cancer therapy, the combination of active targeting and the EPR effect represents a significant potential for overcoming the limitations of conventional chemotherapy. The ability of active nanocarrier platforms to specifically target cancer cells while minimizing off-target effects paves the way for more effective and personalized treatments [113].

4. Nanoparticles for cancer treatment

NPs have emerged as crucial tools for drug delivery, modifying the drug's pharmacokinetics to optimize effectiveness and mitigate certain side effects [114]. Focused on increasing the therapeutic properties and efficacy of drugs, DDS function as reservoirs for drug storage, precisely releasing drugs at specific locations and times, thereby influencing the body's pharmacokinetic and drug distribution processes [115].

The key benefits of NPs as carriers for anticancer agents include the capacity to deliver drugs to tumors, facilitate tumor imaging, proficient storage of numerous drug molecules, and the capacity to overcome challenges related to solubility, stability, and resistance. This not only enhances the bioavailability and biodistribution of drugs in the bloodstream but also ensures biocompatibility [116].

4.1. Polymer-based drug delivery systems

Nanocarriers are extremely small vehicles that can transport drugs, vaccines, and other molecules to a specific area or cell in the body. These nanocarriers are designed to be adjusted to specific applications and consist of different types of materials, such as lipids, proteins, and polymers. Among these, polymer-based nanocarriers stand out as a preferred choice due to their flexibility, biocompatibility, and straightforward synthesis process [117].

Nanocarriers offer several advantages over conventional DDS. The chemical composition, size, and structure of these systems can be manipulated to provide properties that are easily adjustable [58]. They can deliver drugs to specific targets and shield drugs from the body's metabolic processes, eliminating the necessity of administering high doses throughout the entire body and prolonging their half-life. It is also worth noting their ability to create a protective barrier for hydrophobic drugs, thereby improving their aqueous solubility [118]. Consequently, this approach results in a reduction in side effects and enhanced therapeutic outcomes. Another significant advantage is the capacity to design and target specific types of cells, such as cancer cells. This can be achieved by modifying the surface of the nanocarrier with ligands [119]. Surface modifications involve the alteration of a material’s surface properties to enhance its performance

or functionality. In the context of polymer-based nanocarriers, surface modification can improve their stability, biocompatibility, and targeting abilities. This can be accomplished by attaching ligands or other macromolecules and functional groups to the polymer surface, or by coating the surface with another material to alter its properties (Figure 10). This indicates that drugs can be released gradually over a specific period, allowing for a lower overall dose to be administered to the entire body [120,121].

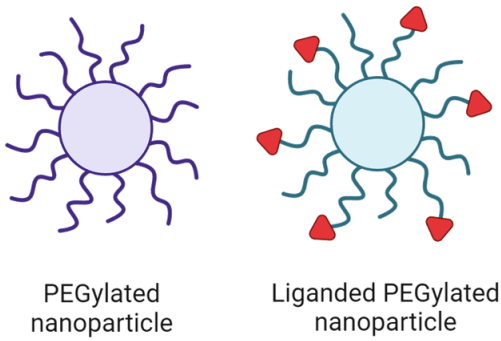

Figure 10. Schematic representation of attaching ligands to the polymer surface to alter its properties. Created in Biorender.

There are several techniques that allow loading drugs into the nanocarrier, such as physical entrapment, chemical conjugation, and electrostatic interactions. The latter involves noncovalent interactions, which are particularly advantageous for loading charged drugs. In this process, drug molecules are attracted to the surface of the nanocarrier by electrostatic forces between the charged groups on the drug and the polymer matrix of the nanocarrier [122]. Furthermore, electrostatic interactions present the possibility of controlling the release kinetics. This can be accomplished by adjusting the pH of the surrounding environment, influencing the strength of the electrostatic interaction between the drug and the nanocarrier. For instance, a nanocarrier designed for the treatment of cancer could be modified to respond to the acidic tumor microenvironment, enabling the selective release of the drug at the tumor site [121].

One of the most crucial aspects of creating and designing polymer-based nanocarriers is the meticulous selection of the most appropriate material. The selection of the polymer depends on the specific properties that are required for the nanocarrier. These properties may include biocompatibility, biodegradability, stability, drug loading capacity, nanocarrier release kinetics, and the ability to interact with and transport cargo to specific sites [117]. Polymers such as polyethyleneimine (PEI) and polyethylene glycol (PEG) are well-known for their biocompatibility, biodegradability, and the ability to finely tune and control their physicochemical properties [121].

4.1.1. Polyethyleneimine

PEI is a cationic polymer composed of repeating units of amine groups and two aliphatic carbons, which has gained significant attention in the field of drug delivery due to its unique properties. PEI can assume either a branched or linear configuration. Linear PEI contains only secondary and primary amino groups, while branched PEI contains primary, secondary, and tertiary amino groups, as illustrated in Figure 11. Branched PEI has a high charge density of amine groups, which makes it more chemically reactive, and is often used as a cationic polyelectrolyte [123–126]. Additionally, lower molecular weight PEIs, 22 and 25 kDa, exhibit reduced toxicity compared to high molecular weight PEIs (800 kDa) [127].

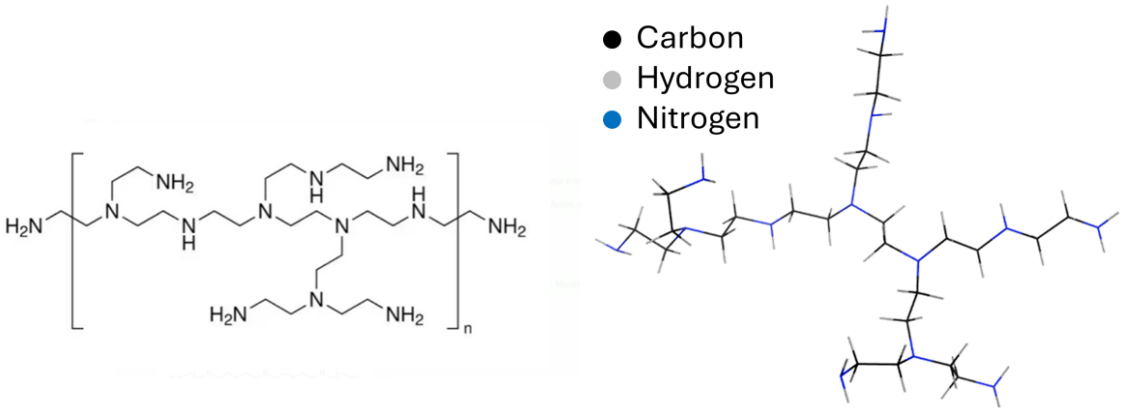

Figure 11- Chemical structures of branched PEI. Structure created in Molecular Operating Environment (MOE) 2015.10 software [20].

PEI is soluble in water and due to its high charge density can form complexes or stable NPs through electrostatic interactions with negatively charged molecules, such as DNA, RNA, and proteins. This versatility renders it invaluable tool for the delivery of a wide range of therapeutic agents, including genes, proteins, and small molecules [105,124].

PEI has been widely studied and used in a variety of applications, including gene therapy, tissue engineering, drug delivery, and cancer therapy. In gene therapy, PEI is an efficient gene delivery vector, due to its high charge density and ability to form stable complexes with DNA and RNA, which can penetrate the cell membrane and enter the cell nucleus [128]. Also, PEI has been explored for use in tissue engineering applications, as it can also promote cell adhesion and proliferation. This polymer can be used to create scaffolds for tissue regeneration and cell culture. PEI-based scaffolds can support cell attachment, proliferation, and differentiation, making them promising tools [125,129]. In addition, PEI has also been used as a drug delivery vehicle, due to its ability to form stable NPs with drugs. The NPs can protect the drug from degradation, improve its solubility, and enhance its bioavailability [123,130]. One of the most promising applications of

PEI is in cancer therapy [125]. PEI is effective in delivering anticancer drugs, such as DOX and paclitaxel, to cancer cells. PEI-based DDS can improve the solubility and stability of these drugs, as well as enhance their cellular uptake and retention in cancer cells, resulting in improved therapeutic efficacy [105,124,125].

However, despite its potential, there are also several challenges associated with the use of PEI for biomedical applications. One of the main challenges is its potential toxicity and immunogenicity due to the high positive charge. PEI has been shown to induce cytotoxicity and inflammation *in vitro* and *in vivo*, which can limit its use in some applications. Efforts have been made to modify the polymer structure or use alternative biodegradable polymers. To reduce its toxicity and improve its biocompatibility, such as the development of modified PEI-based DDS, for example, PEGylated PEI and acid-sensitive PEI. However, more research is needed to fully understand the safety and efficacy of PEI-based materials and to address the potential challenges associated with their use in biomedical applications [125].

PEI has emerged as a polyvalent polymer with considerable recognition, in the field of DDS. Its distinctive attributes render it an exceptional contender for augmenting the efficiency and efficacy of drug delivery platforms [105,124,125]. Furthermore, PEI's remarkable transfection efficiency renders it highly appealing for biomedical applications [124]. Moreover, PEI can be tailored through modifications to enhance its biocompatibility and targeting capabilities, thereby expanding its applicability in DDS. Its capacity to form stable complexes with diverse drugs enables controlled release and targeted delivery to specific tissues or cells [125]. PEI-based DDS can overcome barriers such as poor solubility and bioavailability, thereby enhancing the therapeutic efficacy of encapsulated drugs [123].

4.1.2. Polydopamine

Polydopamine (PDA) is a synthetic polymer that is inspired by the adhesive properties of natural dopamine [131]. It was first reported in 2007, and since then, it has been extensively studied for its unique properties and potential applications in a variety of fields, including biomedicine, materials science, and environmental remediation [131,132]. Researchers discovered that the polymerization of dopamine in an alkaline solution produced a black coating that exhibited strong adhesion to a variety of surfaces. The resulting polymer exhibits a high degree of surface reactivity and can be used to coat a variety of surfaces, including metals, plastics, and ceramics [131,133]. PDA displays several unique properties that make it attractive for diverse applications. One of its most remarkable features is its high surface reactivity (as depicted in Figure 12), which allows it to form strong bonds with a wide range of substrates [133]. Another important property of PDA is its ability to form conformal coatings on surfaces [133,134]. This means that the coating can adapt the shape of the surface to which it is applied, which can be useful in a variety of applications.

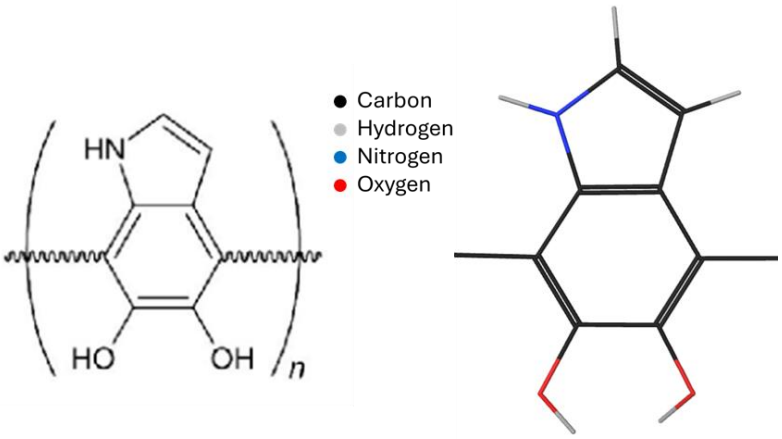

Figure 12. Chemical structures of branched PDA. Structure created in Molecular Operating Environment (MOE) 2015.10 software [20].

PDA finds application across multiple domains, with a particular interest in some specific areas, such as surface modification, drug delivery, and tissue engineering. This property has been explored for the development of functional materials with enhanced surface properties. For example, PDA coatings have been used to improve the adhesion of implants, create superhydrophobic surfaces, and enhance the optical properties and materials biocompatibility [45,135,136]. In drug delivery, the high surface reactivity of PDA allows for the attachment of a variety of molecules, including drugs and targeting moieties, which can improve efficacy and specificity. This approach has been used for the targeted delivery of drugs to cancer cells [131,137]. Additionally, in tissue engineering, the high surface reactivity of PDA allows for the attachment of biological molecules, such as growth factors and extracellular matrix proteins, to scaffolds. This approach has been used to enhance cell adhesion and proliferation, leading to improved tissue regeneration [131,138].

Despite its potential, there are some limitations associated with the use of PDA in biomedical applications, including potential cytotoxicity issues [131]. Some studies have demonstrated that PDA can induce cell death and inflammation *in vitro* and *in vivo*. However, the exact mechanism of toxicity remains unclear [139]. Further research is needed to fully understand the safety and efficacy of PDA-based materials and to address the potential challenges associated with their use in biomedical applications.

PDA has emerged as a promising material in the area of DDS, offering unique advantages and applications. The inherent adhesive properties of PDA enable strong interactions with a wide range of substrates. This property can be exploited to coat drug-loaded carriers, thereby enhancing their stability, biocompatibility, and targeting capabilities [131,137]. Furthermore, PDA exhibits pH-responsive behavior, allowing a controlled drug release in response to changes in the local microenvironment. This property enables precise spatiotemporal control over drug delivery, thereby minimizing off-target effects and optimizing therapeutic outcomes [137]. In addition to its

role in drug encapsulation and release, PDA can also serve as a versatile platform for surface functionalization. The introduction of functional groups onto PDA-coated carriers allows for the facilitation of specific interactions with target cells or tissues, thus enabling targeted drug delivery and enhanced therapeutic efficacy [137].

Overall, the use of PDA holds considerable potential for improving the efficacy of DDS. The adhesive properties, pH responsiveness, and surface functionalization capabilities make it a valuable means for enhancing the efficiency and specificity of DDS.

4.2. Clay-based drug delivery systems

Many NPs, nanodisks, or nanotubes have been identified as having potential therapeutic applications in cancer. DDS have been successfully modified using clays and clay minerals [140]. Nano-clays have attracted considerable interest due to their high specific surface area, biocompatibility, biodegradability, enhanced cellular uptake behaviors, controlled drug release capacity, and interlayer spacing, which can be employed for drug encapsulation with a high retention capacity [89,141,142]. At present, there is a particular focus on Laponite® (LAP), a type of synthetic silicate nanoparticle, which has been used as a drug carrier [143,144].

4.2.1. Laponite

The first report of LAP was developed by Dr. Barbara S. Neumann in the United Kingdom during the 1960s. It was initially employed as a rheological additive in drilling fluids for the oil and gas industry [145]. Since then, it has been used in a variety of applications, such as a thickener in personal care products and as a dispersant in paint and ink formulations [135]. In recent years, there has been a marked increase in interest in the use of LAP.

LAP is a type of synthetic clay composed of magnesium and aluminum silicate disks bonded together by sodium ions (25 nm in diameter and 0.92 nm in thickness) [146]. It has unique properties, including a high surface area (up to 700 square meters per gram) and a high degree of aqueous swelling [135,136]. The surface of the disks exhibits a negative charge, while the edges of the disks may acquire a positive charge, depending on the solution's pH [147].

Another property of LAP is its ability to form stable water suspensions. This property is attributed to the high surface area and the presence of negative charges on the surface of clay particles, which repel each other and prevent aggregation. LAP can also be functionalized with different molecules, such as polymers or drugs, to create nanocomposites that have unique properties and can be used for a variety of applications [135,148].

According to Y. Li *et al*., (2011) [146], LAP can degrade when exposed to acidic environments into nontoxic products like Na^+, $Si(OH)_4$, Mg^{2+}, and Li^+ [146,149]. Consequently, a

series of drugs (including DOX), biological molecules, and fluorescent dye molecules, such as amoxicillin [150], glutathione [151], and Nile-red [152], have been incorporated into LAP nanohybrids through intercalation, as depicted in Figure 13.

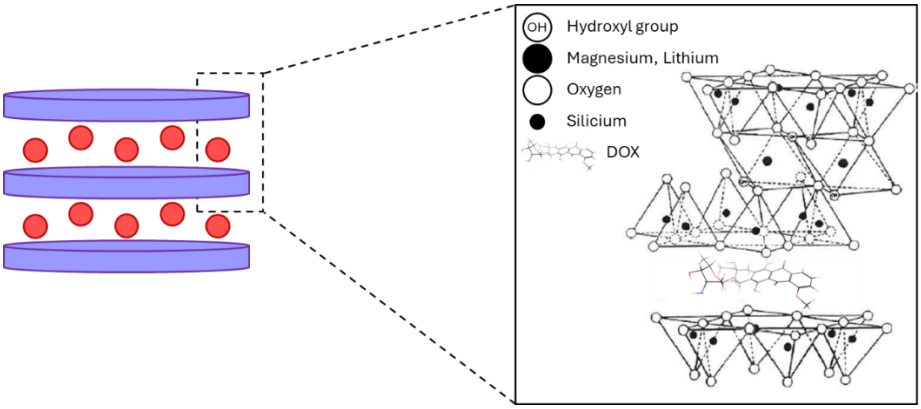

Figure 13. Schematic Illustration of the intercalation of DOX into LAP. Created in Biorender (adapted from Teyssier *et al.,* 2005 [153]).

LAP has an extremely high surface area due to its layered structure. This makes it useful for a variety of applications where surface area is important, such as in adsorption or catalysis [135,148]. Its electrokinetic properties, allow it to be charged by the addition of ions or by changes in pH. This makes it useful in applications such as drug delivery and as a stabilizer in emulsions [147].

Within the drug delivery field, LAP has attracted significant attention to be used as a carrier, due to its electrokinetic properties and high surface area, which facilitate the adsorption and encapsulation of drugs or therapeutic molecules. This adsorption capability allows for the controlled release of the encapsulated drug over time, leading to improved therapeutic efficacy and reduced side effects [135,148]. Moreover, LAP can also be functionalized or modified to further tailor their properties for specific drug delivery applications. It can be functionalized with targeting moieties, such as antibodies or peptides, to selectively bind to specific cells or tissues and improve drug efficacy by allowing for sustained release [148]. For example, an investigation led by Wu *et al*., 2020, [154] reported a LAP-based nanoplatform covalently modified with FA for tumor-targeted delivery.

4.3. DOX-based nanotherapeutics currently in the clinic

DOX is a potent chemotherapeutic agent used in the treatment of various cancer types, so, several DOX-based nanotherapeutics are currently undergoing clinical trials or are already in use.

Prior commercialization, drugs undergo a rigorous selection process starting with preclinical studies. These studies assess pharmacodynamics and pharmacokinetic, determining the drug's pharmacokinetic/pharmacodynamic profile and establishing safe dosages for initial human trials. The progression of Human trials is contingent upon the specific protocols that have been established for each phase. These protocols delineate the criteria for participants, the study duration, the dosage, and the methodology for data collection. After market availability, the drug's performance is monitored during active medical use via post-market surveillance [40].

The first type of DOX-based nanotherapeutics authorized for medical applications has been Liposomes-based. Diverse commercial versions of this system are currently available, including Doxil® and Myocet®, which differ in composition (Table 1).

Table 1: Approved liposome nanoformulations and their composition containing DOX.

Product name	Composition	Approved treatment	Refs
Doxil®	HSPC, cholesterol, and DSPE-PEG2000	Kaposi's sarcoma, multiple myeloma, breast, and ovarian cancer	Gabizon *et al*. [51] Franco Muggia *et al*. [155] Symon *et al*. [156] Orlowski *et al*. [157]
Myocet®	EPC and cholesterol	Metastatic breast cancer	Bulbake *et al*. [158] Chan *et al*. [159] Leonard *et al*. [160]

4.3.1. Doxil®

The first nanosystem to achieve clinical approval by the Food and Drug Administration was Doxil® in 1995 [161]. An enhanced liposomal formulation carrying DOX has presented a better pharmacokinetic profile and less cardiotoxicity commonly associated with free DOX administration [40,162]. Doxil®, which is marketed as Caelyx® in Europe, was a pioneer in the field of drug carriers on the US market [161]. Doxil® was initially accepted for the management of Kaposi's sarcoma associated with AIDS, and later, in 1998, for the treatment of recurrent ovarian cancer [155], in 2003 for metastatic breast cancer [156], and in 2007 for multiple myeloma [40,157].

This system has a mean diameter of between 80 and 90 nm and is based on a PEGylated liposome that contains DOX in the interior cavity [51]. The hydrogenated soy phosphatidylcholine (HSPC), cholesterol, and 1,2-distearoyl-sn-glycero-3-phosphoethanolamine-N-(methoxy-PEG) (DSPE-PEG) [conjugation of distearoyl-phosphatidylethanolamine to PEG] are the three primary lipid components that make up a Doxil® liposome (Figure 14). Once these lipids are consumed and found on cell membranes, they are regarded as harmless [40,51].

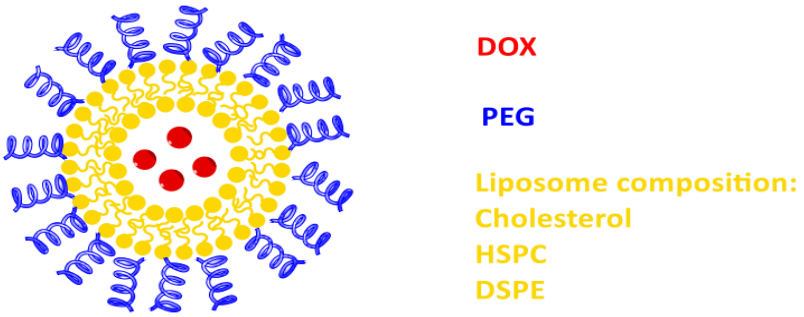

Figure 14. Illustration of a PEGylated Doxil® liposome [40].

4.3.2. Myocet

Another example of a liposomal DOX formulation is Myocet®, a non-PEGylated liposomal DOX, approved five years after Doxil® in Europe and Canada [163]. This formulation was approved as a first-line treatment for metastatic breast cancer in combination with cyclophosphamide [159,160].

Similar to Doxil®, Myocet® utilizes liposomes to encapsulate DOX, improving its pharmacokinetic profile and reducing cardiotoxicity. These liposomal formulations offer improved patient outcomes and quality of life (fewer symptoms, such as nausea, vomiting, and stomatitis) compared to conventional DOX therapy [159,164,165].

Myocet® liposome presents a diameter size of around 150-250 nm and is composed of cholesterol, egg phosphatidylcholine (Egg PC), and, in the interior, a DOX citrate complex (Figure 15) [40,158].

Figure 15. Illustration of the Myocet® liposome [40].

Chapter 2 - Thesis objectives

This thesis aims to develop and compare complexes based on PDA and PEI for the targeted delivery of DOX. To this end, a series of complexes were prepared using LAP, PEG, FA, and Fluorescein Isothiocyanate (FI) to create complexes that would meet the desired conditions.

LAP has been selected for this study due to its low toxicity and its ability to interact strongly with numerous chemical compounds. This makes it an attractive option for protecting drugs from degradation in the physiological environment by intercalating them into crystal stacks, improving the drug efficacy by allowing a sustained release [148,166]. PEG has been shown to increase the half-life of NPs by encapsulating them within the structure, thereby preventing their detection and clearance by the immune system. Consequently, PEG prolongs their circulation time [167]. FA is a frequently utilized ligand in cancer therapy and diagnostics due to its efficacy in active targeting, and usually associated with an overexpression in various cancer types [104,105]). Lastly, FI, a fluorescent compound, was conjugated so that it could be possible to track the complexes inside the cell through confocal microscopy.

This thesis presents a series of studies performed with the following primary goals:

a. Synthesis of LAP-coated PDA to identify optimal conditions to generate small, highly negatively charged complexes by varying LAP concentration and using three different approaches (continuous magnetic stirring, ultrasonic bath, and microsonication) and the effect of the addition of mannitol as a stabilizer agent.
b. Loading DOX into LAP nanodisks, followed by calculating the encapsulation efficiency (EE) and Loading capacity (LC) of DOX in the nanodisks.
c. Synthesis of LAP/DOX/PEI(FI-PEG-FA) and LAP/DOX/PDA(FI-PEG-FA) complexes.
d. Characterization of the synthesized compounds using suitable physicochemical techniques, namely by Nuclear Magnetic Resonance (^{1}H NMR), Dynamic Light Scattering (DLS), Electrophoretic Light Scattering (ELS), and Ultraviolet/Visible spectroscopy (UV/Vis).
e. Comparative study of the cumulative release (Cr) of DOX from the synthesized complexes over time.
f. Evaluation of the *in vitro* cytotoxicity of the complexes using a metabolic activity assay (resazurin reduction assay) to correlate with cell viability.

Chapter 3 - Materials and Methods

1. Materials

Dual functional PEG with one end of a carboxyl group and the other end of an amine group (NH_2–PEG–COOH, MW = 2 kDa) was from Seebio Biotech. 1-ethyl-3-(3-dimethylaminopropy) carbodiimide hydrochloride (EDC) was obtained from TCI chemicals. Dopamine hydrochloride was purchased from Alfa Aesar. N-hydroxysuccinimide (NHS), branched PEI (MW = 25 kDa), FA, and FI were supplied by Sigma-Aldrich. Doxorubicin hydrochloride was from Biosynth. Laponite® XLG was kindly donated by BYK, Germany. Dimethyl sulfoxide (DMSO) was from Fisher Chemical. Regenerated cellulose dialysis membranes with molecular weight cut-off (MWCO) of 1 or 25 kDa were acquired from Spectrum™ (Spectra/Por™). MCF-7 cells were supplied from the CQM cryopreservation cell bank. Roswell Park Memorial Institute (RPMI), fetal bovine serum (FBS), and antibiotic-antimycotic (AA) were from Gibco™ (Thermo Fisher Scientific). All chemicals and materials were used as received. Water used in all experiments was purified using a Milli-Q Direct 3 UV Water Purification System with a resistivity higher than 18.2 MΩ·cm.

2. Coating of LAP

LAP-coated PDA complexes were obtained using an adapted protocol from Zheng *et. al* (2014) [168]. LAP was dispersed in distilled water and placed in an ultrasonic bath at room temperature (22°C) for 30 minutes. Two different concentrations of LAP were tested (1 and 3 mg/mL). A 2 mg/mL solution of DA was prepared in 10 mM Tris-HCl buffer at pH 8.5.

The LAP-coated PDA complexes were prepared by mixing LAP:DA solutions in a 1:2 (V/V) ratio in three different conditions. One sample experienced continuous magnetic stirring (500 rpm), another was treated in an ultrasonic bath, and the last one was subjected to a microsonicator (Bioblock Scientific). Each treatment lasted for 1 hour at 22°C. Subsequently, the reaction mixtures were left at 22°C with constant magnetic stirring (500 rpm) for an additional 2 hours. After that, the reaction mixture was precipitated by centrifugation at a speed of 35,000xg for 10 minutes, three times, each one after washing with 3 mL of distilled water. The precipitate, corresponding to the LAP/PDA complexes, was lyophilized for 3 days and kept at -20ºC for further studies. The study was performed in duplicate, in one of which the complexes were lyophilized after the addition of 5% mannitol.

3. Loading of DOX into LAP Nanodisks

To obtain the DOX-loaded LAP complexes, as illustrated in Figure 16, an adapted protocol based on the one described by Wang *et. al* (2013) was used [169].

LAP was dispersed in distilled water and kept in an ultrasonic bath at 22°C for 30 minutes. A 3 mg/mL LAP solution and a 1 mg/mL DOX aqueous solution was previously prepared. The DOX-loaded LAP complexes were prepared in a 1:1 (V/V) ratio. The reaction mixture was kept at 22°C, protected from light, under constant magnetic stirring (500 rpm) for 24 hours. After that, the reaction mixture was precipitated by centrifugation at a speed of 35,000xg for 10 minutes, three times, each one after washing with 3 mL of distilled water. The precipitate, corresponding to the LAP/DOX complexes, was lyophilized for 3 days and kept at -20ºC for further studies. The free DOX present in the supernatant was collected after each centrifugation step and kept at 4ºC for later measurement in UV-Vis for further calculation of the EE% and LC%.

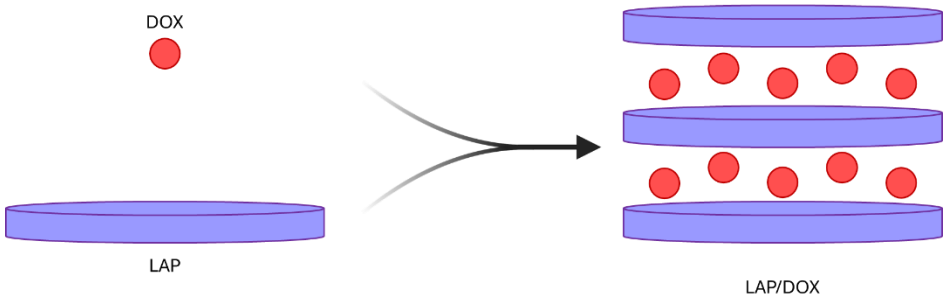

Figure 16. Schematic representation of DOX-loaded LAP complexes. Created in Biorender.

DOX quantification in the supernatants was determined at 480 nm through a standard calibration curve to determine the EE of DOX and subsequently the LC. Equations 1 and 2 represents the DOX EE and LC of the complexes, respectively, where m0 is the initial mass of DOX, mS is the mass of DOX in the supernatant, and mN is the final mass of the complexes.

$$Equation\ 1\ \rightarrow\ EE\ (\%) = \frac{m0 - mS}{m0} \times 100$$

$$Equation\ 2\ \rightarrow LC\ (\%) = \frac{m0 - mS}{mN} \times 100$$

4. Synthesis

For all the following syntheses, an adapted protocol based on the methodology developed by Chen *et al.*,2016, [170] was employed. Each synthesis was carefully adjusted to fit the specific requirements of this study.

4.1. Synthesis of FA-PEG-COOH

For the synthesis of FA-PEG-COOH (Figure 17), FA (8.8 mg) dissolved in DMSO (5 mL) was activated by EDC/NHS (1 mol. equiv. of FA, 3.10 mg EDC and 2.29 mg NHS) under vigorous magnetic stirring for 3 hours (500 rpm). Then, the activated FA was added dropwise to a DMSO solution of NH2-PEG-COOH (0.5 mol. equiv. of FA, 19.94 mg, 10 mL) with magnetic stirring for 3 days (1000 rpm). The reaction mixture was extensively dialyzed against phosphate-buffered saline (PBS, 3 times, 2 L) and water (6 times, 2 L) for 3 days using a dialysis membrane (MWCO = 1 kDa) to remove the excess reactants and by-products, followed by lyophilization to obtain the product of FA-PEG-COOH.

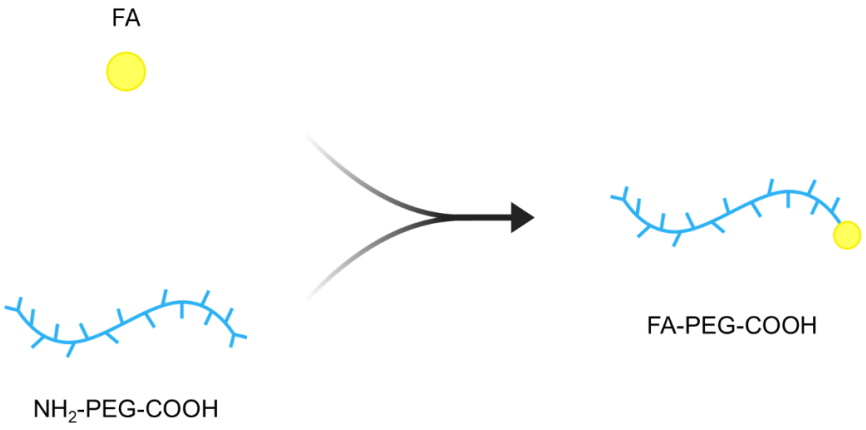

Figure 17. Schematic representation of the synthesis of FA-PEG-COOH. Created in Biorender.

4.2. Synthesis of LAP/DOX/PEI(FI-PEG-FA)

To produce the LAP/DOX/PEI(FI-PEG-FA) complex, it was necessary to synthesize first the FA-PEG-PEI-FI before proceeding to create the desired complex (Figure 18).

The FA-PEG-PEI-FI compound was prepared by dissolving the FA-PEG-COOH in DMSO (10 mol. equiv. of PEI, 19.84 mg, 5 mL) and activated by EDC/NHS (5 mol. equiv. of FA-PEG-COOH, 12.60 mg EDC and 9.35 mg NHS) under vigorous magnetic stirring for 3 hours at 22°C (500 rpm). The activated FA-PEG-COOH was added dropwise into a DMSO solution of PEI (25.00

mg, 10 mL) under magnetic stirring for 3 days (1000 rpm), followed by the addition of FI (10 mol. equiv. of PEI, 3.89 mg, 5 mL in DMSO) into the above mixture solution. After 24 hours, the mixture was extensively dialyzed against PBS (3 times, 2 L) and water (6 times, 2 L) for 3 days using a dialysis membrane (MWCO = 25 kDa) to remove the excess reactants and by-products, followed by lyophilization to get the product of FA-PEG-PEI-FI. The intermediate products of FA-PEG-PEI were also collected, purified, and characterized.

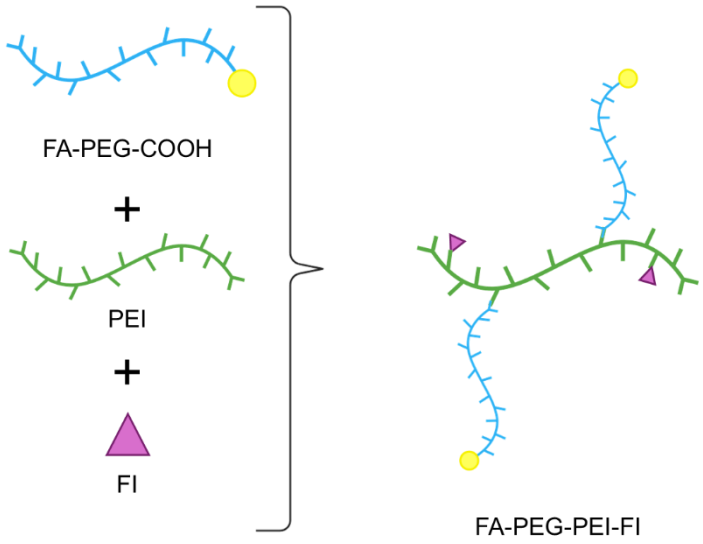

Figure 18. Schematic representation of the synthesis of FA-PEG-PEI-FI. Created in Biorender.

Considering the previous trials, the best conditions for the coating were the LAP:DA 1:2 (V/V) ratio, with a DA concentration of 2 mg/mL and an LAP concentration of 3 mg/mL. Therefore, for the LAP/DOX coating by FA-PEG-PEI-FI (illustrated in Figure 19), the used conditions were described above. A solution of 2 mg/mL FA-PEG-PEI-FI was prepared in distilled water and the LAP/DOX complexes were dispersed in distilled water at a concentration of 3 mg/mL. The FA-PEG-PEI-FI solution was then added at a ratio of 1:2 (V/V). The reaction mixture was kept in an ultrasonic bath for 1 hour at 22°C. Subsequently, the reaction mixture was left at 22°C with constant magnetic stirring (500 rpm) for an additional 2 hours. After this time, the reaction mixture was precipitated by centrifugation at a speed of 35,000xg for 10 minutes, three times, each one after washing with 3 mL of distilled water. The precipitate, corresponding to the LAP/DOX/PEI(FI-PEG-FA) complexes, was lyophilized for 3 days and kept at -20ºC for further studies.

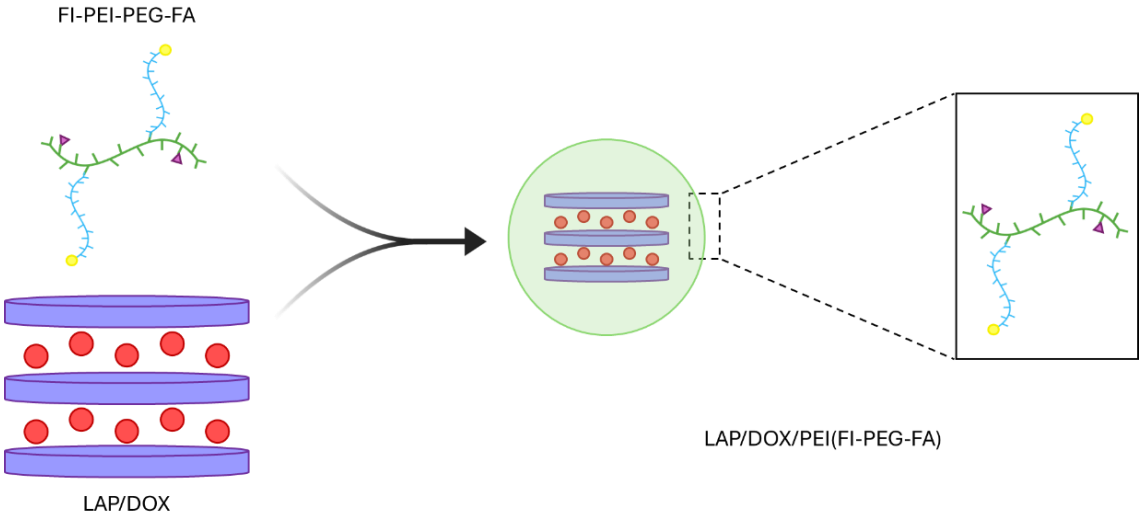

Figure 19. Schematic representation of the synthesis of LAP/DOX/PEI(FI-PEG-FA). Created in Biorender.

4.3. Synthesis of LAP/DOX/PDA(FI-PEG-FA)

To synthesize the LAP/DOX/PDA(FI-PEG-FA) complex, we must first synthesize the LAP/DOX/PDA before proceeding to create the intended formulation.

Considering the previous experiments, the optimal conditions for the coating were the LAP:DA 1:2 (V/V) ratio, with a DA concentration of 2 mg/mL and an LAP concentration of 3 mg/mL. So, for the coating of the LAP/DOX complexes by PDA (as shown in Figure 20), the conditions described above were used. A solution of 2 mg/mL DA was prepared in 10 mM Tris-HCl buffer at pH 8.5. The LAP/DOX complexes were dispersed in distilled water at a concentration of 3 mg/mL. The DA solution was then added at a 1:2 (V/V) ratio. The reaction mixture was kept in an ultrasonic bath for 1 hour at 22°C. Subsequently, the reaction mixture was left at 22°C with constant magnetic stirring (500 rpm) for an additional 2 hours. After this time, the reaction mixture was precipitated by centrifugation at a speed of 35,000xg for 10 minutes, three times, each one after washing with 3 mL of distilled water. The precipitate, corresponding to the LAP/DOX/PDA complexes, was lyophilized for 3 days, after the addition of 5% mannitol, and kept at -20ºC for further studies.

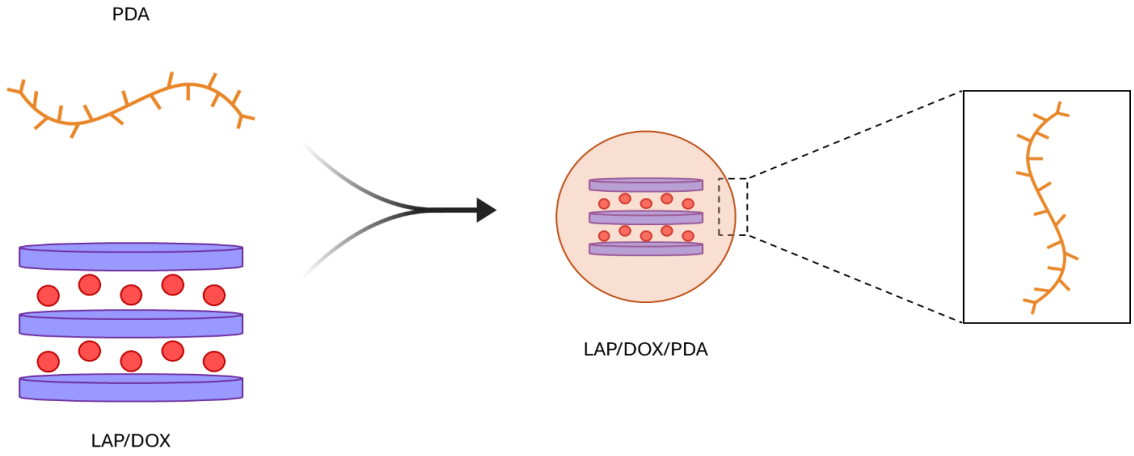

Figure 20. Schematic representation of the synthesis of LAP/DOX/PDA. Created in Biorender.

Following the LAP/DOX/PDA preparation, the synthesis proceeded for the intended complex, as illustrated in Figure 21. FA-PEG-COOH dissolved in DMSO (1 mol. equiv. of PDA, 41.00 mg, 10 mL) was activated by EDC/NHS (5 mol. equiv. of FA-PEG-COOH, 26.04 mg EDC and 19.33 mg NHS) under vigorous magnetic stirring for 3 hours at 22°C (500 rpm). The activated FA-PEG-COOH was added dropwise into a DMSO solution of LAP/DOX/PDA (10.00 mg, 5 mL) under stirring for 3 days (1000 rpm), followed by addition of FI (2 mol. equiv. of PDA, 16.22 mg, 5 mL in DMSO) into the above mixture solution. After 24 hours, the mixture was extensively dialyzed against PBS (3 times, 2 L) and water (6 times, 2 L) for 3 days using a dialysis membrane (MWCO = 1 kDa) to remove the excess reactants and by-products, followed by lyophilization to get the product of LAP/DOX/PDA(FI-PEG-FA). The intermediate products were also collected, purified, and characterized.

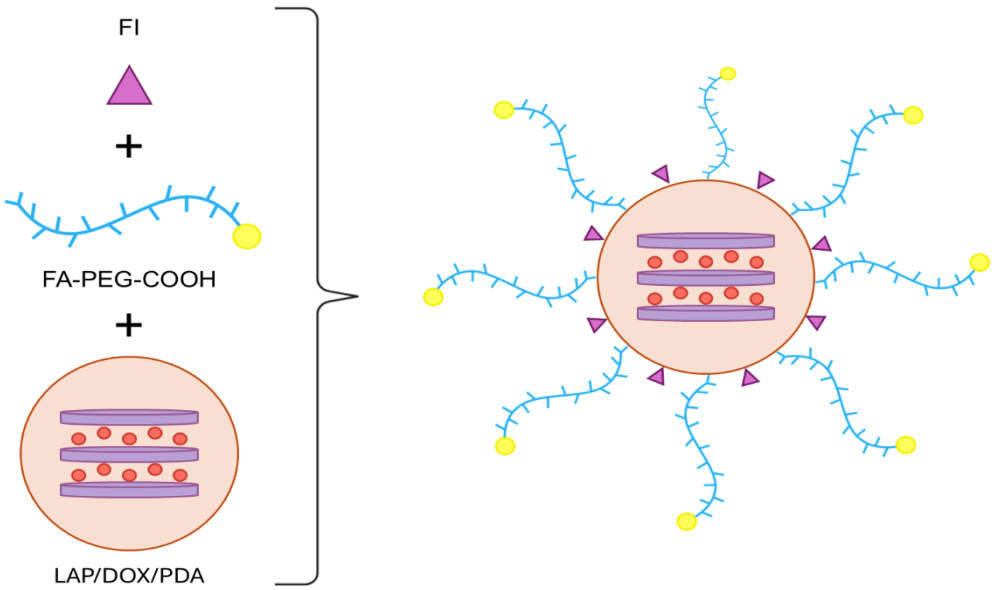

Figure 21. Schematic representation of the synthesis of LAP/DOX/PDA(FI-PEG-FA). Created in Biorender.

5. Drug release

Drug release studies were performed considering the methodology described by Bi, D. *et. al* (2018) [171]. After performing a series of trials for the determination and quantification of DOX, it was selected a 2.5 µg/mL fixed concentration of DOX (data not shown). In the case of the complexes, the LC was used to ensure that the mass of DOX was identical in all samples. Briefly, 300 µL of each solution was transferred to dialysis cassettes (MWCO = 2 kDa, Slide-A-Lyzer MINI Thermo Fisher Scientific). The cassettes were placed in vials containing 10 mL of 1x PBS pH 7.4 and incubated at 37°C. At different time intervals, 100 µL aliquots of PBS were withdrawn for fluorescence analysis using a microplate reader (Perkin Elmer Victor 3 Multilabel Reader). The withdrawn 100 µL was immediately replenished with fresh PBS (pH 7.4), and the vials were incubated again at 37°C. PBS was used as a control and the amount of DOX was determined using a standard curve.

The Cr of DOX over time was calculated according to Equation 3, where Vl is the volume of the release medium, Cn is the average concentration of DOX at a certain time point (four replicates were performed for each condition, n=4), and m is the initial mass of DOX within the dialysis system; Vt corresponds to the volume of the removed aliquots, and Ci is the corresponding concentrations of DOX in these aliquots.

$$Equation\ 3\ \rightarrow Cr\ (\%) = \frac{Vl.Cn\ + Vt.\sum_{1}^{n-1} Ci}{m} \times 100$$

6. Cytotoxicity evaluation

For the cytotoxicity study, it was used a modified protocol derived from the one described by Chen *et al.*, 2016, [170], with MCF-7 cells (breast cancer cell line).

For the MCF-7 cell expansion, the passage P25 was utilized with a cell seeding density of 3 x 10^5 cells per 100 mm culture dish. First, cryopreserved MCF-7 cells were thawed and centrifuged at 300xg for 8 minutes at 20 °C in a superspeed refrigerated centrifuge (Sigma, Model 3-30K). The pelleted cells were resuspended in 1 mL of complete cell culture medium (RPMI) containing 10% (V/V) FBS and 1% (V/V) AA and cell viability was evaluated through trypan blue dye exclusion. The cells were cultured in 100 mm culture dishes with 10 mL of complete RPMI supplemented with 1% (V/V) 100x NEAA (Gibco), 1 mM Sodium Pyruvate (Sigma-Aldrich), and 3.3 µg/mL human insulin (Biomedicals). The cells were maintained in an incubator (Nuaire) at 37 °C, in a humidified atmosphere with 5 % CO_2, with the medium being changed two times a week. Before reaching maximum confluency, the cells were trypsinized. Briefly, the culture medium was removed, and the cells were washed with PBS. Subsequently, 1 mL of 0.25 % trypsin-EDTA

solution (Thermo Fisher Scientific) was added to each culture dish, followed by an incubation at 37°C for 5 minutes. After cell detachment, 2 mL of complete medium was added to stop the trypsin action. Viability and cell density were determined using a 0.2% (W/V) trypan blue (Sigma-Aldrich) solution and a hemocytometer (Neubauer chamber).

For the cell culture experiments, the cells were seeded in 48-well plates for 24 hours at a density of $5x10^4$ cells per well. The following day, solutions at 0.1, 0.5, 1.0, 1.5, and 2.0 µM (with equivalent DOX concentrations) were prepared in filtered distilled water and added to the cell culture. After 48 hours of compound exposure, the resazurin reduction assay was performed to assess cell viability. The cell culture medium was replaced with fresh medium containing 10% (V/V) of a resazurin solution (0.1% (W/V) in PBS) and incubated at 37°C for 3 hours. Subsequently, 100 µL aliquots of the medium were transferred to an opaque 96-well plate, and the fluorescence of resorufin was measured in a microplate reader at λex = 530 nm and λem = 590 nm (Perkin Elmer Victor 3 Multilabel Reader). Cell viability was indirectly quantified by measuring the metabolic activity of the cultured cells. The study was performed in duplicate, and all samples were carried out in quadruplicate. The results are expressed as a percentage of cell viability in relation to the control (cells not exposed to the complexes).

Cell imaging throughout this work was acquired with a widefield and confocal microscopy platform (Mica, Leica Microsystems). The cells were fixed with 200 µL formaldehyde (3.7%) for 25 min at 22°C, and counterstained with 4',6-diamidino-2-phenylindole (DAPI, 2.5 µg/mL, in 200 µL PBS) for 20 min at 22°C.

7. Characterization techniques

^{1}H NMR spectra were recorded on a Bruker Avance II+ UltraShield™ 400 Plus Ultra Long Hold NMR spectrometer. Samples were dissolved into D_2O before NMR measurements. UV-Vis spectroscopy was carried out using a Genesys 180 ultraviolet-visible spectrophotometer from Thermo Fisher Scientific. Samples were dissolved in water. DLS and ELS were conducted at 25ºC with a Zetasizer Nano ZS (Malvern Panalytical), with a measurement angle of 173°. All measurements were performed in triplicate with 11 runs each, using filtered distilled water as a solvent, except for DA, for which a filtered 10 mM pH 8.5 tris-HCl buffer was used.

Chapter 4 - Results and discussion

1. Coating of LAP

Considering that the main purpose of this thesis was the preparation of DOX-loaded LAP complexes coated with different polymers, such as PEI and PDA, for a targeted and sustained drug delivery, the first step in this phase of the study was to obtain complexes that are both small and possess a maximized negative charge. The process started with the dispersion of LAP in distilled water, followed by an ultrasonic bath at room temperature for 30 minutes. The concentrations of LAP tested were 1 and 3 mg/mL. Simultaneously, a DA solution of 2 mg/mL was prepared with a 10 mM Tris-HCl buffer pH 8.5, as the polymerization of DA is favored in an alkaline environment [172].

The polymerization process of DA can be monitored by observing changes in the color of the solution: initially, the solution is transparent (Figure 22.A), and gradually changes to black (Figure 22.B). The black color of the solution is due to the oxidation of o-quinone groups [173].

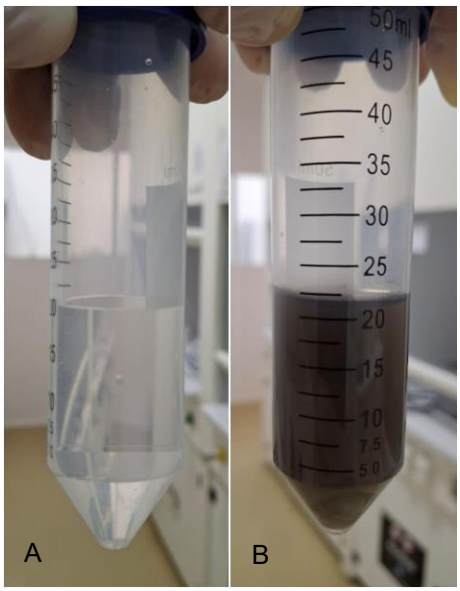

Figure 22. Color change in DA solution, before (A) and after (B) stirring for 3 hours.

The LAP:DA solutions were formulated in a 1:2 (V/V) ratio under three distinct conditions. The first experienced continuous magnetic stirring at 500 rpm, the second an ultrasonic bath, and the third a microsonication. Each treatment spanned 1 hour at room temperature. Following this, the reaction mixtures were left at room temperature with constant magnetic stirring at 500 rpm for an additional 2 hours. Subsequently, the reaction mixtures were precipitated by centrifugation at a speed of 35,000xg for 10 minutes, three times, each one after washing with 3 mL of distilled water. The resulting precipitates, corresponding to the LAP/PDA complexes, were lyophilized for

3 days and stored at -20ºC for further studies. This study was performed in duplicate. In one instance, the complexes were lyophilized after adding a 5% mannitol solution to assess whether its presence would result in smaller complex sizes, as demonstrated by Guimarães (2019), for freeze-dried liposomes in drug encapsulation. In this study, the size of liposomes without saccharides in their composition increased from 113.8 ± 0.99 nm to 859.0 ± 56.14 nm after undergoing the freeze-drying process. However, with the addition of Mannitol, the size of the liposomes post-freeze-drying was reduced to approximately 500 nm [174].

Using the ELS/DLS technique, the zeta potential and hydrodynamic size of the complexes were determined, as shown in Tables 2 and 3, respectively (in supplementary information Figures S1 and S2 show the Volume mean (%) particle size distribution of complexes, with and without Mannitol, respectively).

Table 2: Zeta potential of LAP/PDA complexes.

	Sample Condition	**Zeta Potential (mV)**	
		Without Mannitol	With Mannitol
LAP 3 mg/mL	Continuous magnetic stirring	-54.40 ± 3.73	0.01 ± 0.86
	Ultrasonic bath	-56.30 ± 1.66	-29.20 ± 1.19
	Microsonication	-63.60 ± 4.38	-26.60 ± 2.03
LAP 1 mg/mL	Continuous magnetic stirring	-53.20 ± 1.40	-25.25 ± 0.35
	Ultrasonic bath	-46.35 ± 0.05	-25.20 ± 0.55
	Microsonication	-56.30 ± 2.30	-24.60 ± 1.02

Note: All data represent the mean ± standard deviation (n = 4).

Table 3: Hydrodynamic diameter and polydispersity index (PdI) of LAP/PDA complexes.

	Sample Condition	**Without Mannitol**		**With Mannitol**	
		Volume mean (nm)	PdI	Volume mean (nm)	PdI
LAP 3 mg/mL	Continuous magnetic stirring	1974.50 ± 669.95	0.43	251.85 ± 64.98	1.00
	Ultrasonic bath	1360.00 ± 197.21	0.48	165.15 ± 75.69	1.00
	Microsonication	1424.00 ± 190.96	0.40	204.45 ± 77.33	1.00
LAP 1 mg/mL	Continuous magnetic stirring	604.50 ± 171.57	1.00	320.35 ± 166.74	1.00
	Ultrasonic bath	429.35 ± 120.77	1.00	332.00 ± 56.27	0.94
	Microsonication	754.40 ± 171.57	0.80	408.75 ± 68.02	0.95

Note: All data represent the mean ± standard deviation (n = 4).

After the analysis of the acquired data and considering the aim to create small complexes with the highest negative charge possible, the most favorable condition for the study revealed to be LAP 3 mg/mL, DA 2 mg/mL (in a 1:2 ratio), using an ultrasonic bath with the addition of mannitol. These conditions returned complexes with sizes around 165.15 nm and a surface charge of -29.2 mV. Therefore, the study proceeded under these conditions.

2. Loading of DOX into LAP Nanodisks

To proceed with the DOX loading into the LAP nanodisks, a solution of LAP (3 mg/mL) was mixed with a DOX solution (1 mg/mL) in a 1:1 (V/V) ratio. The reaction mixture was kept at room temperature for 24 hours, protected from light, under constant magnetic stirring (500 rpm) to promote the encapsulation of DOX through the electrostatic interactions between the surfaces of the negatively charged LAP disks and the positively charged DOX [169]. The fact that DOX is encapsulated through a cation exchange mechanism, rather than covalent bonds, allows the interactions between the drug and the discs to be both strong enough to transport DOX, but also weak enough for it to be released easily and effectively at lower pH sites (pH<7.2) [169]. Figure 23 shows the appearance of the LAP/DOX complexes before (A) and after (B) centrifugation. It can be seen that the DOX has been loaded efficiently, as the supernatant is almost clear.

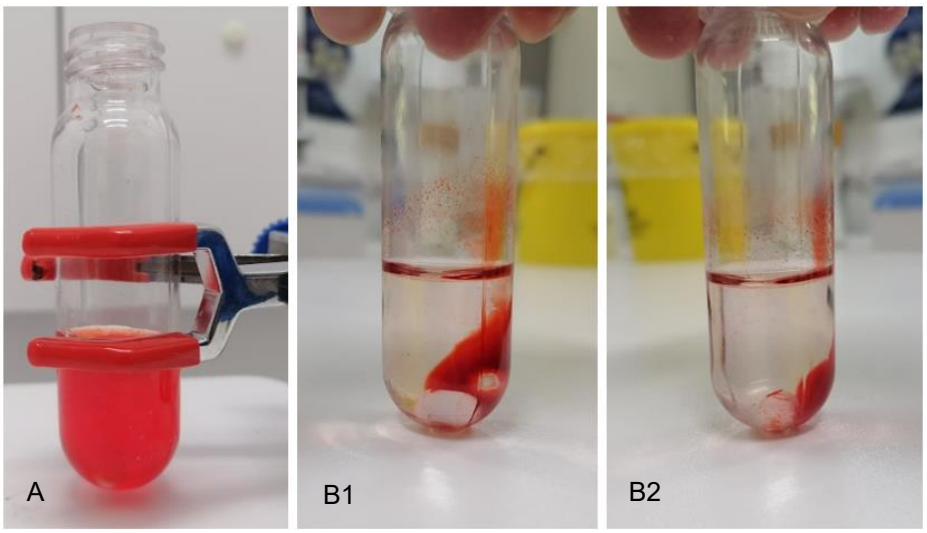

Figure 23. Appearance of the LAP/DOX complexes before (A) and after one centrifugation cycle B1 and B2 showing different viewpoints.

The EE and LC of DOX were determined by quantifying the drug remaining in the supernatant. To do this, a calibration curve was drawn (Figure S3 in the supplementary

information, r^2= 0.9915,) and the absorbance of the supernatant was measured at 480 nm, which corresponds to the maximum absorption wavelength of DOX [169]. From this, it was possible to calculate the EE (equation 1) and LC (equation 2): values of 99.68 ± 2,5×10^{-4} % and 28.53 ± 4,7×10^{-4} % were obtained, respectively (n=4). The value obtained for the EE is in line with the results obtained by Wang *et al.* (2013) [169].

3. Synthesis

To verify the successful synthesis of FA-PEG-COOH by ^{1}H NMR, the starting material (NH_2- PEG-COOH) was also characterized by the same technique to identify the signals that will arise from the FA in the conjugation.

A solution of NH_2-PEG-COOH in deuterium oxide (D_2O) was analyzed by ^{1}H NMR, which revealed the presence of the respective chemical groups. This data is illustrated in Figure 24. It was possible to see two signals, one at δ = 3.71 ppm and the second at δ = 4.79. The first one, identified with number 1, corresponds to the repeating CH_2−CH_2−O units and the other corresponds to the solvent (D_2O). The signals detected from de NH_2-PEG-COOH are in agreement with those found in the literature [175].

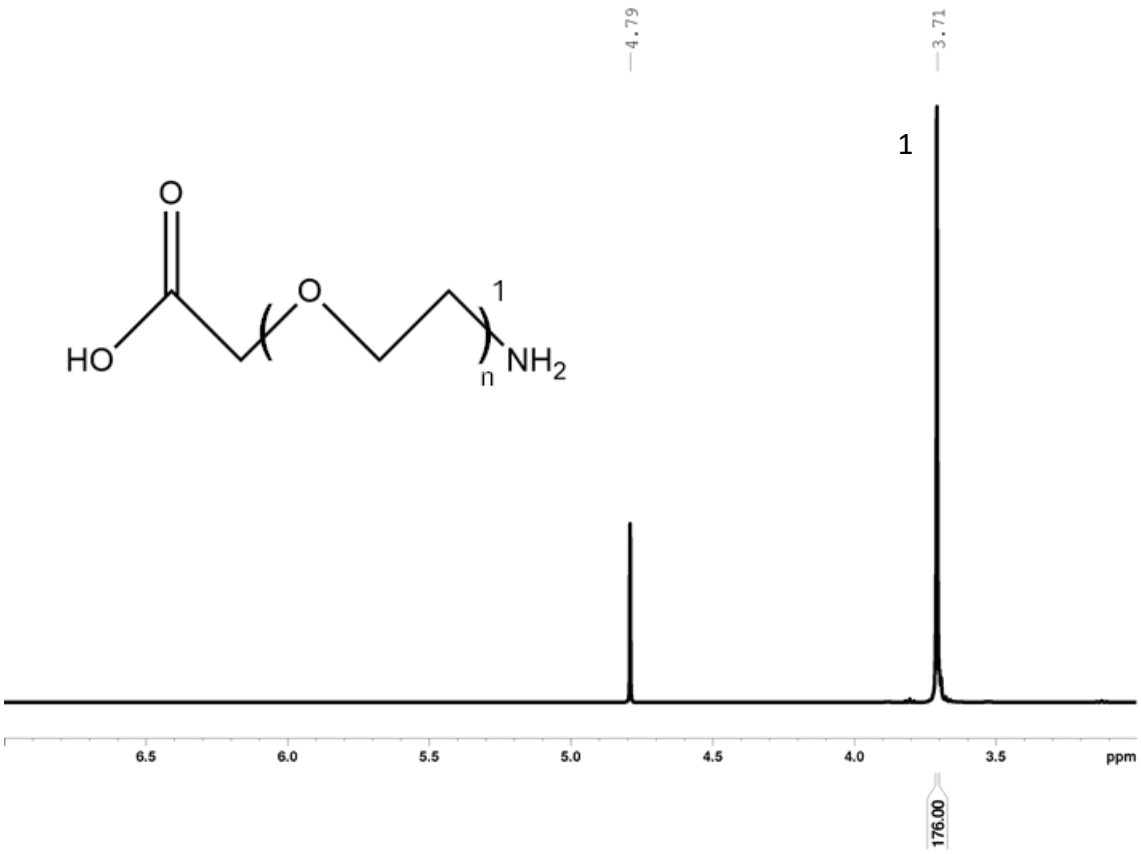

Figure 24. ^{1}H NMR spectrum for NH_2-PEG-COOH in D_2O.

After this analysis, we proceeded to characterize the synthesized FA-PEG-COOH through ^{1}H NMR spectroscopy, being dissolved in D_2O. Its molecular structure with identified chemical groups that produced signals in the NMR spectrum and the obtained spectrum are represented in Figure 25. Three signals corresponding to FA were identified in the spectrum at δ = 6.91, 7.68 and 8.77 ppm. The first signal corresponds to the protons of the two C*H*$_2$ groups from the aromatic ring, labeled as number 4 in the structure. The second, at δ = 7.68 ppm, corresponds to the other C*H*$_2$ groups from the same aromatic ring, identified as number 3 in the structure. Lastly, the signal at δ = 8.77 ppm, corresponds to the C*H* group labeled as number 2. The signals detected from the FA molecule agree with those found in the literature [176]. With this in mind, we have been able to obtain the FA-PEG-COOH.

The number of FA moieties conjugated onto each PEG chain can be estimated by comparing the difference among the ^{1}H NMR integration areas. The average number of FA moieties conjugated onto each PEG was estimated to be 0.11. Since the integration area of the signal at δ = 3.70 ppm corresponds to a PEG molecule and considering that for every 176 we have 0.11 in the area at δ = 8.77 ppm, and this signal is unique to the FA molecule, therefore, for every 1 PEG, we have 0.11 of FA.

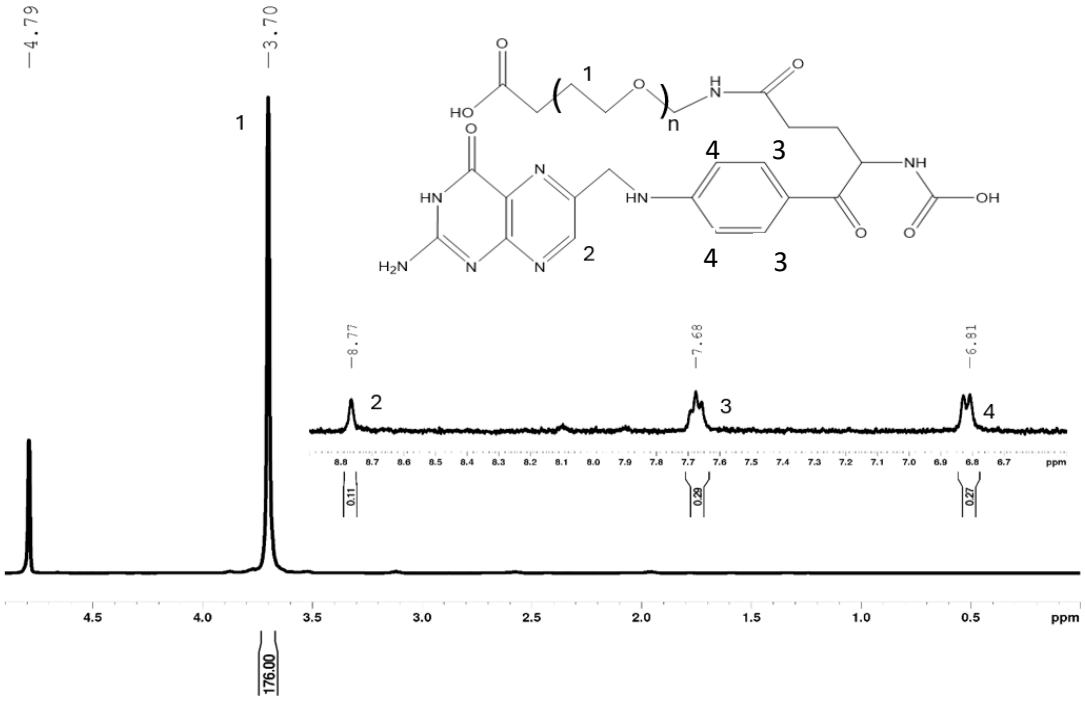

Figure 25. ^{1}H NMR spectrum for FA-PEG-COOH in D_2O.

To verify the formation of the FA-PEG-PEI by ^{1}H NMR, the signals from FA-PEG-PEI were compared to those from FA-PEG-COOH using the same technique to identify the signals that will arise from the PEI in the conjugation.

FA-PEG-PEI was also dissolved in D_2O and the chemical groups present in its structure produced the respective signals in the ^{1}H NMR spectrum that is present in Figure 26. It was possible to observe the signal at δ = 2.60-3.60 ppm, which corresponds to the repetitive C*H*$_2$-C*H*$_2$-NH units of the PEI structure identified as number 5. The signal detected from de FA-PEG-PEI agrees with those found in the literature [123]. Considering this, the synthesis to obtain the FA-PEG-PEI was successful.

To determine the number of PEG molecules conjugated to each PEI molecule, the integration area of the PEI signal was set to 1, so the PEG integration area was estimated at 1.40. This means that for each PEI molecule, there are 1.40 PEG molecules.

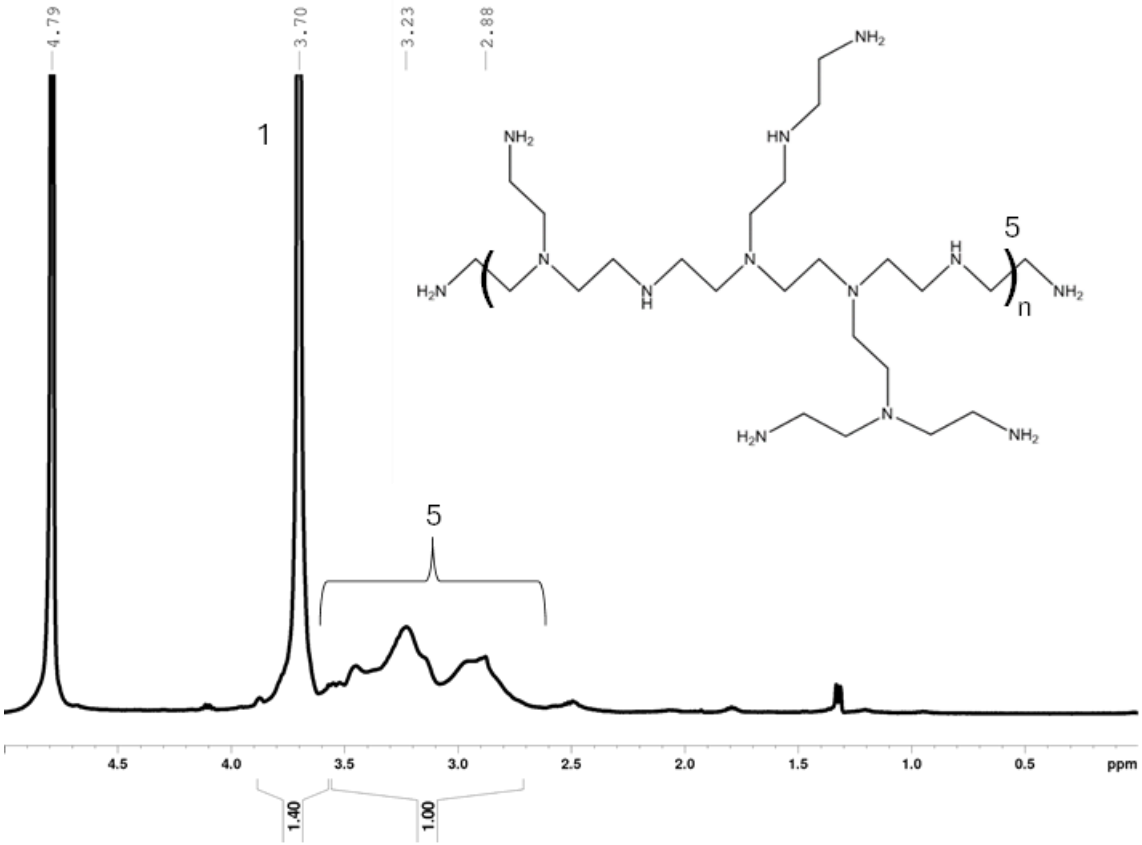

Figure 26. ^{1}H NMR spectrum for FA-PEG-PEI in D_2O.

To ensure the conjugation, UV-Vis spectroscopy was employed to verify the modification of FI onto the PEI surface, because no signals could be seen in the ^{1}H NMR spectrum. The resultant FA-PEG-PEI-FI complex exhibits a peak at 500 nm, as can be seen in Figure 27, indicating successful conjugation of FI onto the PEI surface, consistent with the literature [170].

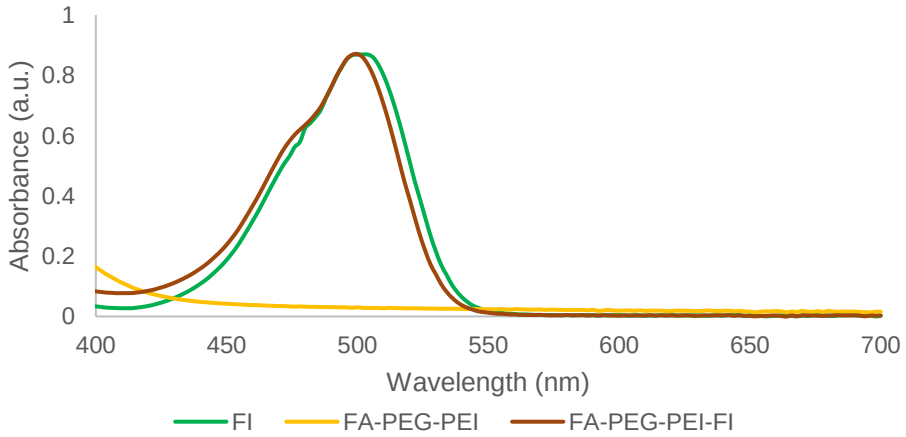

Figure 27. UV-Vis spectrum of FI, FA-PEG-PEI, and FA-PEG-PEI-FI complexes.

4. Dynamic Light Scattering and Electrophoretic Light Scattering analysis

After synthesis, starting materials such DOX, LAP, PEI, DA, PDA, and the synthesized complexes like LAP/DOX, LAP/PEI, LAP/PDA, LAP/DOX/PEI, LAP/DOX/PDA, LAP/DOX/PDA(FI-PEG-FA), and LAP/DOX/PEI(FI-PEG-FA) were characterized by DLS and ELS.

These techniques allow the determination of the hydrodynamic size (volume, intensity, and number means), PdI, and zeta potential (this last one through ELS), to provide critical insights into their size distribution and stability.

The hydrodynamic diameter was determined through DLS, which measures the time-dependent fluctuations in the intensity of scattered light due to the Brownian motion of the particles. The PdI is a measure of the broadness of the size distribution of particles in a sample. Where samples with values close to or equal to 1 mean that the sample is very heterogeneous or with clusters, samples with values close to 0 represent samples with little particle size diversity. A lower PdI is desirable for many applications, including drug delivery. Zeta potential analysis was carried out to obtain the surface charge of the particles, which can affect their stability and interaction with biological systems [177,178].

The DLS analysis provides comprehensive data on the size distribution of various drug delivery systems, highlighting the influence of different components on the hydrodynamic diameter. The variability in particle sizes, especially in complex systems, underscores the importance of optimizing formulation processes to achieve the desired therapeutic outcomes [179]. The hydrodynamic diameters, PdI, and the zeta potential means are shown in Table 4.

Table 4: Hydrodynamic diameter, PdI, and zeta potential of complexes.

Sample Name	Hydrodynamic Diameter (nm)	PdI	Zeta Potential (mV)
DOX	424.25 ± 85.92	0.94	17.45 ± 2.01
LAP	8.18 ± 2.96	0.46	-46.35 ± 5.67
PEI	3.69 ± 0.86	1.00	24.95 ± 2.37
DA	557.00 ± 196.55	0.67	-36.05 ± 2.54
PDA	838.60 ± 311.00	0.42	-42.05 ± 0.60
LAP/DOX	497.55 ± 389.59	0.95	-14.10 ± 0.24
LAP/PEI	238.30 ± 77.35	1.00	34.75 ± 5.20
LAP/PDA	165.15 ± 75.69	1.00	-29.20 ± 1.19
LAP/DOX/PEI	366.80 ± 57.29	0.77	71.40 ± 1.37
LAP/DOX/PDA	432.50 ± 128.34	0.99	5.06 ± 0.45
LAP/DOX/PDA(FI-PEG-FA)	214.10 ± 41.80	0.45	-16.60 ± 1.69
LAP/DOX/PEI(FI-PEG-FA)	880.40 ± 124.70	0.41	20.85 ± 2.10

Note: All data represent the mean ± standard deviation (n = 4).

Considering the data obtained, it is possible to see that the complexes were successfully synthesized. However, the high PdI values for DOX, PEI, LAP/DOX, LAP/PEI, LAP/PDA, and LAP/DOX/PDA indicate the formation of large aggregates/ clusters and an undesired distribution of nanoparticle hydrodynamic diameter [178].

Figure 28 illustrates the dispersion graph of the percentage intensity of particles as a function of their hydrodynamic size, revealing the different sizes of particles in the sample, which may include agglomerates of smaller particles. Additionally, Figure 29 depicts a dispersion graph of the percentage volume in relation to the hydrodynamic size of the particles, offering insight into the more abundant particles in the sample and providing a better analysis considering that particles in small volumes will present lower peaks in this graph. Lastly, Figure 30 highlights a dispersion graph plotting the percentage number of particles as a function of their hydrodynamic size, providing valuable insights into the size distribution and uniformity of the synthesized nanoparticles [178]

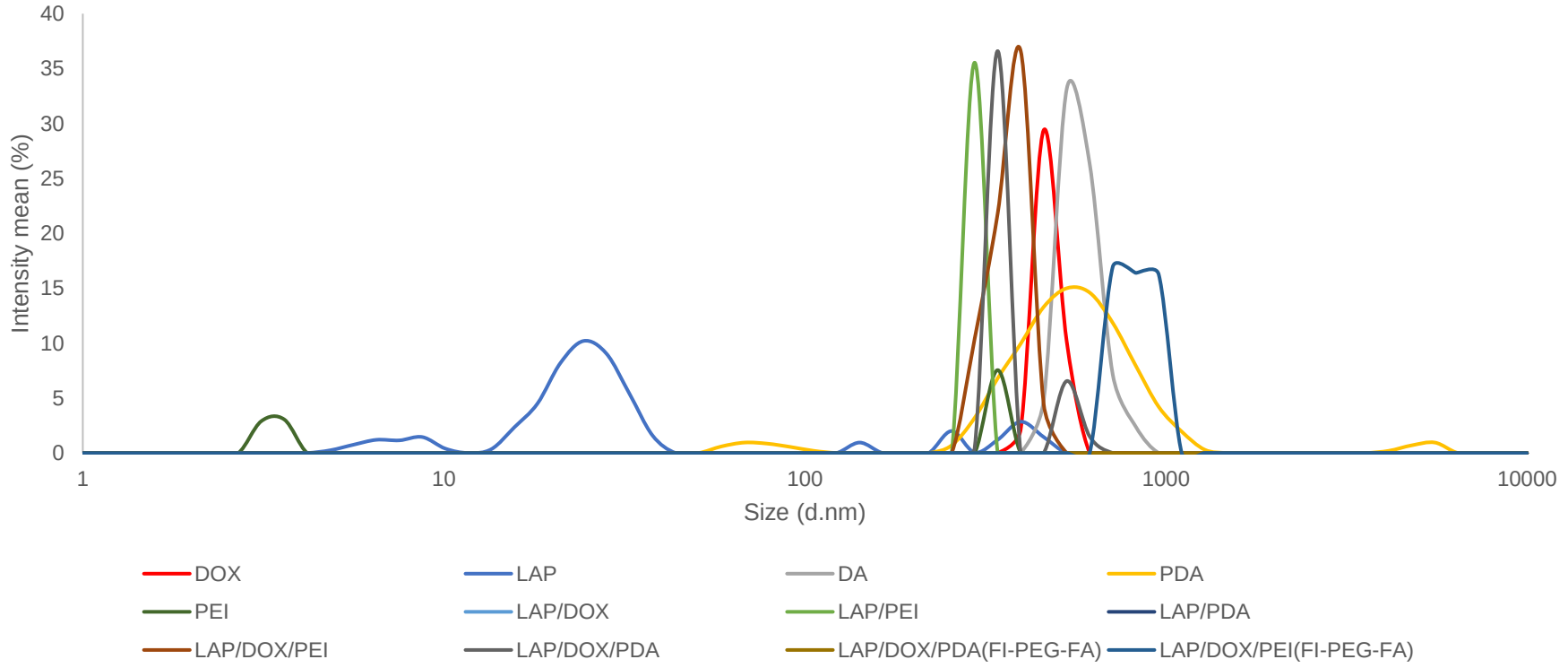

Figure 28. Intensity means (%) vs particle size distribution of samples and complexes.

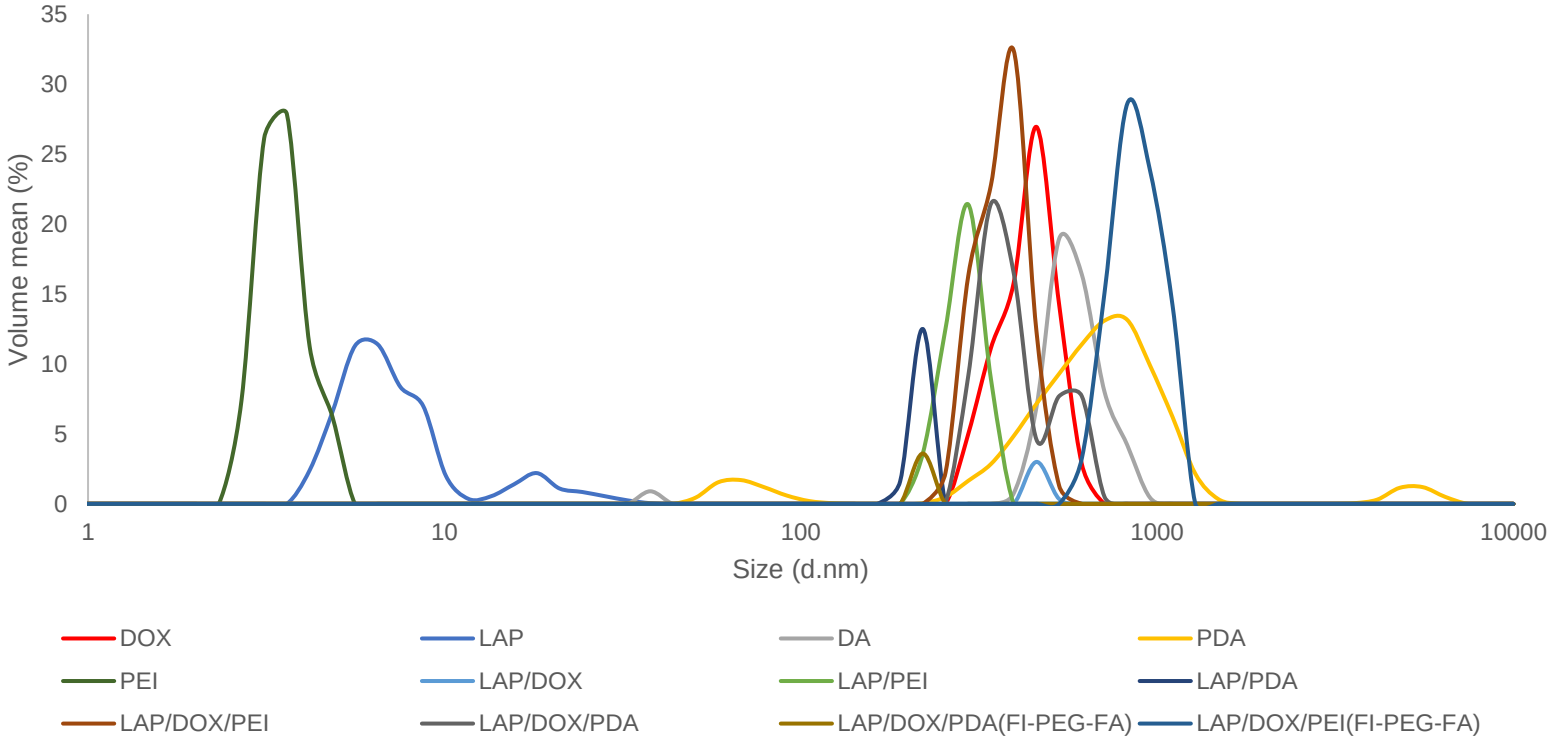

Figure 29. Volume means (%) vs particle size distribution of samples and complexes.

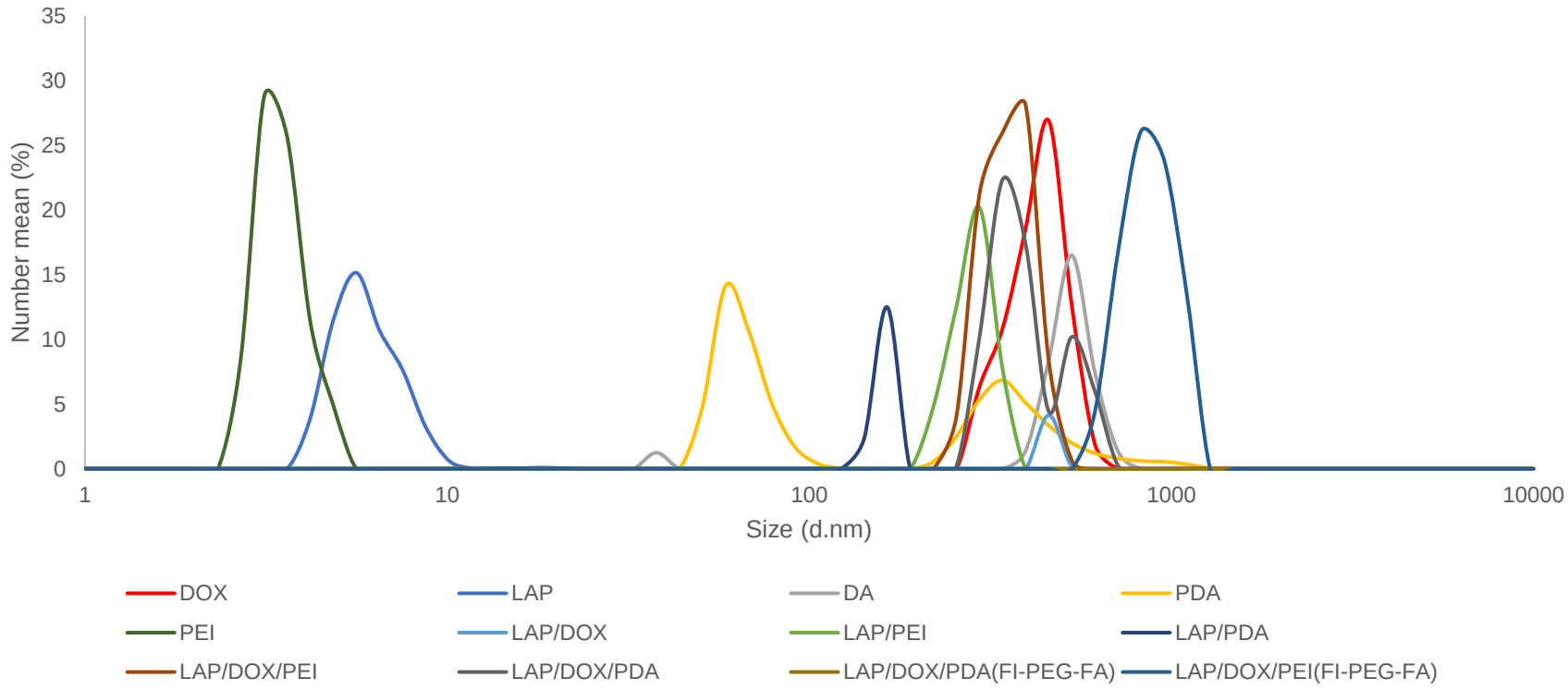

Figure 30. Number means (%) vs particle size distribution of samples and complexes.

Focusing on the final products, Figure 31 presents the key findings. The LAP/DOX/PDA(FI-PEG-FA) complex had a diameter of 214.10 nm, which is relatively good since particles with sizes from 70 nm to 200 nm were shown to remain in the bloodstream for a longer period without being eliminated [179]. The PdI value and a negative superficial charge (-16.60 mV) also revealed to be of relevance, showing that the sample is relatively homogenous and negative enough to interact with the cell membrane [128,180]. In contrast, the LAP/DOX/PEI(FI-PEG-FA) complex had a diameter of 880.40 nm, indicating larger particle sizes that could potentially limit its applicability in certain drug delivery scenarios, since particles with diameters greater than 200 nm are typically sequestered by the spleen and eventually removed by phagocytes [179]. Despite the bigger diameter this sample exhibited a similar PdI value to the one obtained for the LAP/DOX/PDA(FI-PEG-FA) complex and a positive surface charge of 20.85 mV.

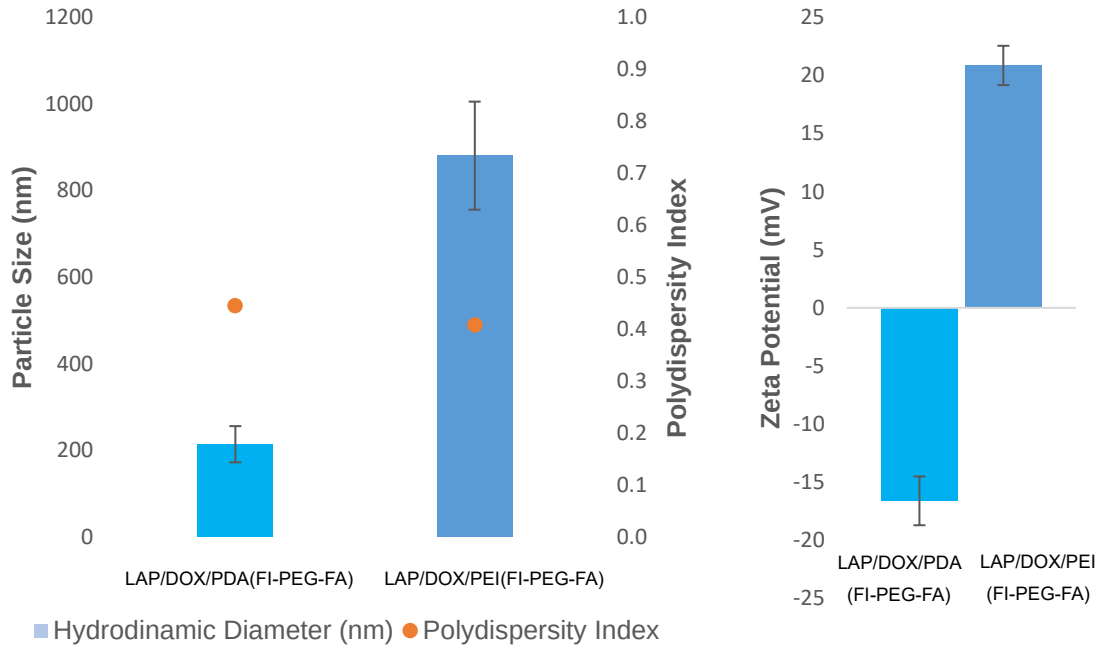

Figure 31. Hydrodynamic diameter, PdI, and zeta potential of LAP/DOX/PDA(FI-PEG-FA) and LAP/DOX/PEI(FI-PEG-FA). Note: All data represents the mean ± standard deviation (n=4).

5. Drug release

For the *in vitro* drug release study, a DOX concentration of 2.5 µg/mL was selected. For the complexes, the LC was considered to ensure that the mass of DOX was consistent across all samples. The drug release was performed in PBS at pH 7.4 to simulate the physiological

environments, for 2 weeks at 37°C [171]. At different time intervals, aliquots were collected for fluorescence analysis to quantify the amount of DOX released. The drug Cr% over time was calculated based on the amount of DOX released, as illustrated in Figure S4 in the supplementary information.

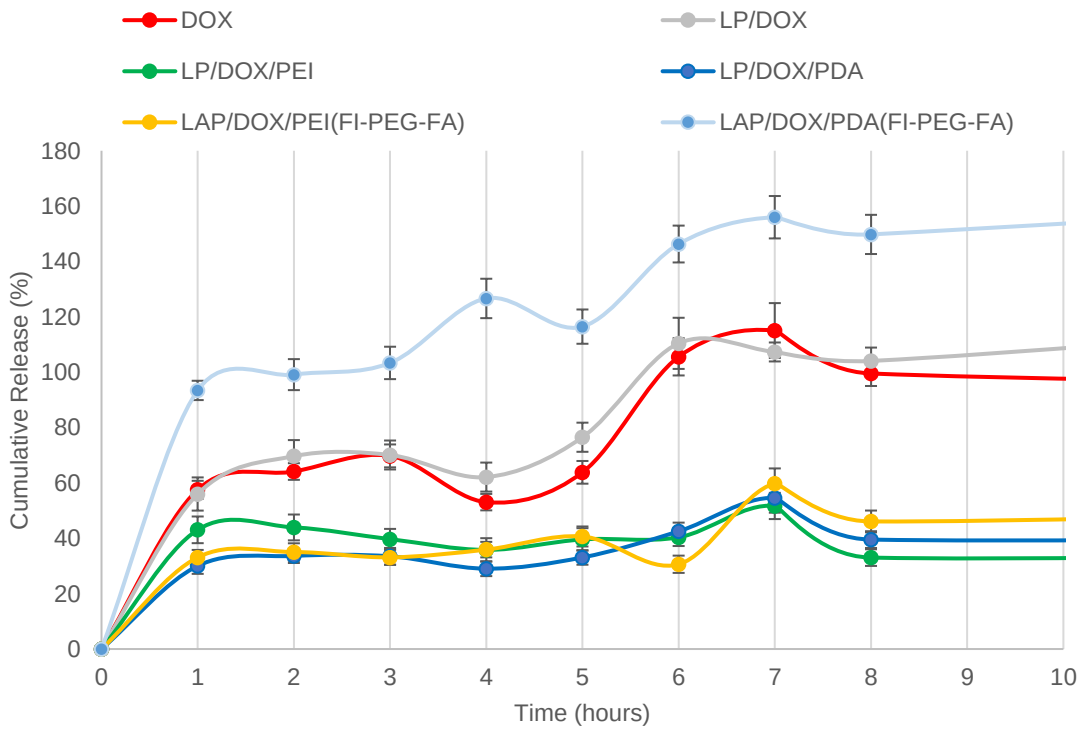

Figure 32. Drug release of DOX in PBS, pH 7.4 at 37 °C as a function of time (10 hours).

Based on Figure 32, which depicts the Cr% in the first 8 hours, it is evident that DOX release was significant in the initial hours. Generally, the subsequent hours showed a gradual release of the drug, with slightly decreasing variations that could reflect fluorescence measurement errors.

After 8 hours, around 100% of the free DOX and the DOX from the LAP/DOX complex had been entirely released, whereas the polymer-coated complexes showed significantly lower release levels as intended, except for the LAP/DOX/PDA(FI-PEG-FA) complex, which released about 150%, an unexpected outcome. The LAP/DOX/PEI complex released 33% of DOX, the LAP/DOX/PDA complex released about 40%, and the LAP/DOX/PEI(FI-PEG-FA) complex released 46%. At 48 hours, all complexes showed an increased DOX release as expected. The LAP/DOX/PEI, LAP/DOX/PDA, LAP/DOX/PEI(FI-PEG-FA), and LAP/DOX/PDA(FI-PEG-FA) complexes released about 45%, 50%, 59%, and 253% of DOX, respectively.

These findings indicate that the complexes generally allow for a more controlled drug release over time (except for the LAP/DOX/PDA(FI-PEG-FA) complex). However the differences are not extremely pronounced for some complexes, such as in the study by BI, D. *et al*., 2018, [171], which reported only 22.4% drug release for the DOX/PDA complex throughout 48 h. Notably, the LAP/DOX/PEI, LAP/DOX/PDA, and LAP/DOX/PEI(FI-PEG-FA) complexes showed the least DOX release in a physiological environment.

These results contradict the purpose of the FI-PDA-PEG-FA coating on the LAP/DOX/PDA(FI-PEG-FA) complex, which was supposed to allow a more controlled drug release. Therefore, additional characterization methods should be conducted to confirm the presence of the coating and evaluate its thickness and dimension. Additionally, since this study was conducted in PBS at pH 7.4, and bearing in mind that previous studies have reported a greater release of DOX at lower pH, it would be beneficial for future research to test DOX release at pH 5 and 6.5, which is representative of the endosomal or lysosomal systems of tumor cells and the tumor microenvironment, respectively [169,171,181].

6. Cytotoxicity evaluation

The cytotoxicity of the complexes was determined using the resazurin reduction assay, an indirect measure of cell viability, which correlates cellular metabolic activity with the number of viable cells in culture. This assay is based on the principle that only living cells are metabolically active and can reduce resazurin (a membrane-permeable compound), into resorufin (a fluorescent product), while non-viable cells lack this capability. Resazurin enters the cells and is reduced to resorufin, which is then excreted and accumulates in the medium [182,183]. When excited at a wavelength of 579 nm, resorufin emits a fluorescent signal at 584 nm, providing a measure of cell viability. The assay's reliance on the unique fluorescence properties of resorufin, rather than resazurin, ensures accurate measurement of metabolic activity and, consequently, cell viability [184].

Figure 33 represents the metabolic activity of cells exposed to different complexes at different DOX concentrations (0.1, 0.5, 1, 1.5, and 2 μM), with the metabolic activity expressed as a percentage relative to the solvent control, which is set at 100%.

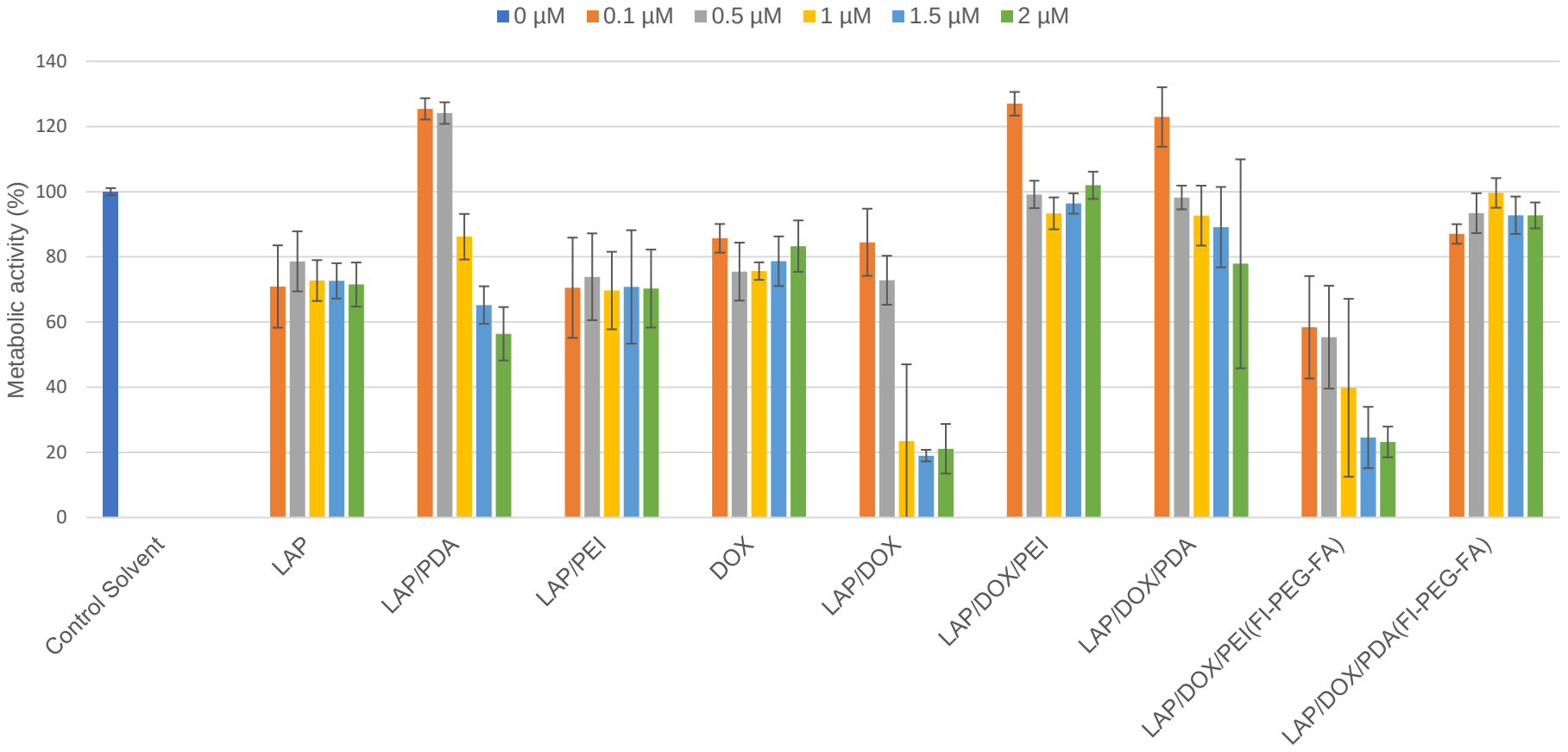

Figure 33. Cell viability of MCF-7 cells after 48h exposure to the complexes (at different concentrations). Data are expressed as the mean ± SD.

The metabolic activity of LAP ranges between approximately 70 - 80% across all concentrations, indicating a consistent reduction in metabolic activity compared to the control, but it does not show a trend with increasing concentration. LAP/PDA displays notably higher metabolic activity at 0.1 and 0.5 μM, reaching around 120%. However, as the concentration increases, the activity drops significantly to about 60% at 2 μM, indicating that higher concentrations of LAP/PDA reduce the number of viable cells. Both LAP/PEI and DOX exhibit similar behavior to LAP, showing no evident trend with increasing concentration, with metabolic activity remaining fairly stable at around 70-75% and 75-85%, respectively. The LAP/DOX complex shows a decrease in metabolic activity (greater cytotoxicity), with increasing concentration. At lower concentrations (0.1 and 0.5 μM), the metabolic activity is similar, but it drops significantly to around 20% at 1 μM and higher. The LAP/DOX/PDA and LAP/DOX/PEI complexes exhibit high metabolic activity at 0.1 μM (around 120%), similar to LAP/PDA, but the metabolic activity decreases to around 80-90% at other concentrations. The LAP/DOX/PEI(FI-PEG-FA) complex demonstrates a substantial reduction in metabolic activity at higher concentrations, indicating its cytotoxic effect. At 0.1 μM, the activity is around 60%, but it drops drastically to about 20% at 2 μM. In contrast, the LAP/DOX/PDA(FI-PEG-FA) complex maintains relatively high metabolic activity, ranging from 85% to 100% at all concentrations, indicating that increasing concentration does not significantly affect metabolic activity.

The primary objective of this cell viability assessment was to determine if cells retained their proliferative ability when exposed to the complexes. Only in some of the complexes, such as LAP/DOX and LAP/DOX/PEI(FI-PEG-FA), did higher concentrations result in a considerable lower activity. At lower concentrations (0.1 μM), some complexes, such as LAP/PDA, LAP/DOX/PEI, and LAP/DOX/PDA, exhibit higher metabolic activity compared to the control, indicating that, at this concentration, the complexes are not toxic to the cells and that low doses can stimulate cellular activity. This may be because when cells are exposed to an unknown compound, their metabolic activity increases as a defense response. Therefore, at lower concentrations, this increase in activity as a defense reaction turns out to be higher compared to the control.

The presence of DOX in the complexes was expected to reduce metabolic activity due to its cytotoxic nature, which targets and kills cancer cells, as demonstrated by Chen *et al.*, 2016, [170] study. In that work, the PEI-FI-(PEG-HA)/DOX complex exhibited a roughly 20% reduction in metabolic activity compared to the same complex without DOX (at a DOX concentration of 4.0 μg/mL). However, this anticipated effect is not observed in complexes such as LAP/PEI, LAP/PDA, LAP/DOX/PEI, and LAP/DOX/PDA, since these complexes (the ones without DOX) show lower cell viability.

From the data collected, it is evident that, among the two final complexes, the LAP/DOX/PEI(FI-PEG-FA) complex most significantly reduces the metabolic activity of the cells. Even at the lowest concentration, this complex resulted in a greater reduction in cell viability than any of the concentrations tested for LAP/DOX/PDA(FI-PEG-FA).

To further validate the therapeutic efficacy of the complexes, the morphology of MCF-7 cells was observed (Figure 34). It can be seen that the MCF-7 cells treated with the complexes display strong green (due to FI conjugation) and red (due to the loaded DOX) fluorescence signals. Notably, a significant portion of the cells appeared rounded and detached after being exposed to the complexes for 48 hours, indicative of cell death. The images captured for the LAP/DOX/PEI(FI-PEG-FA) and LAP/DOX/PDA(FI-PEG-FA) complexes align with the results obtained from the resazurin reduction assay. A higher number of viable cells were observed in the assays where cells were exposed to the LAP/DOX/PDA(FI-PEG-FA) complex, correlating with its higher metabolic activity values. Conversely, the images of cells treated with the LAP/DOX/PEI(FI-PEG-FA) complex reveal more detached and rounded cells, which are clear indicators of cell death. Notably, this complex demonstrated the greatest reduction in metabolic activity, with only 59% of DOX released after 48 hours.

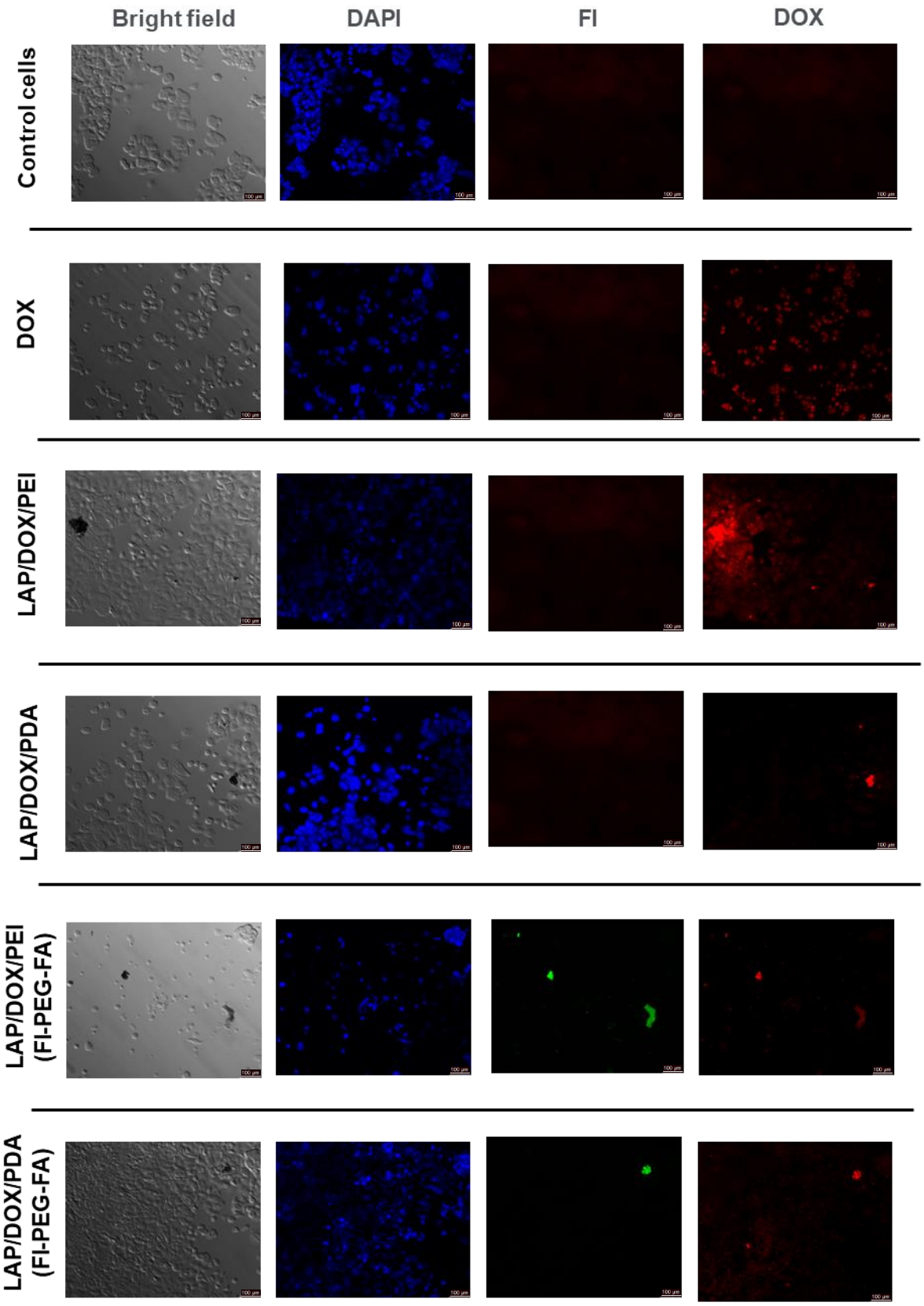

Figure 34. Confocal microscopy: staining with DAPI of MCF-7 cells treated with free DOX, LAP/DOX/PEI, LAP/DOX/PDA, LAP/DOX/PEI(FI-PEG-FA) and LAP/DOX/PDA(FI-PEG-FA) complexes at [1.5] μM after 48 h exposure at 37°C. Scale bar = 100 μm.

Chapter 5 - Conclusions and future perspectives

Cancer remains one of the deadliest diseases today, with the number of cases expected to rise in the coming years. Despite significant advancements in medicine and healthcare, effective therapies capable of completely eradicating tumors remain elusive for many cancer types due to their distinct characteristics. Chemotherapy remains the most widely used treatment, yet it is often accompanied by severe side effects and can sometimes result in treatment failure. In recent years, NPs have garnered increasing attention as drug carriers and tools for cancer diagnosis, imaging, and therapy. These nanocarriers enhance the solubility of anti-cancer drugs, target the tumor site more effectively, improve bioavailability, reduce side effects, and increase the half-time in circulation, among other benefits.

In this thesis, the well-established properties of the PEI and PDA polymers were exploited, including their high charge density, the ability to form stable NPs with drugs, protect them from degradation, improve solubility, and enhance bioavailability. These characteristics make them an ideal platform for surface functionalization to carry DOX, a widely used drug in cancer treatments. DOX exerts its cytotoxic effects primarily through two mechanisms: DNA intercalation and the production of ROS, targeting multiple molecular pathways.

In addition to these polymers, other molecules were incorporated into the complexes. LAP was chosen due to its low toxicity and strong interactions with various chemical compounds, making it an appealing option for protecting drugs from degradation in the physiological environment. PEG was also chosen as it has been shown to extend the lifetime circulation of NPs by camouflaging them, thus preventing their detection and elimination by the immune system. FA was also selected as it is often used in cancer therapy and diagnosis due to its efficacy in active targeting, attributed to its overexpression in many types of cancer. Finally, FI, a fluorescent compound, was conjugated to allow microscopy techniques to be used for screening and analysis.

Regarding the synthesis of LAP-coated PDA, the most favorable condition for this study was LAP 3 mg/mL, DA 2 mg/mL (in a 1:2 ratio), using an ultrasonic bath together with the addition of mannitol. DOX loading into LAP nanodisks achieved an EE high value of 99.68 % and LC of 28.53%, similar to what is reported in the literature. Considering the performed synthesis, the complexes were successfully obtained and characterized by ^{1}H NMR, DLS, ELS, and UV/Vis. The LAP/DOX/PDA(FI-PEG-FA) complex exhibited a diameter of 214.10 nm, a PdI of 0.45, and a negative surface charge of -16.60 mV. In contrast, the LAP/DOX/PEI(FI-PEG-FA) complex displayed a larger diameter of 880.40 nm, a PdI of 0.41, and a positive surface charge of 20.85 mV. The Cr% results of DOX from the synthesized complexes over time, allowed to conclude that the LAP/DOX/PEI(FI-PEG-FA) complex is more effective than LAP/DOX/PDA(FI-PEG-FA) in terms of achieving a sustained DOX release in a physiological environment. Finally, the evaluation of the *in vitro* cytotoxicity of the complexes, between the two final complexes, showed that the

LAP/DOX/PEI(FI-PEG-FA) complex exhibits the most substantial reduction in cellular metabolic activity even at the lowest concentration. Based on this findings, Laponite-based nanocomplexes functionalized with FI-PEI-PEG-FA show great potential as efficient carriers for the controlled delivery of DOX, presenting promising applications in cancer treatment.

According to the results obtained, further studies are needed to assess the effectiveness of the FI-PDA-PEG-FA and FI-PEI-PEG-FA coating processes. These studies should include characterization techniques to confirm the presence of the coatings and evaluate their thickness and dimensions, as these factors can significantly impact DOX release. Additionally, future research should investigate DOX release at pH levels of 5 and 6.5, which represent the endosomal or lysosomal environments of tumor cells and the tumor microenvironment, respectively, given that previous studies have shown increased DOX release under acidic conditions. It would also be interesting to evaluate the cellular uptake and the targeting capabilities and how effectively FA binds to cancer cells, including its effectiveness in different types of cancer. The efficacy of active binding depends on several factors, including the degree of receptor overexpression in the target cells and the strength of the bond between the binding ligand and the receptor.

References

[1] F. Bray, M. Laversanne, H. Sung, J. Ferlay, R.L. Siegel, I. Soerjomataram, A. Jemal, Global cancer statistics 2022: GLOBOCAN estimates of incidence and mortality worldwide for 36 cancers in 185 countries, CA: A Cancer Journal for Clinicians 74 (2024) 229–263. https://doi.org/10.3322/caac.21834.

[2] K. Kim, J.H. Kim, H. Park, Y.S. Kim, K. Park, H. Nam, S. Lee, J.H. Park, R.W. Park, I.S. Kim, K. Choi, S.Y. Kim, K. Park, I.C. Kwon, Tumor-homing multifunctional nanoparticles for cancer theragnosis: Simultaneous diagnosis, drug delivery, and therapeutic monitoring, Journal of Controlled Release 146 (2010) 219–227. https://doi.org/10.1016/j.jconrel.2010.04.004.

[3] J. Shen, Q. He, Y. Gao, J. Shi, Y. Li, Mesoporous silica nanoparticles loading doxorubicin reverse multidrug resistance: Performance and mechanism, Nanoscale 3 (2011) 4314–4322. https://doi.org/10.1039/c1nr10580a.

[4] B. Sumer, J. Gao, Theranostic nanomedicine for cancer, Nanomedicine 3 (2008) 137–140. https://doi.org/10.2217/17435889.3.2.137.

[5] S. Vrignaud, J.P. Benoit, P. Saulnier, Strategies for the nanoencapsulation of hydrophilic molecules in polymer-based nanoparticles, Biomaterials 32 (2011) 8593–8604. https://doi.org/10.1016/j.biomaterials.2011.07.057.

[6] S. Luo, E. Zhang, Y. Su, T. Cheng, C. Shi, A review of NIR dyes in cancer targeting and imaging, Biomaterials 32 (2011) 7127–7138. https://doi.org/10.1016/j.biomaterials.2011.06.024.

[7] K.C. Barick, S. Singh, N. V. Jadhav, D. Bahadur, B.N. Pandey, P.A. Hassan, PH-responsive peptide mimic shell cross-linked magnetic nanocarriers for combination therapy, Advanced Functional Materials 22 (2012) 4975–4984. https://doi.org/10.1002/adfm.201201140.

[8] J. Zugazagoitia, C. Guedes, S. Ponce, I. Ferrer, S. Molina-Pinelo, L. Paz-Ares, Current Challenges in Cancer Treatment, Clinic Therapeutics 38 (2016) 1551–1566. https://doi.org/10.1016/j.clinthera.2016.03.026.

[9] L. Wei, J. Chen, S. Zhao, J. Ding, X. Chen, Thermo-sensitive polypeptide hydrogel for locally sequential delivery of two-pronged antitumor drugs, Acta Biomaterialia 58 (2017) 44–53. https://doi.org/10.1016/j.actbio.2017.05.053.

[10] S. Wen, H. Liu, H. Cai, M. Shen, X. Shi, Targeted and pH-responsive delivery of doxorubicin to cancer cells using multifunctional dendrimer-modified multi-walled carbon nanotubes, Advanced Healthcare Materials 2 (2013) 1267–1276. https://doi.org/10.1002/adhm.201200389.

[11] D. Li, X. Feng, L. Chen, J. Ding, X. Chen, One-Step Synthesis of Targeted Acid-Labile Polysaccharide Prodrug for Efficiently Intracellular Drug Delivery, ACS Biomaterials Science & Engineering 4 (2018) 539–546. https://doi.org/10.1021/acsbiomaterials.7b00856.

[12] N. Amiryaghoubi, M. Fathi, J. Barar, H. Omidian, Y. Omidi, Advanced nanoscale drug delivery systems for bone cancer therapy, Biochimica et Biophysica Acta - Molecular Basis of Disease 1869 (2023). https://doi.org/10.1016/j.bbadis.2023.166739.

[13] X. Liu, H. Tao, K. Yang, S. Zhang, S.T. Lee, Z. Liu, Optimization of surface chemistry on single-walled carbon nanotubes for in vivo photothermal ablation of tumors, Biomaterials 32 (2011) 144–151. https://doi.org/10.1016/j.biomaterials.2010.08.096.

[14] A. Fujiwara, T. Hoshino, J.W. Westley, Anthracycline Antibiotics, Critical Reviews in Biotechnology 3 (1985) 133-157. https://doi.org/10.3109/07388558509150782.

[15] R B Weiss, The anthracyclines: will we ever find a better doxorubicin?, Seminares in Oncology (1992) 670-686.

[16] G. Minotti, P. Menna, E. Salvatorelli, G. Cairo, L. Gianni, Anthracyclines: Molecular advances and pharmacologie developments in antitumor activity and cardiotoxicity, Pharmacological Reviews 56 (2004) 185–229. https://doi.org/10.1124/pr.56.2.6.

[17] X. Peng, B. Chen, C.C. Lim, D.B. Sawyer, The cardiotoxicology of anthracycline chemotherapeutics: translating molecular mechanism into preventative medicine, Molecular Interventions 5 (2005) 163-171. https://doi.org/10.1124/mi.5.3.6.

[18] G.N. Hortobdgyi, Anthracyclines in the Treatment of Cancer: An Overview, Drugs 54 (1997) 1-7. https://doi.org/10.2165/00003495-199700544-00003.

[19] C. Carvalho, R.X. Santos, S. Cardoso, S. Correia, P.J. Oliveira, M.S. Santos, P.I. Moreira, Doxorubicin: The Good, the Bad and the Ugly Effect, Current Medicinal Chemistry 16 (2009) 3267-3285. https://doi.org/10.2174/092986709788803312.

[20] Molecular Operating Environment (MOE), Version 2015; Chemical Computing Group Inc.: Montreal, Quebec, Canada, 2015.

[21] A. Marco, G. Cassinelli, F. Arcamone, The discovery of daunorubicin, Cancer Treatment Reports 65 (1981) 3–8.

[22] C. Tan, H. Tasaka, K.-P. Yu, M.L. Murphy, D.A. Karnofsky, Daunomycin, an antitumor antibiotic, in the treatment of neoplastic disease. Clinical evaluation with special reference to childhood leukemia 20 (1967) 333-353. https://doi.org/10.1002/1097-0142(1967)20:3<333::aid-cncr2820200302>3.0.co;2-k.

[23] F. Arcamone, G. Cassinelli, G. Fantini, A. Grein, P. Orezzi, C. Pol, C. Spalla, Adriamycin, 14-Hydroxydaunomycin, a New Antitumor Antibiotic from S.peucetius var. caesius,

Biotechnology Bioengineering 11 (1969) 1101–1110. https://doi.org/10.1002/bit.260110607.

[24] S. Rivankar, An overview of doxorubicin formulations in cancer therapy, Journal of Cancer Research and Therapeutics 10 (2014) 853–858. https://doi.org/10.4103/0973-1482.139267.

[25] G. Bonadonna, S. Monfardini, M. Lena, F. Fossati-Bellani, Clinical Evaluation of Adriamycin, a New Antitumour Antibiotic, British Medical Journal 3 (1969) 503-506 https://doi.org/10.1136/bmj.3.5669.503.

[26] A.P. Launchbury, N. Habboubit, " Farmitalia, Epirubicin and doxorubicin: a comparison of their characteristics, therapeutic activity and toxicity, Cancer Treatment Reviews 19 (1993) 197-228. https://doi.org/10.1016/0305-7372(93)90036-q.

[27] World Health Organization. World Health Organization Model List of Essential Medicines, 21st List (2019). World Health Organization: Geneva, Switzerland, 2019.

[28] K.C. Weng, C.O. Noble, B. Papahadjopoulos-Sternberg, F.F. Chen, D.C. Drummond, D.B. Kirpotin, D. Wang, Y.K. Horn, B. Hann, J.W. Park, Targeted tumor cell internalization and imaging of multifunctional quantum dot-conjugated immunoliposomes in vitro and in vivo, Nano Letters 8 (2008) 2851–2857. https://doi.org/10.1021/nl801488u.

[29] F.P. Seib, E.M. Pritchard, D.L. Kaplan, Self-assembling doxorubicin silk hydrogels for the focal treatment of primary breast cancer, Advanced Functional Materials 23 (2013) 58–65. https://doi.org/10.1002/adfm.201201238.

[30] J.H. Maeng, D.H. Lee, K.H. Jung, Y.H. Bae, I.S. Park, S. Jeong, Y.S. Jeon, C.K. Shim, W. Kim, J. Kim, J. Lee, Y.M. Lee, J.H. Kim, W.H. Kim, S.S. Hong, Multifunctional doxorubicin loaded superparamagnetic iron oxide nanoparticles for chemotherapy and magnetic resonance imaging in liver cancer, Biomaterials 31 (2010) 4995–5006. https://doi.org/10.1016/j.biomaterials.2010.02.068.

[31] H.T. Ta, C.R. Dass, I. Larson, P.F.M. Choong, D.E. Dunstan, A chitosan-dipotassium orthophosphate hydrogel for the delivery of Doxorubicin in the treatment of osteosarcoma, Biomaterials 30 (2009) 3605–3613. https://doi.org/10.1016/j.biomaterials.2009.03.022.

[32] O. Tacar, P. Sriamornsak, C.R. Dass, Doxorubicin: An update on anticancer molecular action, toxicity and novel drug delivery systems, Journal of Pharmacy and Pharmacology 65 (2013) 157–170. https://doi.org/10.1111/j.2042-7158.2012.01567.x.

[33] W. Yeo, T.K.H. Lau, C.C.H. Kwok, K.T. Lai, V.T.C. Chan, L. Li, V. Chan, A. Wong, W.M.T. Soo, E.W.M. Yeung, K.H. Wong, N.L.S. Tang, J.J.S. Suen, F.K.F. Mo, NEPA efficacy and tolerability during (neo)adjuvant breast cancer chemotherapy with cyclophosphamide and doxorubicin, BMJ Supportive & Palliative Care 12 (2022) 264–270. https://doi.org/10.1136/bmjspcare-2019-002037.

[34] F. khaki-khatibi, M. Ghorbani, M. Sabzichi, F. Ramezani, J. Mohammadian, Adjuvant therapy with stattic enriches the anti-proliferative effect of doxorubicin in human ZR-75-1 breast cancer cells via arresting cell cycle and inducing apoptosis, Biomedicine and Pharmacotherapy 109 (2019) 1240–1248. https://doi.org/10.1016/j.biopha.2018.10.183.

[35] M. Kciuk, A. Gielecińska, S. Mujwar, D. Kołat, Ż. Kałuzińska-Kołat, I. Celik, R. Kontek, Doxorubicin—An Agent with Multiple Mechanisms of Anticancer Activity, Cells 12 (2023). https://doi.org/10.3390/cells12040659.

[36] Y. Pommier, E. Leo, H. Zhang, C. Marchand, DNA topoisomerases and their poisoning by anticancer and antibacterial drugs, Chemistry & Biology 17 (2010) 421–433. https://doi.org/10.1016/j.chembiol.2010.04.012.

[37] C.A. Frederick, L. Dean Williams, G. Ughetto, I.A. Gijs van der Mare, J.H. van Boom, A. Rich, A. H-J Wang, Structural Comparison of Anticancer Drug-DNA Complexes: Adriamycin and Daunomycin, Biochemistry 29 (1990) 2538–2549. https://doi.org/10.1021/bi00462a016.

[38] D.B. Zorov, M. Juhaszova, S.J. Sollott, Mitochondrial Reactive Oxygen Species (ROS) and ROS-Induced ROS Release, Physiological Reviews 94 (2014) 909–950. https://doi.org/10.1152/physrev.00026.2013.-Byproducts.

[39] F. Arcamone, G. Cassinelli, G. Franceschi, S. Penco, C. Pol, S. Redaelli, A. Selva, Structure and physicochemical properties of Adriamycin (Doxorubicin). In: S.K. Carter, A.D. Marco, M. Ghione, I.H. Krakoff, G. Mathé. *International Symposium on Adriamycin*. Springer, Berlin, Heidelberg, (1972) 15-31. https://doi.org/10.1007/978-3-642-95227-2_2.

[40] M. Gonçalves, S. Mignani, J. Rodrigues, H. Tomás, A glance over doxorubicin based-nanotherapeutics: From proof-of-concept studies to solutions in the market, Journal of Controlled Release 317 (2020) 347–374. https://doi.org/10.1016/j.jconrel.2019.11.016.

[41] M. Cagel, E. Grotz, E. Bernabeu, M.A. Moretton, D.A. Chiappetta, Doxorubicin: nanotechnological overviews from bench to bedside, Drug Discovery Today 22 (2017) 270–281. https://doi.org/10.1016/j.drudis.2016.11.005.

[42] T.G. Burke, T.R. Tritton, Structural Basis of Anthracycline Selectivity for Unilamellar Phosphatidylcholine Vesicles: An Equilibrium Binding Study, Biochemistry 24 (1985) 1768-1776. https://doi.org/10.1021/bi00328a030.

[43] F. Barcelo, I. Barcelo, F. Gavilanes, J.A. Ferragut, S. Yanovich, J.M. Gonzalez-Ros, Interaction of anthracyclines with nucleotides and related compounds studied by spectroscopy, Biochimica et Biophysica Acta 884 (1986) 172-181. https://doi.org/10.1016/0304-4165(86)90241-2.

[44] L.Y. Rizzo, B. Theek, G. Storm, F. Kiessling, T. Lammers, Recent progress in nanomedicine: Therapeutic, diagnostic and theranostic applications, Current Opinion in Biotechnology 24 (2013) 1159–1166. https://doi.org/10.1016/j.copbio.2013.02.020.

[45] K.K. Karukstis, E.H.Z. Thompson, J.A. Whiles, R.J. Rosenfeld, Deciphering the fluorescence signature of daunomycin and doxorubicin, Biophysical Chemistry 73 (1998) 249-263 https://doi.org/10.1016/S0301-4622(98)00150-1.

[46] S. Shah, A. Chandra, A. Kaur, N. Sabnis, A. Lacko, Z. Gryczynski, R. Fudala, I. Gryczynski, Fluorescence properties of doxorubicin in PBS buffer and PVA films, Journal of Photochemistry and Photobiology B: Biology 170 (2017) 65–69. https://doi.org/10.1016/j.jphotobiol.2017.03.024.

[47] M. Theodoulou, C. Hudis, Cardiac Profiles of Liposomal Anthracyclines: Greater Cardiac Safety versus Conventional Doxorubicin?, Cancer 100 (2004) 2052–2063. https://doi.org/10.1002/cncr.20207.

[48] A.I. Minchinton, I.F. Tannock, Drug penetration in solid tumours, Nature Reviews Cancer 6 (2006) 583–592. https://doi.org/10.1038/nrc1893.

[49] Y. Chen, S.R. Bathula, J. Li, L. Huang, Multifunctional nanoparticles delivering small interfering RNA and doxorubicin overcome drug resistance in cancer, Journal of Biological Chemistry 285 (2010) 22639–22650. https://doi.org/10.1074/jbc.M110.125906.

[50] B.-J. Fang, M.L. Yu, S.G. Yang, L.M. Liao, J.W. Liu, R. CH Zhao, Effect of O-4-ethoxyl-butyl-berbamine in combination with pegylated liposomal doxorubicin on advanced hepatoma in mice, World Journal of Gastroenterology 10 (2004) 950-953. https://doi.org/10.3748/wjg.v10.i7.950.

[51] A. Gabizon, H. Shmeeda, Y. Barenholz, Pharmacokinetics of Pegylated Liposomal Doxorubicin Review of Animal and Human Studies, Clinical Pharmacokinetics 42 (2003) 419-436. https://doi.org/10.2165/00003088-200342050-00002.

[52] S.M. Ansar, T. Mudalige, Characterization of doxorubicin liposomal formulations for size-based distribution of drug and excipients using asymmetric-flow field-flow fractionation (AF4) and liquid chromatography-mass spectrometry (LC-MS), International Journal of Pharmaceutics 574 (2020). https://doi.org/10.1016/j.ijpharm.2019.118906.

[53] M. Slingerland, H.J. Guchelaar, H. Gelderblom, Liposomal drug formulations in cancer therapy: 15 years along the road, Drug Discovery Today 17 (2012) 160–166. https://doi.org/10.1016/j.drudis.2011.09.015.

[54] M.L. Tan, A.M. Friedhuber, D.E. Dunstan, P.F.M. Choong, C.R. Dass, The performance of doxorubicin encapsulated in chitosan-dextran sulphate microparticles in an osteosarcoma model, Biomaterials 31 (2010) 541–551. https://doi.org/10.1016/j.biomaterials.2009.09.069.

[55] S. Park, H.S. Kim, W.J. Kim, H.S. Yoo, Pluronic@Fe_3O_4 nanoparticles with robust incorporation of doxorubicin by thermo-responsiveness, International Journal of Pharmaceutics 424 (2012) 107–114. https://doi.org/10.1016/j.ijpharm.2011.12.044.

[56] J. Park, P.M. Fong, J. Lu, K.S. Russell, C.J. Booth, W.M. Saltzman, T.M. Fahmy, PEGylated PLGA nanoparticles for the improved delivery of doxorubicin, Nanomedicine 5 (2009) 410–418. https://doi.org/10.1016/j.nano.2009.02.002.

[57] L.M. Kaminskas, B.D. Kelly, V.M. McLeod, G. Sberna, D.J. Owen, B.J. Boyd, C.J.H. Porter, Characterisation and tumour targeting of PEGylated polylysine dendrimers bearing doxorubicin via a pH labile linker, Journal of Controlled Release 152 (2011) 241–248. https://doi.org/10.1016/j.jconrel.2011.02.005.

[58] K.E. Uhrich, S.M. Cannizzaro, R.S. Langer, K.M. Shakesheff, Polymeric Systems for Controlled Drug Release, Chemical Reviews 99 (1999) 3181–3198. https://doi.org/10.1021/cr940351u.

[59] Z. Teng, X. Zhu, G. Zheng, F. Zhang, Y. Deng, L. Xiu, W. Li, Q. Yang, D. Zhao, Ligand exchange triggered controlled-release targeted drug delivery system based on core-shell superparamagnetic mesoporous microspheres capped with nanoparticles, Journal of Materials Chemistry 22 (2012) 17677–17684. https://doi.org/10.1039/c2jm32331a.

[60] J.Z. Du, X.J. Du, C.Q. Mao, J. Wang, Tailor-Made dual pH-sensitive polymer-doxorubicin nanoparticles for efficient anticancer drug delivery, Journal of the American Chemical Society 133 (2011) 17560–17563. https://doi.org/10.1021/ja207150n.

[61] M. Shi, K. Ho, A. Keating, M.S. Shoichet, Doxorubicin-conjugated immuno-nanoparticles for intracellular anticancer drug delivery, Advanced Functional Materials 19 (2009) 1689–1696. https://doi.org/10.1002/adfm.200801271.

[62] B. Mekuye, B. Abera, Nanomaterials: An overview of synthesis, classification, characterization, and applications, Nano Select 4 (2023) 486–501. https://doi.org/10.1002/nano.202300038.

[63] T. Sun, Y.S. Zhang, B. Pang, D.C. Hyun, M. Yang, Y. Xia, Engineered nanoparticles for drug delivery in cancer therapy, Angewandte Chemie - International Edition 53 (2014) 12320–12364. https://doi.org/10.1002/anie.201403036.

[64] A.C. Marques, P.J. Costa, S. Velho, M.H. Amaral, Functionalizing nanoparticles with cancer-targeting antibodies: A comparison of strategies, Journal of Controlled Release 320 (2020) 180–200. https://doi.org/10.1016/j.jconrel.2020.01.035.

[65] J.Z.S. Chiu, A.M. Castillo, I.G. Tucker, A.E. Radunskaya, A. McDowell, Modeling the interaction of polymeric nanoparticles functionalized with cell penetrating peptides at the nano-bio interface, Colloids and Surfaces B: Biointerfaces 217 (2022). https://doi.org/10.1016/j.colsurfb.2022.112626.

[66] Y. Fan, M. Marioli, K. Zhang, Analytical characterization of liposomes and other lipid nanoparticles for drug delivery, Journal of Pharmaceutical and Biomedical Analysis 192 (2021). https://doi.org/10.1016/j.jpba.2020.113642.

[67] S. Bayda, M. Adeel, T. Tuccinardi, M. Cordani, F. Rizzolio, The history of nanoscience and nanotechnology: From chemical-physical applications to nanomedicine, Molecules 25 (2020) 112. https://doi.org/10.3390/molecules25010112.

[68] J. Li, X. Yu, X. Shi, M. Shen, Cancer nanomedicine based on polyethylenimine-mediated multifunctional nanosystems, Prog Mater Sci 124 (2022). https://doi.org/10.1016/j.pmatsci.2021.100871.

[69] N.H. Abd Ellah, S.F. Gad, K. Muhammad, G. E Batiha, H.F. Hetta, Nanomedicine as a promising approach for diagnosis, treatment and prophylaxis against COVID-19, Nanomedicine 15 (2020) 2085–2102. https://doi.org/10.2217/nnm-2020-0247.

[70] B. Hu, K.O. Boakye-Yiadom, W. Yu, Z.W. Yuan, W. Ho, X. Xu, X.Q. Zhang, Nanomedicine Approaches for Advanced Diagnosis and Treatment of Atherosclerosis and Related Ischemic Diseases, Advanced Healthcare Materials 9 (2020). https://doi.org/10.1002/adhm.202000336.

[71] V.K. Chaturvedi, A. Singh, V.K. Singh, M.P. Singh, Cancer Nanotechnology: A New Revolution for Cancer Diagnosis and Therapy, Current Drug Metabolism 20 (2018) 416–429. https://doi.org/10.2174/1389200219666180918111528.

[72] S.C. Baetke, T. Lammers, F. Kiessling, Applications of nanoparticles for diagnosis and therapy of cancer, British Journal of Radiology 88 (2015). https://doi.org/10.1259/bjr.20150207.

[73] D. Giakoumettis, S. Sgouros, Nanotechnology in neurosurgery: a systematic review, Child's Nervous System 37 (2021) 1-10. https://doi.org/10.1007/s00381-020-05008-4.

[74] E. Garbayo, S. Pascual-Gil, C. Rodríguez-Nogales, L. Saludas, A. Estella-Hermoso de Mendoza, M.J. Blanco-Prieto, Nanomedicine and drug delivery systems in cancer and regenerative medicine, Wiley Interdisciplinary Reviews: Nanomedicine and Nanobiotechnology 12 (2020). https://doi.org/10.1002/wnan.1637.

[75] R. Goudarzi, A.R. Dehpour, A. Partoazar, Nanomedicine and regenerative medicine approaches in osteoarthritis therapy, Aging Clinical and Experimental Research 34 (2022) 2305–2315. https://doi.org/10.1007/s40520-022-02199-5.

[76] W.H. De Jong, P.J. Borm, Drug delivery and nanoparticles: Applications and hazards, International Journal of Nanomedicine 3 (2008) 133-149. https://doi.org/10.2147/ijn.s596.

[77] A. Avasthi, C. Caro, E. Pozo-Torres, M.P. Leal, M.L. García-Martín, Magnetic Nanoparticles as MRI Contrast Agents, Topics in Current Chemistry 378 (2020) 30. https://doi.org/10.1007/s41061-020-00302-w.

[78] N. Song, J. Zhang, J. Zhai, J. Hong, C. Yuan, M. Liang, Ferritin: A Multifunctional Nanoplatform for Biological Detection, Imaging Diagnosis, and Drug Delivery, Accounts of Chemical Research 54 (2021) 3313–3325. https://doi.org/10.1021/acs.accounts.1c00267.

[79] J.C.G. Esteves da Silva, H.M.R. Gonçalves, Analytical and bioanalytical applications of carbon dots, TrAC - Trends in Analytical Chemistry 30 (2011) 1327–1336. https://doi.org/10.1016/j.trac.2011.04.009.

[80] D.F. Emerich, Nanomedicine - Prospective therapeutic and diagnostic applications, Expert Opinion on Biological Therapy 5 (2005) 1–5. https://doi.org/10.1517/14712598.5.1.1.

[81] K. Qiao, L. Xu, J. Tang, Q. Wang, K.S. Lim, G. Hooper, T.B.F. Woodfield, G. Liu, K. Tian, W. Zhang, X. Cui, The advances in nanomedicine for bone and cartilage repair, Journal of Nanobiotechnology 20 (2022). https://doi.org/10.1186/s12951-022-01342-8.

[82] N. Lewinski, V. Colvin, R. Drezek, Cytotoxicity of nanopartides, Small 4 (2008) 26–49. https://doi.org/10.1002/smll.200700595.

[83] A. Wicki, D. Witzigmann, V. Balasubramanian, J. Huwyler, Nanomedicine in cancer therapy: Challenges, opportunities, and clinical applications, Journal of Controlled Release 200 (2015) 138–157. https://doi.org/10.1016/j.jconrel.2014.12.030.

[84] L. Zhang, Y. Jiang, Y. Zheng, Y. Zeng, Z. Yang, G. Huang, D. Liu, M. Gao, X. Shen, G. Wu, X. Yan, F. He, Selective killing of Burkitt's lymphoma cells by mBAFF-targeted delivery of PinX1, Leukemia 25 (2011) 331–340. https://doi.org/10.1038/leu.2010.261.

[85] F. Ravar, E. Saadat, M. Gholami, P. Dehghankelishadi, M. Mahdavi, S. Azami, F.A. Dorkoosh, Hyaluronic acid-coated liposomes for targeted delivery of paclitaxel, in-vitro characterization and in-vivo evaluation, Journal of Controlled Release 229 (2016) 10–22. https://doi.org/10.1016/j.jconrel.2016.03.012.

[86] K. Szczepanowicz, M. Bzowska, T. Kruk, A. Karabasz, J. Bereta, P. Warszynski, Pegylated polyelectrolyte nanoparticles containing paclitaxel as a promising candidate for drug carriers for passive targeting, Colloids and Surfaces B: Biointerfaces 143 (2016) 463–471. https://doi.org/10.1016/j.colsurfb.2016.03.064.

[87] B. Haley, E. Frenkel, Nanoparticles for drug delivery in cancer treatment, Urologic Oncology: Seminars and Original Investigations 26 (2008) 57–64. https://doi.org/10.1016/j.urolonc.2007.03.015.

[88] J.Y. Lee, U. Termsarasab, J.H. Park, S.Y. Lee, S.H. Ko, J.S. Shim, S.J. Chung, H.J. Cho, D.D. Kim, Dual CD44 and folate receptor-targeted nanoparticles for cancer diagnosis and

anticancer drug delivery, Journal of Controlled Release 236 (2016) 38–46. https://doi.org/10.1016/j.jconrel.2016.06.021.

[89] Y. Yang, J. Li, F. Chen, S. Qiao, Y. Li, W. Pan, Synthesis, Formulation, and Characterization of Doxorubicin-Loaded Laponite/Oligomeric Hyaluronic Acid-Aminophenylboronic Acid Nanohybrids and Cytological Evaluation against MCF-7 Breast Cancer Cells, American Association of Pharmaceutical Scientists PharmSciTech 21 (2020). https://doi.org/10.1208/s12249-019-1533-6.

[90] H. Maeda, G.Y. Bharate, J. Daruwalla, Polymeric drugs for efficient tumor-targeted drug delivery based on EPR-effect, European Journal of Pharmaceutics and Biopharmaceutics 71 (2009) 409–419. https://doi.org/10.1016/j.ejpb.2008.11.010.

[91] P.S. Low, W.A. Henne, D.D. Doorneweerd, Discovery and development of folic-acid-based receptor targeting for imaging and therapy of cancer and inflammatory diseases, Accounts of Chemical Research 41 (2008) 120–129. https://doi.org/10.1021/ar7000815.

[92] X. Zhang, N. Liang, X. Gong, Y. Kawashima, F. Cui, S. Sun, Tumor-targeting micelles based on folic acid and α-tocopherol succinate conjugated hyaluronic acid for paclitaxel delivery, Colloids and Surfaces B: Biointerfaces 177 (2019) 11–18. https://doi.org/10.1016/j.colsurfb.2019.01.044.

[93] H. Maeda, T. Sawa, T. Konno, Mechanism of tumor-targeted delivery of macromolecular drugs, including the EPR effect in solid tumor and clinical q overview of the prototype polymeric drug SMANCS, Journal of Controlled Release 74 (2001) 47-61. https://doi.org/10.1016/s0168-3659(01)00309-1.

[94] S. Unezaki, K. Maruyama B', J.-I. Hosoda, I. Nagae, Y. Koyanagi, M. Nakata, O. Ishida, M. Iwatsuru, S. Tsuchiya, Direct measurement of the extravasation of polyethyleneglycol-coated liposomes into solid tumor tissue by in vivo fluorescence microscopy, International Journal of Pharmaceutics 144 (1996) 11-17. https://doi.org/10.1016/S0378-5173(96)04674-1.

[95] A.K. Iyer, G. Khaled, J. Fang, H. Maeda, Exploiting the enhanced permeability and retention effect for tumor targeting, Drug Discovery Today 11 (2006) 812–818. https://doi.org/10.1016/j.drudis.2006.07.005.

[96] Y. Malam, M. Loizidou, A.M. Seifalian, Liposomes and nanoparticles: nanosized vehicles for drug delivery in cancer, Trends Pharmacol Sci 30 (2009) 592–599. https://doi.org/10.1016/j.tips.2009.08.004.

[97] E. Gullotti, Y. Yeo, Extracellularly activated nanocarriers: A new paradigm of tumor targeted drug delivery, Molecular Pharmaceutics 6 (2009) 1041–1051. https://doi.org/10.1021/mp900090z.

[98] Y.H. Bae, Drug targeting and tumor heterogeneity, Journal of Controlled Release 133 (2009) 2–3. https://doi.org/10.1016/j.jconrel.2008.09.074.

[99] I.K. Choi, R. Strauss, M. Richter, C.O. Yun, A. Lieber, Strategies to increase drug penetration in solid tumors, Frontiers in Oncology 3 (2013). https://doi.org/10.3389/fonc.2013.00193.

[100] C.H. Heldin, K. Rubin, K. Pietras, A. Östman, High interstitial fluid pressure - An obstacle in cancer therapy, Nature Reviews Cancer 4 (2004) 806–813. https://doi.org/10.1038/nrc1456.

[101] K.F. Pirollo, E.H. Chang, Does a targeting ligand influence nanoparticle tumor localization or uptake?, Trends in Biotechnology 26 (2008) 552–558. https://doi.org/10.1016/j.tibtech.2008.06.007.

[102] N. Bertrand, J. Wu, X. Xu, N. Kamaly, O.C. Farokhzad, Cancer nanotechnology: The impact of passive and active targeting in the era of modern cancer biology, Advanced Drug Delivery Reviews 66 (2014) 2–25. https://doi.org/10.1016/j.addr.2013.11.009.

[103] M. Srinivasarao, P.S. Low, Ligand-Targeted Drug Delivery, Chemical Reviews 117 (2017) 12133–12164. https://doi.org/10.1021/acs.chemrev.7b00013.

[104] R.I. Pinhassi, Y.G. Assaraf, S. Farber, M. Stark, D. Ickowicz, S. Drori, A.J. Domb, Y.D. Livney, Arabinogalactan-folic acid-drug conjugate for targeted delivery and target-activated release of anticancer drugs to folate receptor-overexpressing cells, Biomacromolecules 11 (2010) 294–303. https://doi.org/10.1021/bm900853z.

[105] B. Zhou, L. Zhao, M. Shen, J. Zhao, X. Shi, A multifunctional polyethylenimine-based nanoplatform for targeted anticancer drug delivery to tumors in vivo, Journal of Materials Chemistry B 5 (2017) 1542–1550. https://doi.org/10.1039/c6tb02620f.

[106] G.P. Adams, R. Schier, A.M. Mccall, H.H. Simmons, E.M. Horak, R.K. Alpaugh, J.D. Marks, L.M. Weiner, High Affinity Restricts the Localization and Tumor Penetration of Single-Chain Fv Antibody Molecules, Cancer Research 61 (2001) 4750-4755.

[107] S. Gosk, T. Moos, C. Gottstein, G. Bendas, VCAM-1 directed immunoliposomes selectively target tumor vasculature in vivo, Biochimica et Biophysica Acta - Biomembranes 1778 (2008) 854–863. https://doi.org/10.1016/j.bbamem.2007.12.021.

[108] T.M. Allen, Ligand-targeted therapeutics in anticancer therapy, Nature Reviews Cancer 2 (2002) 750–763. https://doi.org/10.1038/nrc903.

[109] G.A. Wiseman, C.A. White, R.B. Sparks, W.D. Erwin, D.A. Podoloff, D. Lamonica, N.L. Bartlett, J.A. Parker, W.L. Dunn, S.M. Spies, R. Belanger, T.E. Witzig, B.R. Leigh, Biodistribution and dosimetry results from a phase III prospectively randomized controlled trial of Zevalin™ radioimmunotherapy for low-grade, follicular, or transformed B-cell non-

Hodgkin's lymphoma, Critical Reviews in Oncology/Hematology 39 (2001) 181-194. https://doi.org/10.1016/s1040-8428(01)00107-x.

[110] Z. Liu, K. Chen, C. Davis, S. Sherlock, Q. Cao, X. Chen, H. Dai, Drug delivery with carbon nanotubes for in vivo cancer treatment, Cancer Research 68 (2008) 6652–6660. https://doi.org/10.1158/0008-5472.CAN-08-1468.

[111] L. Brannon-Peppas, J.O. Blanchette, Nanoparticle and targeted systems for cancer therapy, Advanced Drug Delivery Reviews 56 (2004) 1649–1659. https://doi.org/10.1016/j.addr.2004.02.014.

[112] K. Li, S. Wang, S. Wen, Y. Tang, J. Li, X. Shi, Q. Zhao, Enhanced in vivo antitumor efficacy of doxorubicin encapsulated within laponite nanodisks, American Chemical Society - Applied Materials & Interfaces 6 (2014) 12328–12334. https://doi.org/10.1021/am502094a.

[113] M. Yang, J. Li, P. Gu, X. Fan, The application of nanoparticles in cancer immunotherapy: Targeting tumor microenvironment, Bioactive Materials 6 (2021) 1973–1987. https://doi.org/10.1016/j.bioactmat.2020.12.010.

[114] N. Karra, S. Benita, The Ligand Nanoparticle Conjugation Approach for Targeted Cancer Therapy, Current Drug Metabolism 13 (2012) 22-41. https://doi.org/10.2174/138920012798356899.

[115] G. Tiwari, R. Tiwari, S. Bannerjee, L. Bhati, S. Pandey, P. Pandey, B. Sriwastawa, Drug delivery systems: An updated review, International Journal of Pharmaceutical Investigation 2 (2012) 2-11. https://doi.org/10.4103/2230-973x.96920.

[116] S. Hua, M.B.C. de Matos, J.M. Metselaar, G. Storm, Current trends and challenges in the clinical translation of nanoparticulate nanomedicines: Pathways for translational development and commercialization, Frontiers in Pharmacology 9 (2018). https://doi.org/10.3389/fphar.2018.00790.

[117] S.S. Dharap, Y. Wang, P. Chandna, J.J. Khandare, B. Qiu, S. Gunaseelan, P.J. Sinko, S. Stein, A. Farmanfarmaian, T. Minko, Tumor-specific targeting of an anticancer drug delivery system by LHRH peptide, Proceedings of the National Academy of Sciences of the United States of America 102 (2005) 12962-12967. https://doi.org/10.1073/pnas.0504274102.

[118] X. Li, Z. Yang, K. Yang, Y. Zhou, X. Chen, Y. Zhang, F. Wang, Y. Liu, L. Ren, Self-Assembled polymeric micellar nanoparticles as nanocarriers for poorly soluble anticancer drug ethaselen, Nanoscale Research Letters 4 (2009) 1502–1511. https://doi.org/10.1007/s11671-009-9427-2.

[119] S. Schmitt, A. Huppertsberg, A. Klefenz, L. Kaps, V. Mailänder, D. Schuppan, H.J. Butt, L. Nuhn, K. Koynov, Fluorescence Correlation Spectroscopy Monitors the Fate of

Degradable Nanocarriers in the Blood Stream, Biomacromolecules 23 (2022) 1065–1074. https://doi.org/10.1021/acs.biomac.1c01407.

[120] C. Amgoth, C. Phan, M. Banavoth, S. Rompivalasa, G. Tang, Polymer Properties: Functionalization and Surface Modified Nanoparticles, in: Role of Novel Drug Delivery Vehicles in Nanobiomedicine, IntechOpen (2020) https://doi.org/10.5772/intechopen.84424.

[121] D.S. Idris, A. Roy, S. Pandit, S. Alghamdi, M. Almehmadi, A.A. Alsaiari, O. Abdulaziz, A. Alsharif, M.U. Khandaker, M.R.I. Faruque, Polymer-based nanocarriers for biomedical and environmental applications, E-Polymers 23 (2023). https://doi.org/10.1515/epoly-2023-0049.

[122] S. Tarafder, K. Nansen, S. Bose, Lovastatin release from polycaprolactone coated β-tricalcium phosphate: Effects of pH, concentration and drug-polymer interactions, Materials Science and Engineering C 33 (2013) 3121–3128. https://doi.org/10.1016/j.msec.2013.02.049.

[123] B. Zhou, J. Yang, C. Peng, J. Zhu, Y. Tang, X. Zhu, M. Shen, G. Zhang, X. Shi, PEGylated polyethylenimine-entrapped gold nanoparticles modified with folic acid for targeted tumor CT imaging, Colloids and Surfaces B: Biointerfaces 140 (2016) 489–496. https://doi.org/10.1016/j.colsurfb.2016.01.019.

[124] Y. Zou, D. Li, M. Shen, X. Shi, Polyethylenimine-Based Nanogels for Biomedical Applications, Macromolecular Bioscience 19 (2019). https://doi.org/10.1002/mabi.201900272.

[125] Z. Chen, Z. Lv, Y. Sun, Z. Chi, G. Qing, Recent advancements in polyethyleneimine-based materials and their biomedical, biotechnology, and biomaterial applications, Journal of Materials Chemistry B 8 (2020) 2951–2973. https://doi.org/10.1039/c9tb02271f.

[126] C.N. Lungu, M. V. Diudea, M. V. Putz, I.P. Grudziński, Linear and branched PEIs (Polyethylenimines) and their property space, International Journal of Molecular Sciences 17 (2016). https://doi.org/10.3390/ijms17040555.

[127] L. Wightman, R. Kircheis, V. Rössler, S. Garotta, R. Ruzicka, M. Kursa, E. Wagner, Different behavior of branched and linear polyethylenimine for gene delivery in vitro and in vivo, Journal of Gene Medicine 3 (2001) 362–372. https://doi.org/10.1002/jgm.187.

[128] W.T. Godbey, K.K. Wu, A.G. Mikos, Poly(ethylenimine) and its role in gene delivery, Journal of Controlled Release 60 (1999) 149-160. https://doi.org/10.1016/s0168-3659(99)00090-5.

[129] R. Guo, S. Chen, X. Xiao, Fabrication and characterization of poly (ethylenimine) modified poly (l-lactic acid) nanofibrous scaffolds, Journal of Biomaterials Science Polymer Edition 30 (2019) 1523–1541. https://doi.org/10.1080/09205063.2019.1648015.

[130] J. Zhao, C. Lu, X. He, X. Zhang, W. Zhang, X. Zhang, Polyethylenimine-grafted cellulose nanofibril aerogels as versatile vehicles for drug delivery, American Chemical Society Applied Materials & Interfaces 7 (2015) 2607–2615. https://doi.org/10.1021/am507601m.

[131] R.S. Ambekar, B. Kandasubramanian, A polydopamine-based platform for anti-cancer drug delivery, Biomaterials Science 7 (2019) 1776–1793. https://doi.org/10.1039/c8bm01642a.

[132] Y. Liu, C. Su, Y. Zu, X. Chen, J. Sha, J. Dai, Ultrafast deposition of polydopamine for high-performance fiber-reinforced high-temperature ceramic composites, Scientific Reports 12 (2022). https://doi.org/10.1038/s41598-022-24971-3.

[133] S. El Yakhlifi, V. Ball, Polydopamine as a stable and functional nanomaterial, Colloids and Surfaces B: Biointerfaces 186 (2020). https://doi.org/10.1016/j.colsurfb.2019.110719.

[134] J. Park, T.F. Brust, H.J. Lee, S.C. Lee, V.J. Watts, Y. Yeo, Polydopamine-based simple and versatile surface modification of polymeric nano drug carriers, American Chemical Society Nano 8 (2014) 3347–3356. https://doi.org/10.1021/nn405809c.

[135] G. Kiaee, N. Dimitrakakis, S. Sharifzadeh, H.J. Kim, R.K. Avery, K.M. Moghaddam, R. Haghniaz, E.P. Yalcintas, N.R. de Barros, S. Karamikamkar, A. Libanori, A. Khademhosseini, P. Khoshakhlagh, Laponite-Based Nanomaterials for Drug Delivery, Advanced Healthcare Materials 11 (2022). https://doi.org/10.1002/adhm.202102054.

[136] G. Li, Y. Guo, R. Guo, X. Shi, M. Shen, LAPONITE® nanodisk-based platforms for cancer diagnosis and therapy, Materials Advances 3 (2022) 6742–6752. https://doi.org/10.1039/d2ma00637e.

[137] Z. Wang, Y. Duan, Y. Duan, Application of polydopamine in tumor targeted drug delivery system and its drug release behavior, Journal of Controlled Release 290 (2018) 56–74. https://doi.org/10.1016/j.jconrel.2018.10.009.

[138] H.A. Lee, Y. Ma, F. Zhou, S. Hong, H. Lee, Material-Independent Surface Chemistry beyond Polydopamine Coating, Accounts of Chemical Research 52 (2019) 704–713. https://doi.org/10.1021/acs.accounts.8b00583.

[139] S. Hong, K.Y. Kim, H.J. Wook, S.Y. Park, K.D. Lee, D.Y. Lee, H. Lee, Attenuation of the in vivo toxicity of biomaterials by polydopamine surface modification, Nanomedicine 6 (2011) 793–801. https://doi.org/10.2217/nnm.11.76.

[140] J.I. Dawson, R.O.C. Oreffo, Clay: New opportunities for tissue regeneration and biomaterial design, Advanced Materials 25 (2013) 4069–4086. https://doi.org/10.1002/adma.201301034.

[141] D. Li, Y.T. Zhang, M. Yu, J. Guo, D. Chaudhary, C.C. Wang, Cancer therapy and fluorescence imaging using the active release of doxorubicin from MSPs/Ni-LDH folate

targeting nanoparticles, Biomaterials 34 (2013) 7913–7922. https://doi.org/10.1016/j.biomaterials.2013.06.046.

[142] R. Rojas, C.E. Giacomelli, Size-tunable LDH-protein hybrids toward the optimization of drug nanocarriers, Journal of Materials Chemistry B 3 (2015) 2778–2785. https://doi.org/10.1039/c4tb01992j.

[143] H. Jung, H.M. Kim, Y. Bin Choy, S.J. Hwang, J.H. Choy, Itraconazole-Laponite: Kinetics and mechanism of drug release, Applied Clay Science 40 (2008) 99–107. https://doi.org/10.1016/j.clay.2007.09.002.

[144] C. Viseras, P. Cerezo, R. Sanchez, I. Salcedo, C. Aguzzi, Current challenges in clay minerals for drug delivery, Applied Clay Science 48 (2010) 291–295. https://doi.org/10.1016/j.clay.2010.01.007.

[145] K. Shafran, C. V. Jeans, S.J. Kemp, K. Murphy, Dr Barbara S. Neumann: Clay Scientist, Industrial Pioneer, Creator of Laponite®, Elements 17 (2021) 69–70. https://doi.org/10.2138/gselements.17.1.69.

[146] Y. Li, D. MacIel, H. Tomás, J. Rodrigues, H. Ma, X. Shi, PH sensitive Laponite/alginate hybrid hydrogels: Swelling behaviour and release mechanism, Soft Matter 7 (2011) 6231–6238. https://doi.org/10.1039/c1sm05345k.

[147] D. Bonn, H. Kellay, H. Tanaka, G. Wegdam, J. Meunier, Laponite: What Is the Difference between a Gel and a Glass?, Langmuir 15 (1999) 7534–7536. https://doi.org/10.1021/la990167.

[148] H. Tomás, C.S. Alves, J. Rodrigues, Laponite®: A key nanoplatform for biomedical applications?, Nanomedicine 14 (2018) 2407–2420. https://doi.org/10.1016/j.nano.2017.04.016.

[149] D.W. Thompson, J.T. Butterworth, The Nature of Laponite and Its Aqueous Dispersions, Journal of Colloid and Interface Science 151 (1992) 236-243. https://doi.org/10.1016/0021-9797(92)90254-J.

[150] S. Wang, F. Zheng, Y. Huang, Y. Fang, M. Shen, M. Zhu, X. Shi, Encapsulation of amoxicillin within laponite-doped poly(lactic-co-glycolic acid) nanofibers: Preparation, characterization, and antibacterial activity, American Chemical Society Applied Materials & Interfaces 4 (2012) 6393–6401. https://doi.org/10.1021/am302130b.

[151] X. Chen, Y. Wang, R. Chai, Y. Xu, H. Li, B. Liu, Luminescent Lanthanide-Based Organic/Inorganic Hybrid Materials for Discrimination of Glutathione in Solution and within Hydrogels, American Chemical Society Applied Materials & Interfaces 9 (2017) 13554–13563. https://doi.org/10.1021/acsami.7b02679.

[152] T. Felbeck, T. Behnke, K. Hoffmann, M. Grabolle, M.M. Lezhnina, U.H. Kynast, U. Resch-Genger, Nile-red-nanoclay hybrids: Red emissive optical probes for use in aqueous dispersion, Langmuir 29 (2013) 11489–11497. https://doi.org/10.1021/la402165q.

[153] J. Teyssier, R. Le Dantec, C. Galez, Y. Mugnier, A. Vrain, J. Bouillot, J.-C. Plenet, Inorganic clay-based nanostructured material for nonlinear optical waveguides, Proceedings of SPIE 5946, Optical Materials and Applications (2006). https://doi.org/10.1117/12.639173.

[154] Y. Wu, K. Li, L. Kong, Y. Tang, G. Li, W. Jiang, M. Shen, R. Guo, Q. Zhao, X. Shi, Functional LAPONITE Nanodisks Enable Targeted Anticancer Chemotherapy in Vivo, Bioconjugate Chemistry 31 (2020) 2404–2412. https://doi.org/10.1021/acs.bioconjchem.0c00473.

[155] B.M. Franco Muggia, J.D. Hainsworth, S. Jeffers, P. Miller, S. Groshen, M. Tan, L. Roman, B. Uziely, L. Muderspach, A. Garcia, A. Burnett, F. Anthony Greco, C. Paul Morrow, L.J. Paradiso, L.-J. Liang, Phase II Study of Liposomal Doxorubicin in Refractory Ovarian Cancer: Antitumor Activity and Toxicity Modification by Liposomal Encapsulation, Journal of Clinical Oncology 15 (1996). https://doi.org/10.1200/JCO.1997.15.3.987.

[156] Z. Symon, A. Peyser, D. Tzemach, O. Lyass, E. Sucher, E. Shezen, A. Gabizon, Selective delivery of doxorubicin to patients with breast carcinoma metastases by stealth liposomes, Cancer 86 (1999) 72–78. https://doi.org/10.1002/(SICI)1097-0142(19990701)86:1<72::AID-CNCR12>3.0.CO;2-1.

[157] R.Z. Orlowski, A. Nagler, P. Sonneveld, J. Bladé, R. Hajek, A. Spencer, J. San Miguel, T. Robak, A. Dmoszynska, N. Horvath, I. Spicka, H.J. Sutherland, A.N. Suvorov, S.H. Zhuang, T. Parekh, L. Xiu, Z. Yuan, W. Rackoff, J.L. Harousseau, Randomized phase III study of pegylated liposomal doxorubicin plus bortezomib compared with bortezomib alone in relapsed or refractory multiple myeloma: Combination therapy improves time to progression, Journal of Clinical Oncology 25 (2007) 3892–3901. https://doi.org/10.1200/JCO.2006.10.5460.

[158] U. Bulbake, S. Doppalapudi, N. Kommineni, W. Khan, Liposomal formulations in clinical use: An updated review, Pharmaceutics 9 (2017). https://doi.org/10.3390/pharmaceutics9020012.

[159] S. Chan, N. Davidson, E. Juozaityte, F. Erdkamp, A. Pluzanska, N. Azarnia, L.W. Lee, Phase III trial of liposomal doxorubicin and cyclophosphamide compared with epirubicin and cyclophosphamide as first-line therapy for metastatic breast cancer, Annals of Oncology 15 (2004) 1527–1534. https://doi.org/10.1093/annonc/mdh393.

[160] R.C.F. Leonard, S. Williams, A. Tulpule, A.M. Levine, S. Oliveros, Improving the therapeutic index of anthracycline chemotherapy: Focus on liposomal doxorubicin (Myocet™), Breast 18 (2009) 218–224. https://doi.org/10.1016/j.breast.2009.05.004.

[161] Y. Barenholz, Doxil® - The first FDA-approved nano-drug: Lessons learned, Journal of Controlled Release 160 (2012) 117–134. https://doi.org/10.1016/j.jconrel.2012.03.020.

[162] S.T. Duggan, G.M. Keating, G. Ferrandina, J.P. Kesterson, Pegylated Liposomal Doxorubicin A Review of its use in Metastatic Breast Cancer, Ovarian Cancer, Multiple Myeloma and AIDS-Related Kaposi's Sarcoma, Drugs 71 (2011) 2531-2558. https://doi.org/10.2165/11207510-000000000-00000.

[163] G. Batist, J. Barton, P. Chaikin, C. Swenson, L. Welles, Myocet (liposome-encapsulated doxorubicin citrate): a new approach in breast cancer therapy, Expert Opinion on Pharmacotherapy 3 (2002) 1739–1751. https://doi.org/10.1517/14656566.3. 12.1739.

[164] G. Batist, G. Ramakrishnan, C.S. Rao, A. Chandrasekharan, J. Gutheil, T. Guthrie, P. Shah, A. Khojasteh, M.K. Nair, K. Hoelzer, K. Tkaczuk, Y.C. Park, L.W. Lee, Reduced cardiotoxicity and preserved antitumor efficacy of liposome-encapsulated doxorubicin and multicenter trial of metastatic breast cancer, Journal of Clinical Oncology 19 (2001) 1444–1454. https://doi.org/10.1200/JCO.2001.19.5.1444.

[165] L. Harris, G. Batist, R. Belt, D. Rovira, R. Navari, N. Azarnia, L. Welles, E. Winer, Liposome-encapsulated doxorubicin compared with conventional doxorubicin in a randomized multicenter trial as first-line therapy of metastatic breast carcinoma, Cancer 94 (2002) 25–36. https://doi.org/10.1002/cncr.10201.

[166] S. Pavlidou, C.D. Papaspyrides, A review on polymer-layered silicate nanocomposites, Progress in Polymer Science (Oxford) 33 (2008) 1119–1198. https://doi.org/10.1016/j.progpolymsci.2008.07.008.

[167] J.S. Suk, Q. Xu, N. Kim, J. Hanes, L.M. Ensign, PEGylation as a strategy for improving nanoparticle-based drug and gene delivery, Advances in Drug Delivery Reviews 99 (2016) 28–51. https://doi.org/10.1016/j.addr.2015.09.012.

[168] Q. Zheng, T. Lin, H. Wu, L. Guo, P. Ye, Y. Hao, Q. Guo, J. Jiang, F. Fu, G. Chen, Mussel-inspired polydopamine coated mesoporous silica nanoparticles as pH-sensitive nanocarriers for controlled release, International Journal of Pharmaceutics 463 (2014) 22–26. https://doi.org/10.1016/j.ijpharm.2013.12.045.

[169] S. Wang, Y. Wu, R. Guo, Y. Huang, S. Wen, M. Shen, J. Wang, X. Shi, Laponite nanodisks as an efficient platform for doxorubicin delivery to cancer cells, Langmuir 29 (2013) 5030–5036. https://doi.org/10.1021/la4001363.

[170] C. Chen, B. Zhou, X. Zhu, M. Shen, X. Shi, Branched polyethyleneimine modified with hyaluronic acid via a PEG spacer for targeted anticancer drug delivery, Royal Society of Chemistry Advances 6 (2016) 9232–9239. https://doi.org/10.1039/c5ra23022e.

[171] D. Bi, L. Zhao, R. Yu, H. Li, Y. Guo, X. Wang, M. Hana, Surface modification of doxorubicin-loaded nanoparticles based on polydopamine with pH-sensitive property for tumor

targeting therapy, Drug Delivery 25 (2018) 564–575. https://doi.org/10.1080/10717544.2018.1440447.

[172] J.H. Ryu, P.B. Messersmith, H. Lee, Polydopamine Surface Chemistry: A Decade of Discovery, American Chemical Society Applied Materials & Interfaces 10 (2018) 7523–7540. https://doi.org/10.1021/acsami.7b19865.

[173] N.F. Della Vecchia, A. Luchini, A. Napolitano, G. Derrico, G. Vitiello, N. Szekely, M. Dischia, L. Paduano, Tris buffer modulates polydopamine growth, aggregation, and paramagnetic properties, Langmuir 30 (2014) 9811–9818. https://doi.org/10.1021/la501560z.

[174] D. Guimarães, J. Noro, C. Silva, A. Cavaco-Paulo, E. Nogueira, Protective Effect of Saccharides on Freeze-Dried Liposomes Encapsulating Drugs, Frontiers in Bioengineering and Biotechnology 7 (2019). https://doi.org/10.3389/fbioe.2019.00424.

[175] J.L. Pasek-Allen, R.K. Wilharm, J.C. Bischof, V.C. Pierre, NMR Characterization of Polyethylene Glycol Conjugates for Nanoparticle Functionalization, American Chemical Society Omega 18 (2022) 4331-4336. https://doi.org/10.1021/acsomega.2c07669.

[176] C. Bonechi, A. Donati, R. Lampariello, S. Martini, M.P. Picchi, M. Ricci, C. Rossi, Solution structure of folic acid: Molecular mechanics and NMR investigation, Spectrochimica Acta Part A: Molecular and Biomolecular Spectroscopy 60 (2004) 1411–1419. https://doi.org/10.1016/j.saa.2003.08.007.

[177] M. Kaszuba, J. Corbett, F.M.N. Watson, A. Jones, High-concentration zeta potential measurements using light-scattering techniques, Philosophical Transactions of the Royal Society A: Mathematical, Physical and Engineering Sciences 368 (2010) 4439–445. https://doi.org/10.1098/rsta.2010.0175.

[178] S. Bhattacharjee, DLS and zeta potential - What they are and what they are not?, Journal of Controlled Release 235 (2016) 337–351. https://doi.org/10.1016/j.jconrel.2016.06.017.

[179] M. Goldberg, R. Langer, X. Jia, Nanostructured materials for applications in drug delivery and tissue engineering, Journal of Biomaterials Science Polymer Edition 18 (2007) 241-268. https://doi.org/10.1163/156856207779996931.

[180] U. Lungwitz, M. Breunig, T. Blunk, A. Göpferich, Polyethylenimine-based non-viral gene delivery systems, European Journal of Pharmaceutics and Biopharmaceutics 60 (2005) 247-266. https://doi.org/10.1016/j.ejpb.2004.11.011.

[181] F. Meng, Y. Zhong, R. Cheng, C. Deng, Z. Zhong, PH-sensitive polymeric nanoparticles for tumor-targeting doxorubicin delivery: Concept and recent advances, Nanomedicine 9 (2014) 487–499. https://doi.org/10.2217/nnm.13.212.

[182] J. O'Brien, I. Wilson, T. Orton, F. Pognan, Investigation of the Alamar Blue (resazurin) fluorescent dye for the assessment of mammalian cell cytotoxicity, Eur J Biochem 267 (2000) 5421–5426. https://doi.org/10.1046/j.1432-1327.2000.01606.x.

[183] E.M. Czekanska, Assessment of Cell Proliferation with Resazurin-Based Fluorescent Dye, Methods in Molecular Biology 740 (2011) 27–32. https://doi.org/10.1007/978-1-61779-108-6_5.

[184] K. Präbst, H. Engelhardt, S. Ringgeler, H. Hübner, Basic colorimetric proliferation assays: MTT, WST, and resazurin, Methods in Molecular Biology 1601 (2017) 1–17. https://doi.org/10.1007/978-1-4939-6960-9_1.

Supplementary information

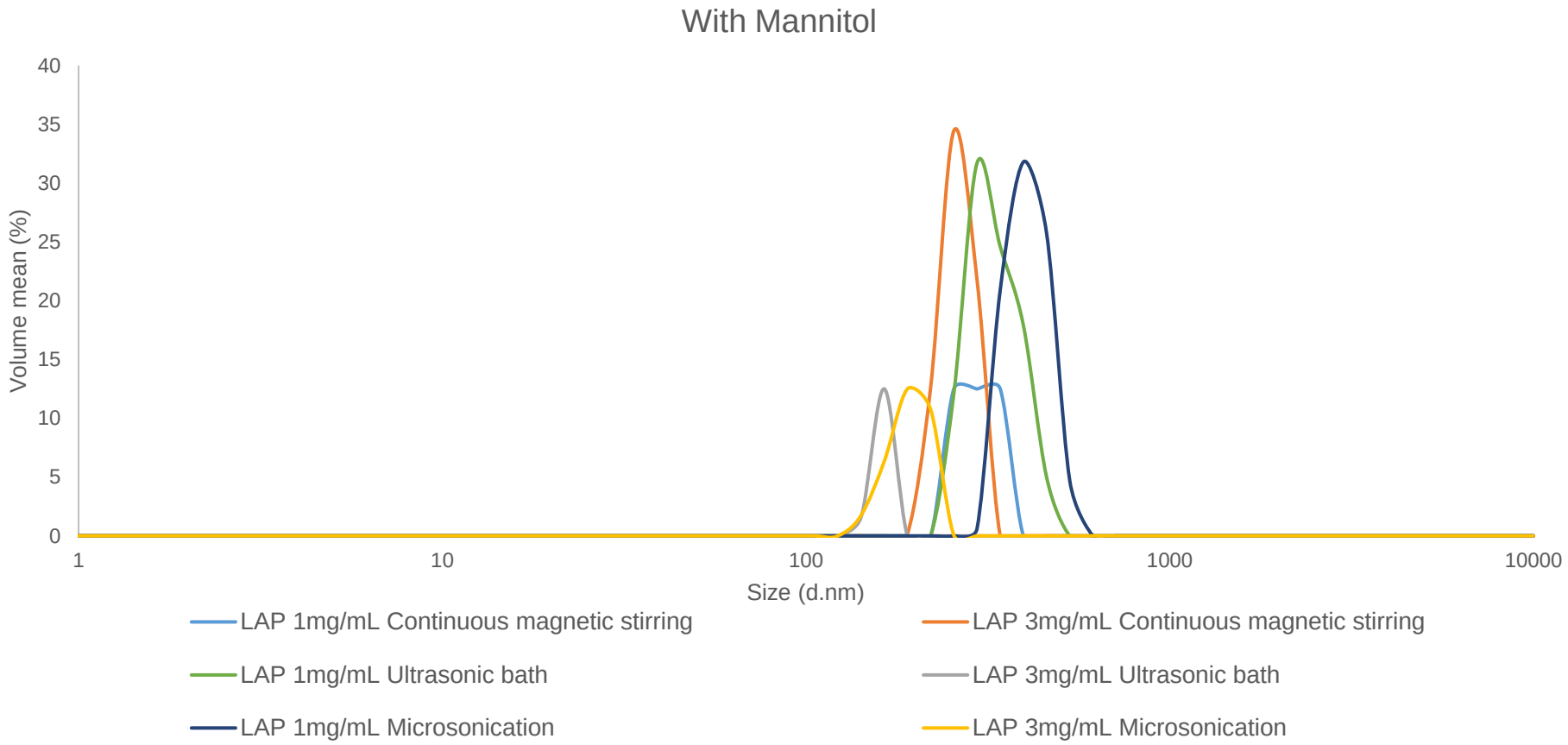

Figure S1. Volume mean (%) vs particle size distribution of all the conditions tested and with the addition of Mannitol.

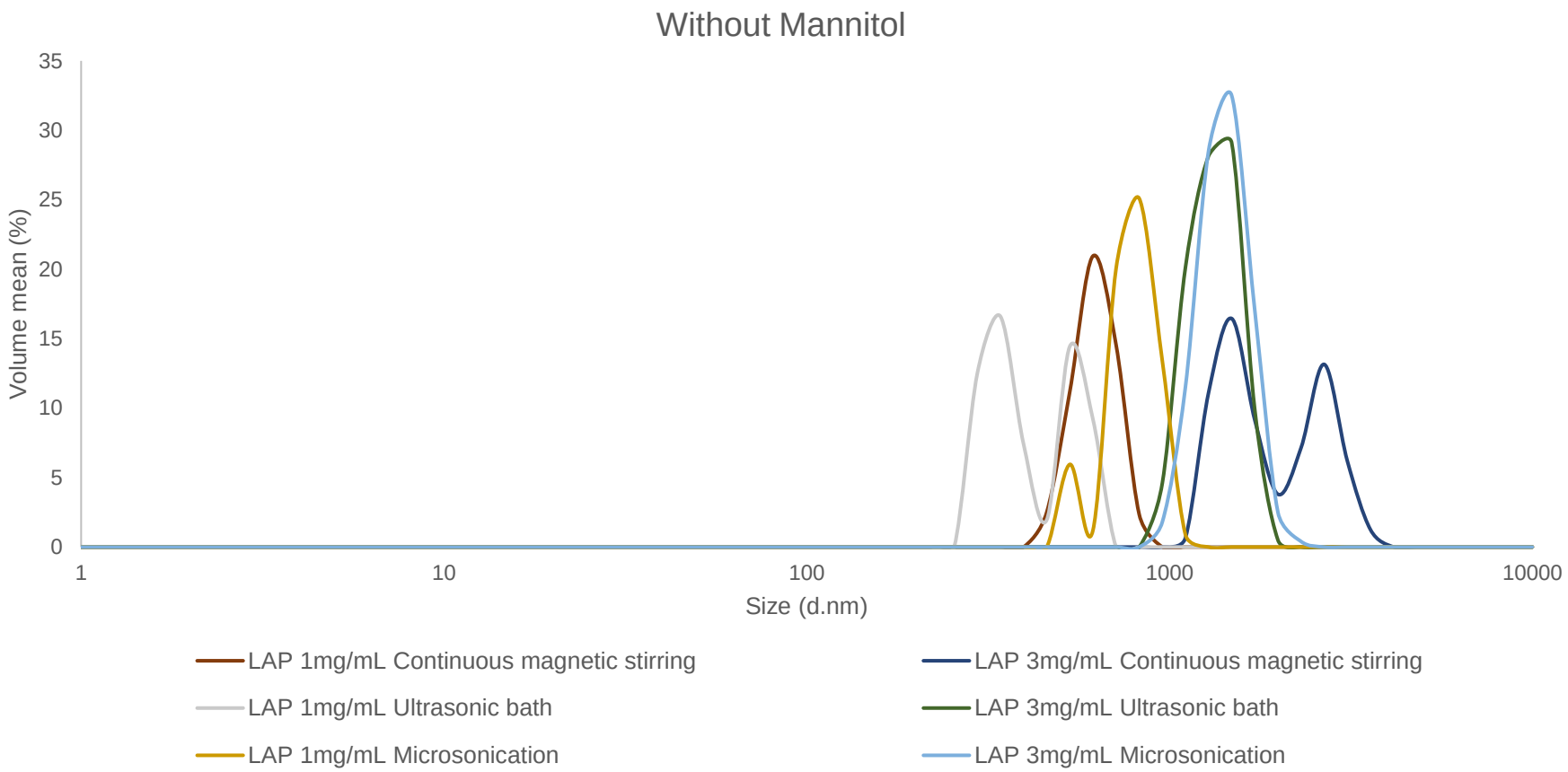

Figure S2. Volume mean (%) vs particle size distribution of all the conditions tested and without the addition of Mannitol.

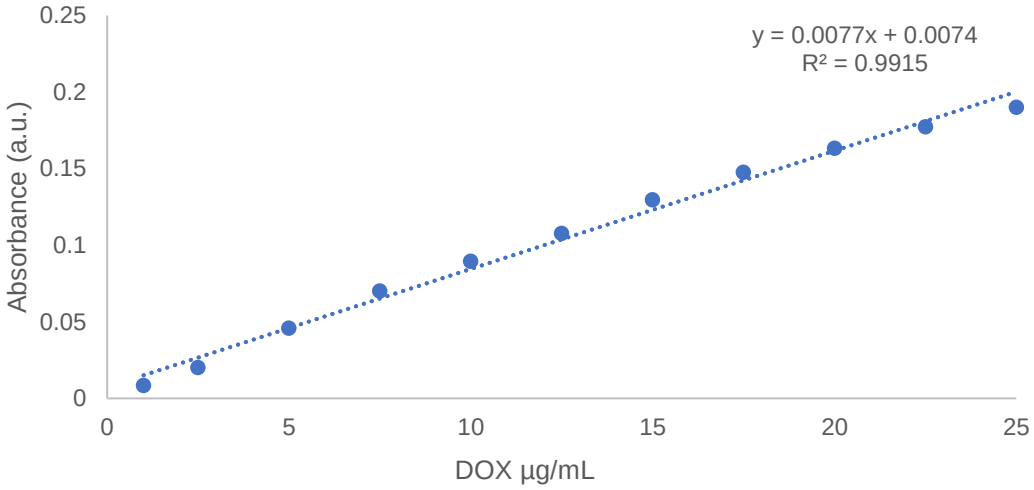

Figure S3. Calibration line for DOX at 480nm.

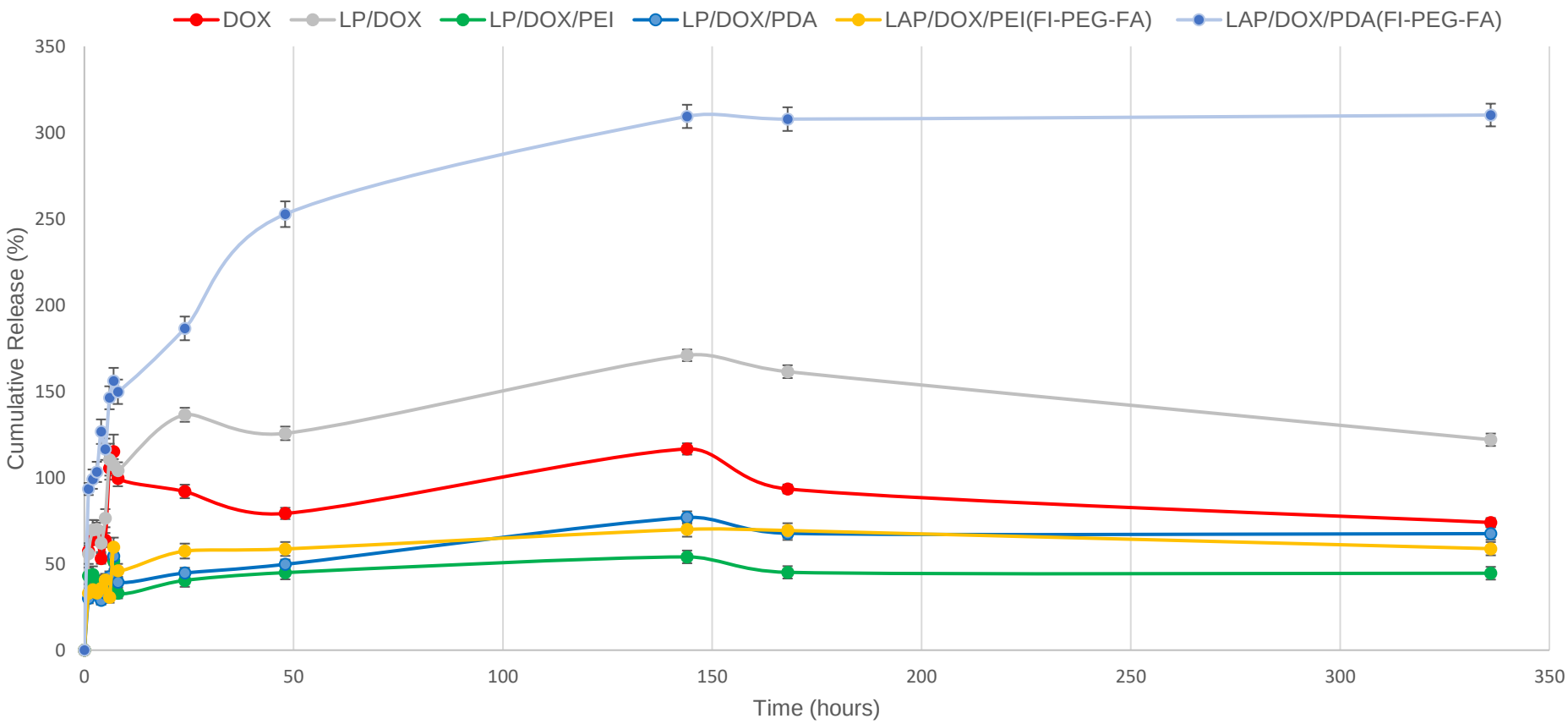

Figure S4. Cr% of DOX in PBS, pH 7.4 at 37 °C as a function of time (2 weeks).

Cofinanciado por: